Université d'Ottawa · University of Ottawa

Université d'Ottawa · University of Ottawa

FACULTÉ DES ÉTUDES SUPÉRIEURES ET POSTDOCTORALES

FACULTY OF GRADUATE AND POSTDOCTORAL STUDIES

Jacinthe LESAGE

AUTEUR DE LA THÈSE - AUTHOR OF THESIS

M. Sc. (Biochemistry - spec. HMG)

GRADE - DEGREE

Department of Biochemistry, Microbiology and Immunology

FACULTÉ, ÉCOLE, DÉPARTEMENT - FACULTY, SCHOOL, DEPARTMENT

TITRE DE LA THÈSE - TITLE OF THE THESIS

Investigation into the Genetic Nature of Familial Congenital Bicuspid Aortic Valve

D. Bulman

DIRECTEUR DE LA THÈSE - THESIS SUPERVISOR

CO-DIRECTEUR DE LA THÈSE - THESIS CO-SUPERVISOR

EXAMINATEURS DE LA THÈSE - THESIS EXAMINERS

M-A. Akimenko

M. Holcik

J.-M. De Koninck, Ph.D.

LE DOYEN DE LA FACULTÉ DES ÉTUDES SUPÉRIEURES ET POSTDOCTORALES

DEAN OF THE FACULTY OF GRADUATE AND POSTDOCTORAL STUDIES

Investigation into the Genetic Nature of Familial Congenital Bicuspid Aortic Valve

by
Jacinthe Le Sage

Thesis submitted to the
Faculty of Graduate and Postdoctoral Studies
in partial fulfillment of the requirements for the
Master of Science degree in Human Molecular Genetics

Department of Biochemistry, Microbiology and Immunology
Faculty of Medicine
University of Ottawa

Your file Votre référence
ISBN: 0-494-01524-1
Our file Notre référence
ISBN: 0-494-01524-1

Abstract

Bicuspid aortic valve (BAV) affects approximately 1% of the general population and its etiology remains unknown. Based on literature reports, we hypothesized that congenital BAV (cBAV) was a developmental defect inherited as an autosomal dominant trait with variable penetrance. We evaluated the *NOS3* candidate gene based on the reported phenotype of a mouse mutant, and the *FBLN2* and *TIMP4* genes based on their role in heart development. DNA sequencing of these genes in our BAV families did not reveal the presence of any potential disease-causing mutations. We also examined the 3p25 region, which showed suggestive linkage at the D3S1259 marker locus in a previous 20 cM genome-wide screen. Linkage analysis with additional markers in the region suggested that the initial hit at D3S1259 had probably been obtained by chance in most families. We are currently recruiting additional families and plan to undertake a 10 cM genome screen to uncover new loci. This work represents the first effort to investigate the genetic nature of cBAV.

Acknowledgements

I would like to thank my supervisor Dr Dennis Bulman for his guidance throughout my project. Dennis, thank you for your patience.

Thank you Dr Chan and Donna Dillon from the Heart Institute; Dr Chan, I'm glad I had an expert on BAV within arms reach. Donna, with your devotion and your strong work ethics, the project was in good hands.

I would like to thank my advisory committee members, Dr David Picketts and Dr Alexander MacKenzie, for their precious time and advice.

I would like to thank the National Sciences and Engineering Research Council of Canada, the Ontario Graduate Scholarship, le Fonds pour la Recherche en Santé du Québec, the University of Ottawa and the Heart and Stroke Foundation of Canada for funding.

Thank you Dr Andrew Patterson from the University of Toronto for helping us with the linkage data.

Many thanks to Lee, Lam, Andrew, Ruobing and Kelly for your contribution to my project; your help came very appreciated at the times when I needed it the most.

Thank you to everyone from the Bulman lab team, past and present, who certainly contributed to making my experience in the lab a most enjoyable one.

Mille mercis à ma famille et à tous mes amis; vous avez été patients et compréhensifs durant de longs mois et vos encouragements constants m'ont aidée à continuer jusqu'à la fin. Marc, merci d'avoir été là pour moi durant mes moments les plus difficiles.

Je vous aime

xxx

Table of Contents

List of Tables

List of Figures

Abbreviations and Symbols

A	Adenosine
a.a.	Amino acid
α	Alpha
Ala or A	Alanine
ASD	Atrial septal defect
Asp	Aspartic acid
AV	Atrioventricular
AVSD	Atrioventricular septal defect
b, bp	Base, base pairs
β	Beta
BAV, cBAV	Bicuspid aortic valve, congenital bicuspid aortic valve
C	Cytidine
°C	Degrees Celsius
CA	Coronary artery
chr.	Chromosome
cM	Centimorgan
CMD	Cystic medial degeneration
dbSNP	SNP database (at NCBI)
ddH_2O	Distilled de-ionized water
DNA	Deoxyribonucleic acid
dNTP	Deoxynucleotide triphosphate
ECM	Extracellular matrix
EDTA	Ethylenediamine tetraacetate
endo.	endocardial
eNOS	Endothelial nitric oxide synthase
FGF	Fibroblast growth factor
G	Guanosine
Glu	Glutamic acid
Gly	Glycine
h	Hour
HA	Hyaluronic acid
HCl	Chloridric acid
I	Isoleucine
i.e.	Id est (latin for: "that is")
K	Lysine
KCl	Potassium chloride
L	Litre
ln	Natural logarithm
LOD	Logarithm of the odds
Log	Logarithm
M, mM, μM	Molar, millimolar, micromolar
MA	Massachusetts
Mb	Megabase
Met	Methionine
$MgCl_2$	Magnesium chloride

min	Minute
ml, µl	Millilitre, microlitre
MMP	Matrix metalloproteinase
µg	Microgram
mRNA	Messenger RNA
N	Nucleotide (G, A, T or C)
NCBI	National Centre for Biotechnology Information
NE	Nebraska
$(NH_4)_2SO_4$	Ammonium sulphate
NJ	New Jersey
NO, NOS	Nitric oxide, nitric oxide synthase
OFT	Outflow tract
OH	Ohio
ON	Ontario
p	Probability value
PCR	Polymerase chain reaction
PDGF	Platelet derived growth factor
pH	– Log (hydrogen ion concentration)
Phe	Phenylalanine
pmol	Picomole
Pro	Proline
pter	p terminal end
R	Arginine
®	Registered
RNA	Ribonucleic acid
s	Second
Ser	Serine
SNP	Single nucleotide polymorphism
STRP	Short tandem repeat polymorphism
T	Thymidine
TE	TRIS-EDTA
TGF-β	Transforming growth factor-β
θ	Theta
Thr	Threonine
™	Trade mark
TNF-α	Tumor necrosis factor-α
TRIS	Tris(hydroxymethyl)aminomethane
UCSC	University of California, Santa Cruz
USA	United States of America
UTR	Untranslated region
Val or V	Valine
VEGF	Vascular endothelial growth factor
VNTR	Variable number of tandem repeats
vs.	Versus
VSD	Ventricular septal defect
Z	LOD score
-/-	homozygote gene null (gene knockout)
+/-	heterozygote wild-type/knockout

Chapter 1. Background Information and Literature Review

1.1 The bicuspid aortic valve disorder – an overview

Bicuspid aortic valve (BAV) is the most common malformation of the heart valves with an estimated incidence ranging from 0.4 to 2.0% in the general population [1-4]. BAV is more prevalent in males than in females, and accounts for about one-third of surgically excised aortic valves [5-7].

The normal *tricuspid* aortic heart valve has three, equal-sized, leaflets (or cusps) and three aortic sinuses (Figure 1.1A). A *bicuspid* aortic valve has only two leaflets, which can be equal or unequal in size, and two commissures (Figure 1.1B, C) [8]. A raphe, which is a mound of fibrous tissue, can also be found at the fused commissure of the conjoint cusp (Figure 1.1). When a raphe is absent, the two cusps are usually of almost equal size [9].

The pathogenesis of BAV is unclear. Reports in the literature usually classify bicuspid aortic valves into two categories, according to their presumed origin. *Congenital BAV* (cBAV) probably results from early fusion of a tricuspid structure during development in the embryo [10]. *Acquired* or *postinflammatory BAV* develops throughout life and results from the fusion of two, adult cusps [11,12] (Figure 1.1D). It is estimated that approximately one third of all cases of BAV are congenital [13].

To date, the cause of cBAV remains unknown and genetic linkage has not been reported for this disorder. However, a genetic abnormality is implicated, as familial clustering has been reported, and BAV is frequently associated with other aortic defects.

Figure 1.1. Morphology of the bicuspid aortic valve compared with the normal aortic valve. **A.** Anatomy of the aortic valve and related structures. A normal aortic valve has three of each of these components: leaflets, aortic sinuses (the expanded region of the aortic root), interleaflet triangles and commissures (the junction between two leaflets). The brief contact between edges of cusps during diastole is called "coaptation". The dotted lines indicate the level of attachment of each leaflet inside the aortic sinuses. The two coronary arteries are not depicted. **B.** Bicuspid valves without a raphe have only two, often nearly equal-sized cusps, but the number of sinuses and interleaflet triangles can vary from two to three. **C.** Bicuspid valves with a raphe usually have three sinuses, and the circumference of the conjoint cusp around the aorta is usually smaller than 240^{o} between the two commissures. The raphe is usually shallower and shorter compared with the ridge of the fused commissure from an acquired bicuspid aortic valve. **D.** In the latter, three sinuses and interleaflet triangles are still identifiable and the circumference around each cusp is nearly equal, as seen in a normal valve.

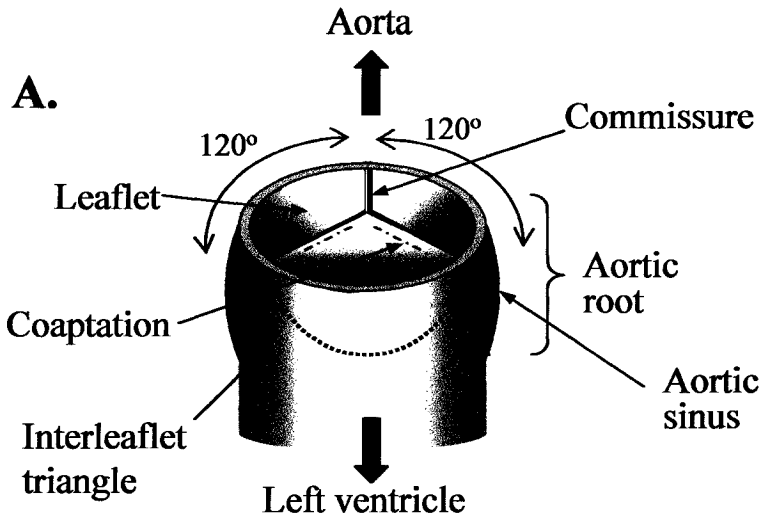
A.
Aorta
120°
120°
Commissure
Leaflet
Aortic root
Coaptation
Aortic sinus
Interleaflet triangle
Left ventricle
Tricuspid aortic valve
B.
~180°
~180°
Without a raphe
C.
≥120°
≤120°
Shallow raphe
With a raphe
Congenital bicuspid aortic valve
D.
120°
120°
Fused commissure (tall ridge)
Acquired bicuspid aortic valve

This association suggests that BAV is part of a more generalized disease of the aortic media [14,15]. Some pedigrees are consistent with a pattern of autosomal dominant inheritance with variable penetrance [13].

1.2 Morphological variants of the congenitally bicuspid aortic valve

Congenitally bicuspid aortic valves present morphologic variants, and several authors have classified them into different categories according to the size and orientation of the leaflets and the number of aortic sinuses (Figure 1.2) [2,6,10,16,17]. In BAVs without a raphe, the two cusps can be oriented in various ways (Figure 1.2B). Similarly, the larger cusp (conjoint cusp) in a BAV with a raphe can involve any cusp (Figure 1.2C). However, certain variants are found more frequently than others (see section 1.9.1). Bicuspid valves can also be classified according to the aspect of the raphe. This fibrous ridge can be tall or shallow, or fenestrated, and vary in length and thickness [5,6,8,10,11,18-20]. In reality, bicuspid valves are not always as "perfect" as depicted in Figure 1.2. A number of intermediate phenotypes are often seen. Some anatomic variants of the coronary arteries have also been reported [17,21].

1.3 Diagnosis

Fifteen years ago, BAV was diagnosed at autopsy or during surgery. Currently, BAV is diagnosed by two-dimensional (2-D) transthoracic echocardiography. This non-invasive imaging modality allows observation of the valve in motion, and has high specificity and sensitivity in detecting bicuspid aortic valves [18,22]. The diagnosis can remain indeterminate in a small percentage of patients because of extensive calcification

Figure 1.2. Morphological variants of the bicuspid aortic valve. **A.** A normal tricuspid aortic valve is depicted. The two coronary arteries each arise from a different aortic sinus. The cusps of the aortic valves are named after the origin of the coronary arteries, i.e. the left, right, and posterior (or non-coronary) cusp. The dotted lines indicate the level of attachment of each leaflet inside the aortic sinuses. CA: coronary artery. **B.** Bicuspid valves without a raphe can have one coronary artery arising from each cusp, or both CAs arising from the same cusp. L: left. R: right. A: anterior. P: posterior. **C.** The conjoint cusp in bicuspid valves with a raphe can involve any two cusps.

A.

Normal tricuspid aortic valve

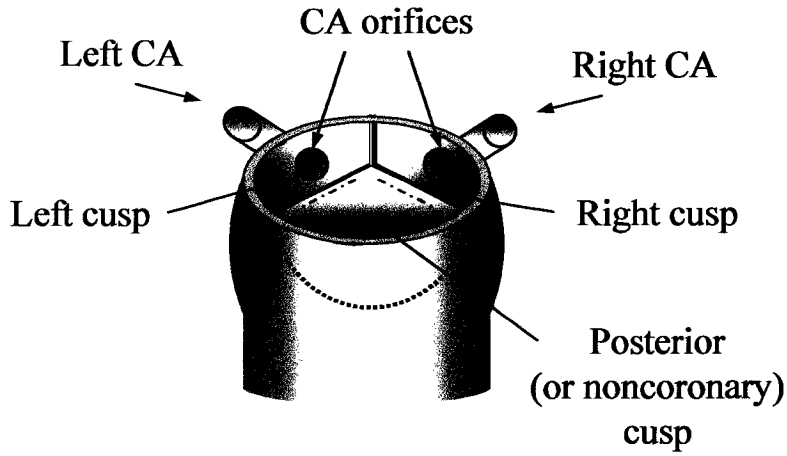

B.

Congenital without a raphe

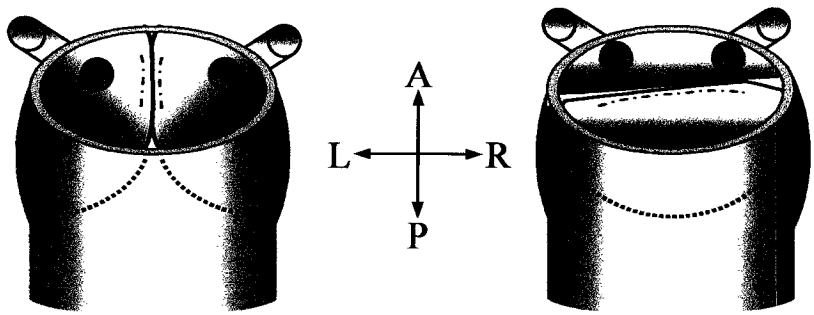

Lateral (left-right) cusps

Anterior-posterior cusps

C.

Congenital with raphe

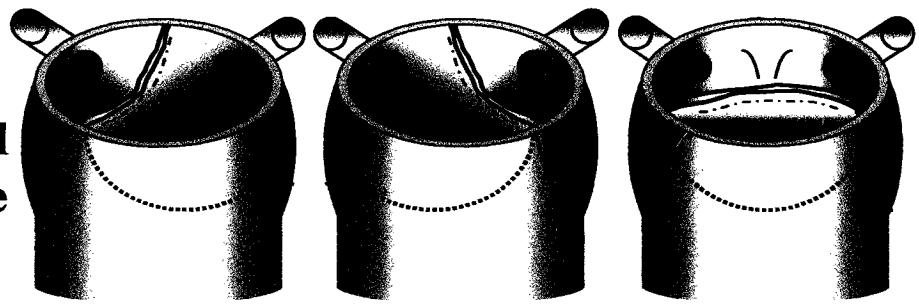

Right-posterior conjoint cusp

Left-posterior conjoint cusp

Left-right conjoint cusp

of the valves [8]. The clinical manifestations of cBAV are varied and cannot be used to establish a diagnosis with precision [8,22]. Age at diagnosis varies widely since the bicuspid valve can remain functional for a number of years before the symptoms appear [2,23-25]. Diagnosis can be made in infancy or childhood when severe valve dysfunction exists, but most patients only start presenting symptoms after 40 years of age [6,26]. BAV can also be an incidental finding at autopsy in an asymptomatic patient [2,24].

During echocardiography, the major elements that help establish a diagnosis are the position of the commissures and shape of the orifice, which has an inverted triangle appearance in a normal valve and assumes a "fish-mouth" appearance in a bicuspid valve during systole [18]. General asymmetry of the valve is usually an indication of BAV [27]. The difference between congenital and acquired bicuspid valves can be made by following certain morphologic criteria that have been described. Briefly, the raphe in a congenital bicuspid valve is usually more vestigial, and the true and fused commissures are not spaced equally at 120^{o} from each other, as seen in acquired BAV (see Figure 1.1) [2,6,8,10].

1.4 Clinical significance

Bicuspid aortic valves have a higher propensity towards complications than normal tricuspid valves. The most common complications include aortic root dilatation, aortic stenosis due to calcification of the cusps, regurgitation (insufficiency) and infection [2,16,24,28-30]. Over time, these changes can open the door to additional complications, which in turn can aggravate the pre-existing condition. Indeed, dilated aortae are subject to dissection and rupture and can lead to insufficiency, while cusp prolapse and especially

infection (infective endocarditis) are major causes of aortic regurgitation in BAV patients [2,3,6,12,24,31]. BAV patients tend to be affected with these cardiac problems at a greater incidence and at a significantly younger age compared with individuals having a tricuspid aortic valve [3,12,24]. Only about 1-30% of patients maintain normal valve function over their lifetime [6,31]. The long-term prognosis is variable in each patient, with consequences ranging from little effect on valve function, to severe symptoms requiring valve replacement or causing death [24].

The nature, severity and progression of the complications are influenced by age, sex, shape and orientation of the cusps and raphe, and the presence of an underlying aortic medial fragility [3,6,9,16,23,24,32,33]. Other unknown genetic and environmental factors are also likely to play a role in the nature of the degenerative changes [2].

1.5 Incidence

Congenital heart disease is found in about 6/1000 live births when moderate and severe forms are considered. This number inflates to 19/1000 live births when bicuspid aortic valve is included [4]. Necropsy studies disclosed an incidence of 0.40% to 2.25% for BAV in the general population in USA and Europe, with an average of 1% [2-4]. A lower incidence is reported in Japan and Brazil (0.023 to 0.350% and 0.650% respectively) [9,34,35], although these figures might not be significant due to the relatively small number of valves studied.

1.6 Congenital BAV: an inherited disorder?

The mode of inheritance of familial congenital BAV is not defined. Over 25 years ago, poor diagnosis methods and thus lack of a confident "affected" status for each family member made pedigree analysis difficult [23]. Moreover, the distinction between congenital and acquired BAV was not always possible. Today, this problem has been overcome, but the mode of inheritance is still unclear in many families [15,36,37], except for a pattern of autosomal dominance with variable penetrance that was observed in some families [1,13,37]. A recent study in Lebanon revealed that several congenital heart defects, namely atrial and ventricular septal defects, aortic stenosis, insufficiency, and bicuspid aortic valve were associated with increased consanguinity [38]. Intriguingly, endogamy is usually associated with recessive traits. The possibility of multiple inheritance patterns for BAV should not be excluded.

Additional support in favour of a genetic involvement in BAV also comes from the unusually high incidence of familial clustering for this disorder. Emanuel *et al* [37] and Huntington *et al* [13] reported that BAV occurs in more than one family member in a minimum of 14.6% and 36.7% of the cases, respectively. They correspondingly found an incidence of 3.7% and 9.1% for BAV in first-degree relatives of the proband, which is well above the 1-2% figures found in the general population. "BAV is clearly more common in first-degree relatives of subjects with a bicuspid aortic valve than in those of subjects with a tricuspid aortic valve" [39]. In addition, a recent study of 74 BAV patients and relatives (total = 309 participants) revealed a heritability of 89% for BAV, supporting a strong genetic effect for this condition [40].

BAV appears to have reduced penetrance especially in females [36]. The affected male:female ratio is 2:1 on average [13,37,39], yet no sex-linked inheritance has been reported. It has been suggested that more women are asymptomatic and remain undetected [29]. However, in several familial cases of BAV, the prevalence in males and females was equal [13,36,37].

The small number of families available for studying congenital BAV certainly impedes genetic analyses. In the past decade, the presence of BAV in more than one family member was still reported to be extremely uncommon [36,39]. Nevertheless, 46 families with cBAV have been published up to this date (reviewed in [36]; see also [13,40,41]), plus 6 additional families from the current project (see Figure 3.1, Chapter 3; ten of our 16 families have been previously published in [13]). The increasing awareness of clinicians about BAV and the recommendation to screen all first degree relatives of affected individuals by echocardiography will contribute to facilitating the detection of additional families in the future [36,42].

1.7 Other associated conditions and disorders

BAV is occasionally associated with aortic and cardiac abnormalities as well as with known genetic disorders and syndromes, which further supports the idea that cBAV is an inherited disorder. The most frequent associations are discussed below.

1.7.1 Aortic abnormalities

Coarctation of the aorta. Coarctation is a congenital narrowing of the aorta, generally localized in the descending aortic arch, with consequent restricted blood flow to

organs. A bicuspid aortic valve is present in 35-85% of patients with coarctation; therefore their association is not coincidental [11,15,28,43-46]. Coarctation affects approximately 0.04% of the general population compared to 1-2% for BAV [4], hence BAV is found in patients with coarctation at least 25 times more often than what would be expected by chance.

Aortic wall fragility and aortic aneurysm, dissection and rupture. Dissections are tears in the inner aortic wall that can cause blood to infiltrate between the layers composing the vessel wall. The weakened aortic wall can rupture, causing sudden death [47]. The association of BAV with aortic dilatation (aneurysm) and aortic dissection is well recognized [3,14,21,48-52]. BAV patients are found to have a dilated ascending aorta 6 to 10 times more frequently than individuals with a normal tricuspid valve [45,53,54]. Viewed from another perspective, a high prevalence of BAV (20%) was also observed in patients with dilated aortic root [30], or dissection (up to 28%) [47]. Aortic dissection occurs nine times more frequently in BAV patients than in normal subjects, therefore BAV is considered to be a risk factor predisposing to intimal tears [3].

In addition, BAV is associated with degenerative changes of the aorta such as abnormal elastic properties and cystic medial necrosis (also called cystic medial degeneration, CMD), even in patients with a non-dilated ascending aorta [53-60]. CMD is seen at the microscopic level by non-inflammatory smooth muscle cell and elastic fibre loss, and an accumulation of basophilic and mucoid material. The aorta from BAV patients shows a greater extent of smooth muscle cell apoptosis than that from individuals with a tricuspid aortic valve, both in the presence and absence of aortic dilatation [61-63].

Whether medial weakness is inherent to the pathology of BAV or a result of turbulent blood flow caused by the diseased valve is strongly debated [49,55,64]. In favour of the altered hemodynamics (blood flow parameters) hypothesis, it is known that turbulent blood flow can dilate vessels [64,65]. Also, a correlation was found between the extent of aortic root dilatation and the grade of aortic wall CMD in patients with acquired *tricuspid* aortic valve disease [66], which suggests that aortic wall abnormalities are secondary to altered valve function. However, some have argued that the clinical manifestations of medial weakness (i.e. aortic aneurysm and dissection) should be studied instead of CMD, which might not be a specific medial weakness marker [34,50]. In this regard, several investigators found a greater extent of aortic root dilatation in BAV patients with *normal* valve function and hemodynamics than in controls, in clinical as well as in community-based studies [48,50-52,67,68]. Similarly, aortic dissections are found to occur in BAV patients with normally functioning valves [3,54]. Furthermore, many have suggested that a neural crest-derived pathology could explain the frequent association of aortic coarctation and aortic abnormalities with BAV [14,15,21,58,69]. The aortic arch and valve are populated in part by neural crest-derived cells, which participate in the development of many tissues including facial structures and the aorta [70,71]. Among coarctation patients, BAV is also a lot more prevalent in patients with head/neck anomalies than in patients without a non-cardiac anomaly [15]. Collectively, these results favour the increasingly accepted idea that aortic abnormalities are intrinsic to the BAV pathology and not merely a consequence of it [21,23,42,50,52,54,60,62,63, 68,69,72].

Aortic medial fragility is also found in patients affected with Ehlers-Danlos syndrome (EDS) type IV [73] and Marfan syndrome (MFN) [74]. EDS and MFN are connective tissue disorders caused by mutations in the genes encoding type III procollagen (chr.2) and fibrillin-1 (chr.15), respectively. Recently, linkage has been reported for familial aortic aneurysm and dissections in different families on chromosomes 11q, 5q and 3p24-25 [75-77]. Collectively, these reports show that genetic causes can be attributed to aortic dilatation in the presence or absence of an associated syndrome.

In summary, the aorta of BAV patients has an increased propensity towards medial degeneration, aneurysm and dissection than individuals with a normal aortic valve. A growing body of evidence supports the idea that these findings are manifestations of a common abnormality involving the aortic valve and aortic arch, although the effects of turbulent blood flow are not negligible in a subset of patients.

1.7.2 Other cardiac abnormalities

Mitral valve prolapse (MVP). MVP affects ~2.4% of the general population, and is inherited as an autosomal dominant trait with variable penetrance. Loci for this condition have been identified on chromosomes 16p and 11p [78,79]. This condition can coexist with BAV and aortic medial fragility [6,13].

Other heart anomalies. In one study of 1,022 hearts, BAV was found to occur in 6.7% of hearts with other congenital heart disease. In 51% of these cases, BAV was associated with ventricular septal defect (VSD) and aortic arch obstruction [21,46].

1.7.3 Chromosomal syndromes

Turner's syndrome. In patients with Turner's syndrome (45 XO), a bicuspid aortic valve represents the most common cardiac abnormality seen and is present in 14-19% of the cases [80]. Aortic coarctation is also very prevalent. Despite this association, X-linked inheritance of bicuspid aortic valve has not been reported.

Trisomy 18. Trisomy 18 patients rarely survive beyond one year of age. Several systems are affected, including the cardiovascular one. Ventricular septal defects and heart valve malformations are the cardiovascular hallmarks of this syndrome, with BAV being the most common malformation of the aortic valve [21,81].

3p- syndrome. The 3p- syndrome is a deletion of the 3p25-pter region, and is characterized by growth and mental retardation and craniofacial anomalies. Molecular analysis revealed that the exact location of the deletion breakpoint varies among affected individuals and correlates with the severity of the disease [82]. Cardiovascular defects are present in a subset of patients, usually the ones with the most extensive deletions [83,84]. Genetic mapping disclosed the presence of a gene involved in normal septation of the heart on chromosome 3p25 between D3S1263 and D3S3594 [85]. No report of BAV was made, but the occasional association of BAV with septation defects makes chromosome 3p25 a region of interest.

In summary, BAV can be found as an isolated defect or in association with other cardiac or non-cardiac anomalies. The prevalence of isolated BAV is unclear.

1.8 Normal aortic valve development

Heart formation in the embryo requires complex morphogenesis of a tubular structure into a functional four-chambered pump. The primitive heart tube is composed of four layers; they are (from inside to outside) the endocardium, the cardiac jelly, the myocardium and the epicardium (Figure 1.3A) [86,87]. The cardiac jelly is a thick layer of extracellular matrix. The tube undergoes looping, remodelling and septation to give rise to a mature, functioning heart. Septation (partitioning) of the heart and outflow tract (OFT, the tube that will develop into the pulmonary artery and aorta) is closely associated with the formation of heart valves.

1.8.1 The cardiac cushions

After looping, the extracellular matrix in the atrioventricular (AV) canal and outflow tract regions of the heart begins to swell. Meanwhile, localized signals from the myocardium induce a subpopulation of cells from the endocardium to undergo transformation into mesenchymal cells, which migrate and invade the cardiac jelly swellings [86-88]. These mesenchymal outgrowths are called the endocardial cushions, the structures that will give rise to the valves and septa. The cushions expand and grow towards each other, thus separating the heart tube into chambers with valves. AV and OFT (or truncal) cushions give rise respectively to the atrioventricular valves (mitral and tricuspid) and to the semilunar valves (aortic and pulmonary) (Figure 1.3B) [70,89]. The aorticopulmonary septum divides the outflow tract into two arteries and also extends downward to fuse with the inferior endocardial cushion, thus completely closing the space between ventricles [90]. Since the formation of both the valves and septa is

Figure 1.3. Formation of the human semilunar valves. **A.** Schematic representation of the four layers composing the heart wall. The heart tube is composed of an inner layer of endothelial cells (endocardium) and a layer of cardiac muscle cells (myocardium). In between those two layers resides a thick layer of extracellular matrix called the cardiac jelly. The outer envelope is the epicardium. Drawing not to scale. **B.** Location of the endocardial cushions in the developing heart. Shown in blue are the endocardial cushions that protrude in the outflow tract (left diagram) to form the aorticopulmonary septum and the semilunar valves, and in the atrioventricular canals (right diagram) to give rise to the ventricular septum and atrioventricular valves. RA: right atrium. LA: left atrium. RV: right ventricle. LV: left ventricle. **C.** Septation of the outflow tract and semilunar valve formation. Left: human heart at 30 days of gestation. The "boxed" region indicates the area of the outflow tract (common trunk) where the semilunar valves will form. Middle: Around the 5^{th} week of human gestation, mesenchymal swellings begin to protrude in the lumen of the outflow tract. Right: By the 9^{th} week, septation of the outflow tract is complete, resulting in two distinct arteries (the aorta and pulmonary artery), each with its own tricuspid semilunar valve. **D.** Longitudinal cut of the aorta at the level of the aortic valve. The arterial and ventricular faces of the cusps are subject to very different blood flow patterns; hemodynamics are a major factor involved in the development of the semilunar valves. C and D: adapted from reference [70].

A.

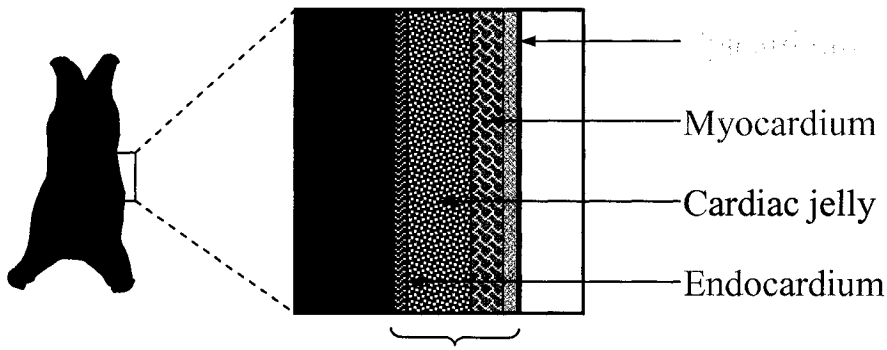
Myocardium
Cardiac jelly
Endocardium
Primitive heart tube
Heart wall

B.

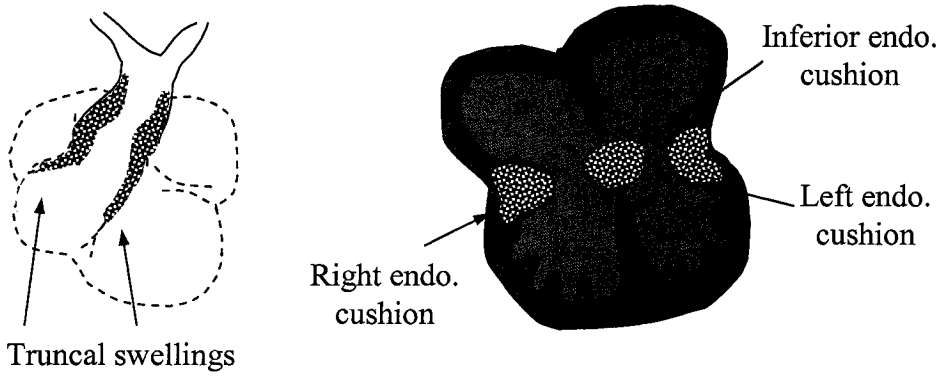
Inferior endo. cushion
Left endo. cushion
Right endo. cushion
Truncal swellings

C.

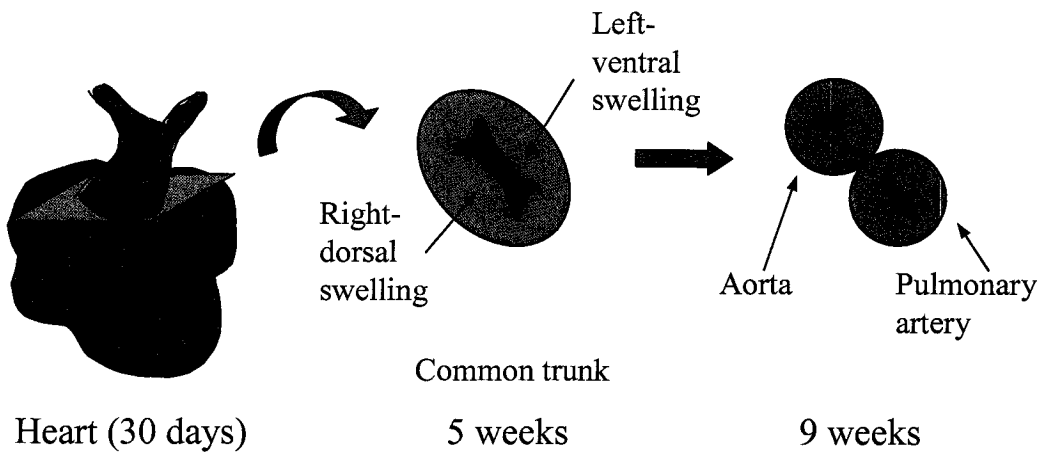
Left-ventral swelling
Right-dorsal swelling
Aorta
Pulmonary artery
Common trunk
Heart (30 days)
5 weeks
9 weeks

D.

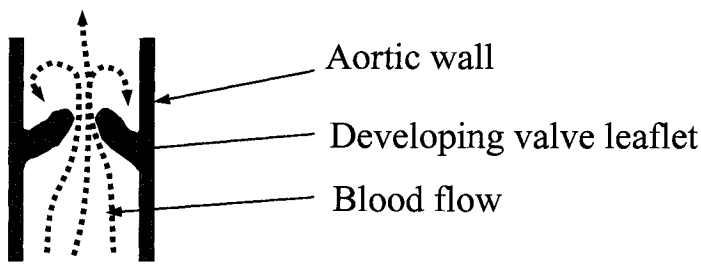
Aortic wall
Developing valve leaflet
Blood flow

dependent on the integrity of the endocardial cushions, it is easy to understand why heart valve anomalies are often accompanied by ventricular septal defects. Septation of the outflow tract involves remodelling and fusion of the two largest truncal cushions (the left and right truncal swellings), resulting in three equal-sized mounds protruding in the lumen of each of the two arteries (Figure 1.3C) [70,90,91]. The bulges consist of a core of mesenchymal cells covered by endocardium. Studies of chick and mouse embryos revealed that the excavation of these structures into cusps and sinuses involves growth of the endocardial layer as well as mesenchymal condensation and cell death at precise locations [92,93]. At least part of this remodelling is contributed to by blood flow changes, which influence cell death and proliferation in the leaflets (Figure 1.3D) [94,95]. The developing cusps finally become thin and fibrous with the differentiation of mesenchymal cells into fibroblasts.

On a molecular level, numerous genes are known to contribute to the formation of the AV and OFT endocardial cushions in mice and avians. Several signalling pathways act in concert to ensure that the correct number of cells invade the cardiac jelly (reviewed in [87,88,96]). Among the molecules known to stimulate the formation of cushions are members of the transforming growth factor β family (TGFβ1, -β2, -β3) and receptors (TBRI, -II, -III), as well as the bone morphogenic proteins (BMP) 2, 4, 5, 6, 7 and receptor (Bmpr2) [97-99]. Several ALKs (activin receptor-like kinases) interact with the TBRs and Bmpr2, and the downstream response of epithelial-to-mesenchymal transformation is mediated by the Smad1, -2, -3, -4, -5 and -8 transcription factors [88]. On the other hand, Smad6 and -7 and vascular endothelial growth factor (VEGF) have an inhibitory effect on cushion transformation in mice [88,100,101]. Matrix

metalloproteinases (MMPs) and tissue inhibitors of MMPs (TIMPs) also participate in cushion remodelling. MMPs are ECM-degrading enzymes which activity is regulated by endogenous inhibitor proteins, the TIMPs [88,102,103].

The cardiac jelly is a functional matrix essential to the propagation of signals between the endocardium and the myocardium. The ECM in the cardiac cushions is an assembled mesh of proteoglycans, glycosaminoglycans and structural proteins, namely hyaluronic acid, versican, perlecan, fibulin-1 and -2, collagens, fibronectin, and fibrillin-2 (reviewed in [86,89]). This matrix undergoes reorganization during the remodelling of cushions into valve leaflets [89]. Hyaluronic acid (HA) is a major scaffold component of the cardiac jelly, and also stimulates the activation or release of soluble factors [88,89]. Targeted inactivation of HA, perlecan or versican alters valvulogenesis in mice [88,89,104]. Acting downstream of HA is the erbB signalling family of receptors (erbB1, -2, -3) and related ligands that activate the ras/MAPK/ERK growth cascade [88,89].

Although several of the genes involved in valve development are expressed in both the AV and the OFT cushions, distinct molecular events take place in the OFT namely because of the presence of neural crest-derived cells.

1.8.2 The neural crest

The neural crest is the name given to a population of cells that originate in the embryonic neural tube. The cells are responsible for the development of an array of structures, namely the nervous system, pigment and skin cells, endocrine tissues and most tissues from the head and face [70]. A subpopulation of neural crest cells migrate to the cardiac outflow tract and contribute to the formation of the aorticopulmonary septum

[71,105]. Notably, neural crest-derived cells are found in the semilunar valve cusps [106,107]. Ablation of the cardiac neural crest in avian models is associated namely with outflow tract and aortic arch anomalies [108]. In addition, elastogenesis (the formation of elastic fibres) originates from cardiac neural crest cells and propagates downstream along the great arteries [108].

A certain proportion of neural crest- and endocardially-derived cells are removed by apoptosis during the normal course of development [88,91,109-111]. It is now known that neural crest-derived and endocardially-derived cushion cells respond to mutual molecular signals that influence their proliferation and fate. Although still largely unexplored, this interaction is essential for proper formation of the aorticopulmonary septum, and probably less important for semilunar valves [91,112].

In summary, the cardiac jelly contributes directly to the cross talk between endocardial, mesenchymal and myocardial cells. A very large number of molecules are implicated in valve development, and their function is tightly regulated in order to obtain a structurally and functionally normal heart. The summary presented here is not exhaustive; numerous other genes are known to be involved in valve formation and are discussed in excellent reviews [86-89,96].

1.9 How do cBAVs arise?

Exactly how congenital bicuspid aortic valves arise remains unknown, but the study of human valves and rodent models has allowed us to gain a better understanding of this malformation.

1.9.1 Insights gained from studying human valves

Knowing that each leaflet originates from a mesenchymal bulge and is supported by its own aortic sinus, two mechanisms have been proposed to explain the occurrence of congenital bicuspid aortic valves in humans. According to the first idea, maldevelopment of the cushion swellings (that is, either failure to develop or abnormal distribution of cushion tissue) would result in BAV [33,113]. In fact, only a minority of the valves are found to have two aortic sinuses and two interleaflet triangles (Figure 1.1A, B), which indicates that they developed from only two cushion swellings [10]. Three sinuses and three interleaflet triangles are found in most bicuspid aortic valves [10]. These observations led to a second hypothesis stating that bicuspid aortic valves would result from the early fusion of an initially tricuspid structure, as indicated by the number of sinuses and the presence of a raphe [6,10,33,46].

The next question that arises then is: what caused this fusion of adjacent cushions? Part of the answer may come from the observation that certain morphologic variants of BAV are found more commonly than others. In congenital BAVs without a raphe, the left-right variant was seen more often than the anterior-posterior type (Figure 1.2B) [2,10,21]. A genetic defect occurring in specific parts of the truncal cushions could explain these findings since cushion regions are molecularly heterogeneous [91]. In congenital BAVs with a raphe, the conjoint cusp involved the right and left cusps most of the time (Figure 1.2C) [6,10,17,21,46] but this was also seen in an *acquired* BAV group. This suggests that non-genetic factors may influence the fusion of cusps [17]. One such factor could be an increased hemodynamic stress on one side of the heart [17,46].

1.9.1.1 BAV and hemodynamics. Hemodynamics consist of studying the forces and factors that influence blood flow. Altered fetal blood flow is directly implicated in the pathogenesis of Fallot's tetralogy, coarctation of the aorta, and other aortic arch and truncus malformations ([46,114] and references therein). Chick embryos with experimentally altered cardiac blood flow were found to develop several heart malformations, including BAV [115-117].

The contribution of blood flow in normal and abnormal cardiac development is twofold. First, the flowing blood itself acts as a mechanical force that is able to induce the remodelling of structures. Endothelial cells lining blood vessels are known to orient in the direction of blood flow and also detach towards the blood stream during valve formation [65,94,95,117-119]. Second, blood flow has indirect effects by inducing the release of shear stress-activated factors, which in turn affect the growth of cardiac structures [120]. Namely, TGFβ1 and the eNOS enzyme are known to be expressed differently under changing shear stress conditions [121,122]. TGFβ1 is involved in cardiac cushion formation and eNOS in endothelial cell proliferation (see sections 1.8.1 and 3.1.1 respectively). Blood flow alterations can also alter cell death patterns in the OFT cushions [91].

In summary, congenital BAVs could form because of alterations in fetal blood flow, which are usually the consequence of another cardiac defect. In absence of any other cardiovascular malformation, a deficiency in the genetic program involved in normal valvulogenesis may cause congenital BAV.

1.9.2 Insights gained from rodent models

1.9.2.1 Syrian hamster. Sans-Coma and his team have studied the occurrence of bicuspid aortic valves in Syrian hamsters for several years [123-125], and have found this condition to be similar to that of humans in many ways. In a highly inbred family of Syrian hamsters, they found a high incidence of bicuspid aortic valve (30.5%), and the percentage of BAV was positively correlated with the inbreeding coefficient of the specimens [124]. The male:female ratio of affected hamsters was 1.1:1.0, which is lower than the average 2:1 ratio found in humans. The same study also disclosed a continuous spectrum of morphological variants of the aortic valve, ranging from a tricuspid valve to a bicuspid valve with various intermediate phenotypes of commissural fusion and aortic sinus size and number [124]. Interestingly, a similar range of phenotypic variants is also observed in humans (sections 1.2 and 1.9.1). In fact, rare cases of unicuspid and quadricuspid aortic valve are also seen in humans, which suggests that the number of cusps reflects a phenotypic continuum [42,126,127]. In Syrian hamsters, the results of various crossing experiments led the investigators to conclude that BAV was probably the result of a genetic predisposition influenced by unknown intrauterine environmental factors [124]. In a subsequent study, examination of hearts from hamster embryos by microscopy revealed that all variants of bicuspid aortic valves formed as a result of the fusion of two valve cushions at the beginning of valvulogenesis, from a structure having initially three cushions [125]. This also appears to be the case in humans (section 1.9.1).

1.9.2.2 Mouse. Bicuspid aortic valves had never been observed in mice until Lee and collaborators reported this condition in mice for the first time four years ago [128]. They had obtained twelve Nos3-null mice, and found a BAV in five of them. Nos3

encodes the endothelial nitric oxide synthase (eNOS) enzyme. Exactly how the deficiency of eNOS in $Nos3^{-/-}$ mice affects valve development remains elusive, but the orthologous gene (*NOS3*) obviously becomes an excellent candidate for the human condition. We have studied this gene in our BAV families as part of this project, therefore further information and discussion about eNOS is deferred to Chapter 3.

A bicuspid aortic valve was only reported in two other mice: the Nkx2-5 and the Fgf8 mutants (Table 1.1). A BAV was found in 11% of Nkx2-5 (a homeobox domain transcription factor) heterozygote mice on a C57Bl/6J background only. However, BAV was not reported in rare human familial cases of *NKX2-5* mutation [129]. Another report described the conditional inactivation of Fgf8 (fibroblast growth factor 8) in specific domains of mouse embryos, which caused bicuspid aortic valve in 23% of these mice in addition to arterial and glandular defects [130].

Other mouse mutants caused semilunar valve anomalies, but not BAV specifically (Table 1.1). Moreover, the phenotypes were not always penetrant and other concomitant cardiac or non-cardiac defects were frequently seen. Mice with null or hypomorphic mutations of the Hspg2 (perlecan), Sox4, Egfr and Gata4 genes all display hyperplasia and sometimes malposition of the truncal cushions, causing semilunar valve defects [104,112,131-133]. Notably, in $Sox4^{-/-}$ mice, it appears that the remodelling, rather than the formation of the cushions, is affected [112], which also appears to be the case in humans (section 1.9.1). On the other hand, the semilunar valves are absent in NF-Atc and Bmpr2 mutant mice, and underdeveloped in the Bmp6/Bmp7 double mutant mice [99,134-136]. Several other mouse mutants also resulted in hypo- or hyperplastic semilunar valves, but the atrioventricular valves were also affected [97,137,138].

Table 1.1. Mouse mutants with semilunar valve and/or truncal endocardial cushion anomalies. The phenotypes of each mouse mutant are indicated by a "✓" and sometimes represent combined data from multiple reports. The phenotypes were often not fully penetrant and other concomitant heart defects were sometimes present. "Outflow tract defects" refers to anomalies such as double-outlet right ventricle, absent septation of the outflow tract (persistent truncus arteriosus) and transposition of the great arteries. Most of the genes listed here encode transcription or growth factors. Gata, Smad, Nf-Atc, Sox and Fog are families of transcription factors, whereas BMP, EGF, FGF and TGF are families of growth factors. The Adam19 enzyme and the perlecan proteoglycan are ECM proteins. **Abbreviations:** BAV: bicuspid aortic valve. SV: semilunar valves. AV: atrioventricular. ASD: atrial septal defect. VSD: ventricular septal defect. ECM: extracellular matrix. $^{ki/ki}$: homozygote gene knockin. $^{\Delta E2}$: exon 2 deleted. hEgfr: human Egfr. $Egfr^{wa2}$: hypomorphic allele of Egfr.

Phenotype / Mouse Mutant	BAV	Hypermorphic, malformed SV/cushions	Hypomorphic or absent SV/cushions	Outflow tract defects	Abnormality of AV valve(s)	ASD	VSD	Non-cardiac defects	References
Adam19$^{-/-}$		✓		✓	✓	✓	✓		[137]
Bmp6$^{-/-}$ + Bmp7$^{-/-}$ (double mutant)			✓		✓	✓	✓	✓	[136]
Bmpr2$^{\Delta E2/\Delta E2}$			✓	✓			✓	✓	[99]
hEgfr$^{ki/ki}$ or Egfr$^{wa2/wa2}$:Ptpn11$^{+/-}$		✓						✓	[131, 132]
Fgf8$^{-/-}$ (conditional inactivation in specific domains)	✓			✓				✓	[130]
Gata4$^{ki/ki}$		✓		✓	✓	✓	✓		[133]
Hspg2$^{-/-}$ (perlecan)		✓		✓				✓	[104]
Madh6$^{-/-}$ (Smad6)		✓		✓	✓				[101]
Nkx2-5$^{+/-}$ (C57Bl/6J)	✓					✓			[129]
NF-Atc$^{-/-}$			✓		✓		✓		[134, 135]
Nos3$^{-/-}$	✓					✓	✓	✓	[128,139-144, 148]
Sox4$^{-/-}$			✓	✓			✓	✓	[112]
Tgf-$\beta_2{}^{-/-}$		✓		✓	✓	✓	✓	✓	[97]
Zfpm2$^{-/-}$ (Fog-2)		✓		✓	✓	✓	✓		[138]

Chapter 2: Scope of thesis

2.1 Statement of purpose

We are studying the genetics of congenital bicuspid aortic valve because it presents the features of an inherited disorder. The ultimate goal of our laboratory is to find the defective gene(s) responsible for congenital BAV. There is a need to define the molecular pathology of this disorder, as very little is known about its development and inheritance. Moreover, the identification of a causative gene(s) could help clarify the origin of BAV (congenital *vs.* acquired) in a subset of patients through genetic testing in the future.

2.2 Hypothesis and experimental approach

Based on pedigree analysis and on current literature reports, we hypothesize that congenital BAV is a developmental defect most likely inherited as an autosomal dominant trait with variable penetrance. Based on the high incidence of cBAV, we also hypothesize that the disorder is genetically heterogeneous. Consequently, we used a positional cloning approach followed by DNA sequencing of candidate genes in samples from affected families in an effort to uncover a genetic defect.

2.3 Objectives for the current Master's project

For the current Master's project, two objectives were put forth:

1. To examine the *NOS3* candidate gene on chromosome 7 (Chapter 3);
2. a. To screen a region on chromosome 3 around marker D3S1259, which might be linked to BAV in certain families (Chapter 4);

   b. To find and examine candidate genes in this region, or to exclude this region in our families (Chapter 5).

Chapter 3: Evaluation of the *NOS3* Candidate Gene on Chromosome 7 by Linkage and Sequence Analysis

3.1 Introduction

The first objective for this project was to evaluate the *NOS3* gene on chromosome 7 as a candidate for cBAV in our families. This gene became of interest to us following a report by Lee *et al* [128], who observed bicuspid aortic valves in mice for the first time. They found 5 of their 12 Nos3 (eNOS)-null mice to have a bicuspid aortic valve, and no other apparent heart malformation. The authors did not speculate why the trait was not fully penetrant. Notably, $eNOS^{-/-}$ mice of the same strain used by Lee's group (C57Bl/6J) were described in other studies before that one, but BAV was not reported [139-142]; the investigators probably did not look at the aortic valve at that time. The phenotypes of these $eNOS^{-/-}$ mice included deficient angiogenesis and vascular remodelling [139,141,143], limb abnormalities [140] and hypertension [144]. The results reported by Lee *et al* are very important for defining the genetic determinants behind heart and valve development in mice and humans: first, it constituted the first report to describe BAV in mice; second, there was an absence of another heart anomaly; and third, BAV appeared to be caused by a single defective gene.

3.1.1 Nitric oxide synthase (NOS) isoforms and eNOS function in cardiovascular development

Endothelial NOS is one of three isozymes of nitric oxide (NO) synthase. Isoform I (neuronal NOS, nNOS) is expressed in neuronal and epithelial cells. Isoform II (inducible NOS, iNOS) is expressed in cytokine-induced cells. Isoform III (endothelial NOS, eNOS)

is expressed in endothelial cells. All three isoforms catalyze the formation of NO from L-arginine and oxygen and require cofactors for their activity [145].

Endothelium-derived NO is a potent vasodilator and has several important functions, namely maintenance of vascular tone, antithrombosis, prevention of leukocyte adhesion to vascular walls and inhibition of vascular smooth muscle cell proliferation [145,146]. In addition, animal studies have shown it to be implicated in the formation of limb vasculature during embryogenesis [140], in post-developmental vascular remodelling, angiogenesis and arteriogenesis [141,143,147] and in proper endothelial cell migration, proliferation and differentiation in the context of wound repair and angiogenesis [139]. In mice, eNOS is also involved in correct septation of the heart [148] and in aortic valve formation [128]. Collectively, these reports demonstrate the important role of eNOS in normal heart and blood vessel development.

Exactly how the deficiency of eNOS in $Nos3^{-/-}$ mice results in a bicuspid aortic valve remains elusive. eNOS is expressed in endothelial cells of blood vessels [122,145], including the monolayer lining the aortic valve leaflets [128]. In light of the above discussion, we can speculate that eNOS dysfunction could affect endothelial cell proliferation in the outflow tract and therefore influence the remodelling of valve leaflets. Other genetic or environmental factors in the womb are likely to play a role since the phenotype was not completely penetrant in mice [128]. Also, it is somewhat surprising that eNOS mutant mice only show cardiovascular phenotypes, knowing that eNOS is expressed in a variety of tissues and cell types [122]. This might be explained by the fact that the other NOS isoforms compensate for the absence of eNOS in other tissues.

A recent case report describes twins believed to be monozygotic that both have a bicuspid aortic valve, with identical commissures and raphe. They also have ocular problems that may be related to eNOS [41]. No molecular biology testing has been done on these patients, but it is tempting to speculate that eNOS dysfunction in these twins could be the origin of both their heart and eye problems.

3.1.2 Introducing our sixteen families affected with cBAV

The work for this thesis was performed in collaboration with Dr Kwan-Leung Chan, a cardiologist from The University of Ottawa Heart Institute (Ottawa, ON) who examined and recruited patients for our study. This study involves sixteen unrelated, multiplex Canadian families in which at least two members are affected with congenital BAV. From these families, we have collected a total of 102 DNA samples, which include 39 affected individuals (Figure 3.1). The families are Caucasian.

3.1.3 Evaluation of *NOS3* in our BAV families

We chose to investigate *NOS3*, the orthologous gene encoding the endothelial nitric oxide synthase (eNOS) enzyme, as a potential cause of cBAV in humans. We studied *NOS3* in our 16 families by linkage and sequence analysis. Genetic linkage is studied by genotyping a polymorphic DNA marker and calculating a "logarithm of the odds ratio" (LOD score), which represents the likelihood of a specific DNA locus to be genetically linked to (or to co-segregate with) the disease gene in a given family [149]. A minimum LOD score of 3.0 is generally accepted as significant evidence in favour of linkage, and –2.0 as evidence against linkage [149,150].

Figure 3.1. Sixteen Canadian families affected with congenital BAV. Symbols: square=male, circle=female, black=affected, white=unaffected, question mark=unknown disease status, diagonal line=deceased. Numbers under the symbols indicate individuals for which DNA has been collected. Arrows indicate the patients chosen for DNA sequencing. Families 1 to 10 were previously published in another study (reference [13]).

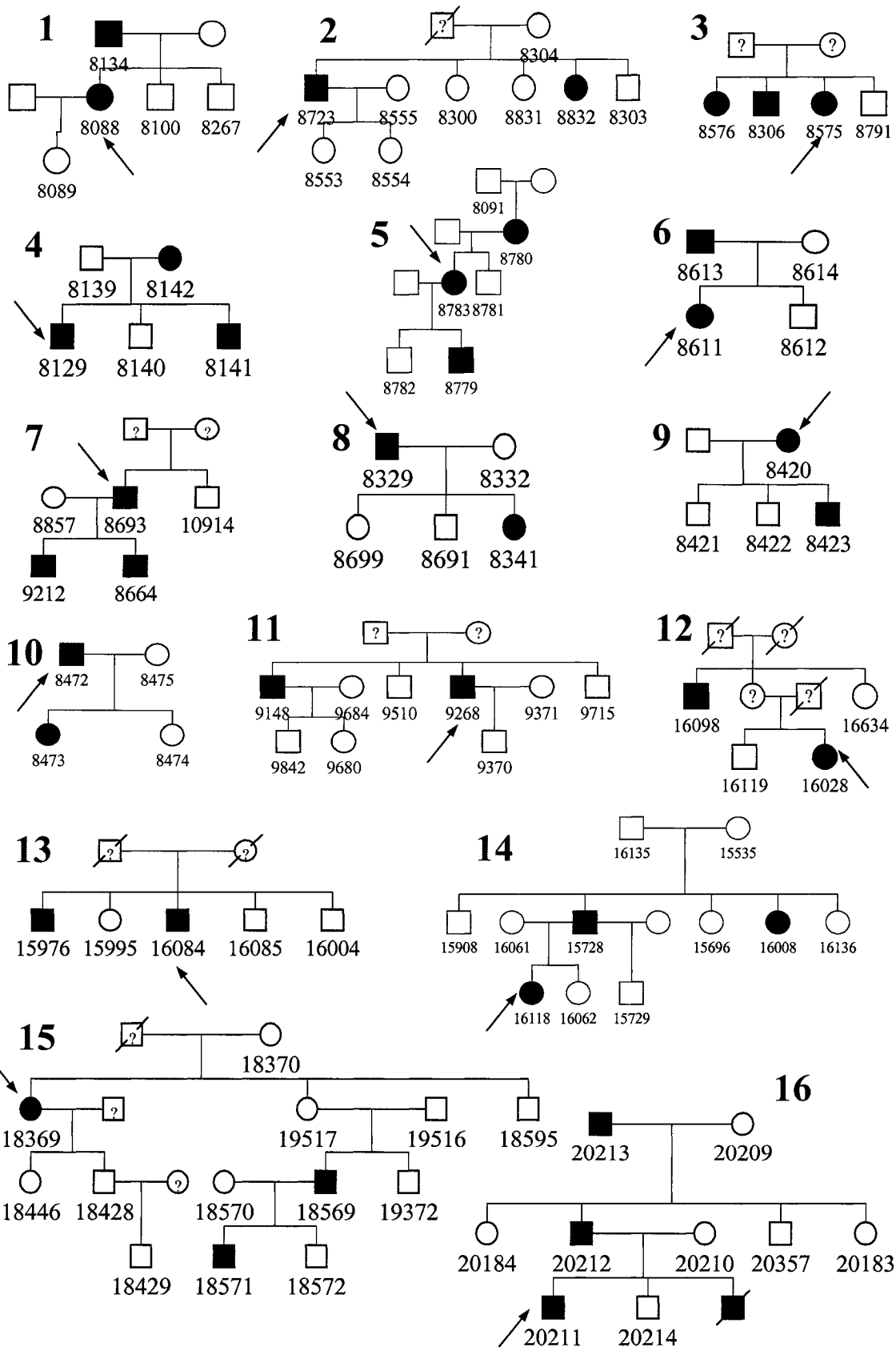
1
8134
8088
8100
8267
8089
2
8304
8723
8555
8300
8831
8832
8303
8553
8554
3
8576
8306
8575
8791
4
8139
8142
8129
8140
8141
5
8091
8780
8783
8781
8782
8779
6
8613
8614
8611
8612
7
8857
8693
10914
9212
8664
8
8329
8332
8699
8691
8341
9
8420
8421
8422
8423
10
8472
8475
8473
8474
11
9148
9684
9510
9268
9371
9715
9842
9680
9370
12
16098
16634
16119
16028
13
15976
15995
16084
16085
16004
14
16135
15535
15908
16061
15728
15696
16008
16136
16118
16062
15729
15
18370
18369
19517
19516
18595
18446
18428
18570
18569
19372
18429
18571
18572
16
20213
20209
20184
20212
20210
20357
20183
20211
20214

3.2 Material and methods

Families and DNA collection

Individuals affected with cBAV and their family members were recruited by our collaborators at The University of Ottawa Heart Institute in Ottawa (ON, Canada), where two-dimensional echocardiography was performed with Sonos 2500, 4500 and 5500 systems (Philips Medical Systems, Andover, MA), in accordance with the recommendations of the American Society of Echocardiography [151]. The distinction between congenital and acquired BAV was made using the criteria described previously [8]. Upon receiving informed consent, blood samples were drawn from participating individuals for DNA extraction. The study was approved by the Research Ethics Board of The Ottawa Hospital.

Genotyping and linkage analysis

Genomic DNA was isolated from whole blood using standard procedures [152]. The D7S636 marker was amplified by polymerase chain reaction (PCR) from genomic DNA. An M13 tail was included in the forward primer sequence (see Appendix II for primers and conditions). M13-IRDye™-labelled DNA fragments were resolved on a 0.4 millimetre thick, 8% acrylamide gel on a Li-Cor® DNA Sequencer model 4000 (Li-Cor, Lincoln, NE). The genotypes were analyzed using the RFLPscan Plus software (version 3.0). Two-point LOD scores were calculated with the MLINK program, and Z_{max} and θ_{max} values were calculated with LODSCORE; both programs are from the FASTLINK linkage software package (version 5.20) [153-156]. Program settings were as follows: the mode of inheritance was autosomal dominant; penetrance was 0.70 or 0.90; the disease

allele frequency was 0.0001; marker allele frequencies were all equal; θ values (for MLINK) were 0.0, 0.01, 0.05, 0.1, 0.2, 0.3 and 0.4. Our exclusion criterion was a LOD score of –2.0 or less at 90% penetrance.

DNA Sequencing

All 26 exons including flanking splice sites and untranslated regions of the *NOS3* gene were amplified by PCR from genomic DNA in one affected individual from each selected family (see arrows in Figure 3.1) and in one unrelated control individual. This control has also been screened by echocardiography to confirm the presence of a normal tricuspid aortic valve. All PCR conditions were optimized for $MgCl_2$ concentration and annealing temperature prior to sequencing. PCR products were treated with ExoSAP-IT (Exonuclease I and shrimp alkaline phosphatase, USB; Cleveland, OH) according to the manufacturer's suggested protocol. Sequencing was performed with Redivue [α-^{33}P] dideoxyNTPs Terminators and the Thermo Sequenase Radiolabeled Terminator Cycle Sequencing kit (Amersham Biosciences; Piscataway, NJ) according to the manufacturer's suggested protocol. Sequencing gels were exposed to X-ray film (Curix Ortho HT-G, Agfa; Toronto, ON) at –80°C for three to ten days, and the sequence was read manually. A list of primers and conditions can be found in Appendix III. All PCRs were performed on a PTC-225 thermal cycler (MJ Research; Waltham, MA). Exons 12, 13 and 16 of the *NOS3* gene could be amplified by PCR, but could not be successfully sequenced under the conditions described above. The PCR products were sent to the Ontario Genomics Innovation Centre (Ottawa, ON) for automated DNA sequencing with an Applied Biosystems 3730 DNA Analyzer and the Big Dye Terminator v3.1 Chemistry. When

looking for alterations in the splice sites, the consensus sequences were as follows: splice donor, (exon)AG — GT(A/G)AGT(intron); splice acceptor, (intron)$(T/C)_nN(C/T)AG$ — G(exon) [157].

Primer design

The PCR primer sequences for amplifying the D7S636 marker were found on the UniSTS web site at NCBI (see Appendix I). All the other PCR and sequencing primers were designed using the Primer3 online software ([158], Appendix I) or the Oligo primer analysis software (version 4.0). All primers were synthesized by Sigma Genosys (Oakville, ON). Lyophilized primers were resuspended in TE (10 mM TRIS, 0.1 mM EDTA, pH 8.3), and diluted to a final 17 μM solution in ddH_20.

Restriction digest of *NOS3* exon 19 with NcoI

To detect the presence of a G/A polymorphism in exon 19 of the *NOS3* gene in family 1, a region of the genomic DNA comprising *NOS3* exons 17-18-19 was first amplified by PCR in DNA samples #8134, 8089, 8088, 8100 and 8267 from family 1 and in the unaffected control. Refer to Appendix IV for PCR conditions. PCR products were then purified with the GFX PCR DNA and Gel Band Purification Kit (Amersham Biosciences; Piscataway, NJ), according to the manufacturer's suggested protocol, with a final elution in 50 μl of ddH_20. Restriction digest of each sample was performed in 20 μl volumes containing 16.5 μl of purified PCR product, 2.0 μl of 10X NEB Buffer #4 and 1.5 μl of the NcoI enzyme (10 000 units/ml, New England Biolabs; Toronto, ON). Samples were incubated at 37 °C for 1.5 hours and then loaded onto a 1.5% agarose gel.

3.3 Results

3.3.1 Exclusion of six families by linkage analysis under an autosomal dominant model

In order to carry out linkage analysis, we first sought a polymorphic DNA marker located near or inside our gene of interest. The *NOS3* gene on chromosome 7 has 26 exons and spans 23,528 bases of genomic DNA (NCBI LocusLink; see Appendix I for electronic database information). Located inside intron 13 resides the highly informative D7S636 dinucleotide repeat polymorphism (heterozygosity index: 0.93). This marker was amplified by PCR in every individual from our sixteen families and the alleles were scored according to the size of the PCR products obtained (data not shown). The genotypes were used to perform two-point linkage analysis between the disorder and the D7S636 marker with the MLINK program to determine if polymorphisms in *NOS3* segregated with cBAV.

It is usually advised not to conduct linkage analysis using equal marker allele frequencies, since they can differ from the frequencies found in the population and thus affect linkage results [149]. We calculated LOD scores (Z) using equal and relative marker allele frequencies. In our 16 families, a total of 15 alleles were found among 204 chromosomes for the D7S636 marker (data not shown). LOD scores were first calculated with equal frequencies for all alleles (1/15), and then with relative frequencies for each allele (for example: the frequency of allele 1 in our families is 10/204, allele 2 is 7/204, etc; data not shown). The LOD scores calculated under both settings were identical in all families (results shown in Table 3.1).

Table 3.1. LOD scores for the *NOS3* gene at the D7S636 intragenic marker locus. The MLINK program was used to calculate two-point LOD scores ($Z(\theta)$) under an autosomal dominant mode of inheritance.

	70% penetrance	90% penetrance		
Family #	$Z(0)$	$Z(0)$	Z_{max}	θ_{max}
1	0.37	0.52	0.52	0.0010
2	-4.55	-6.10	-0.00	0.5010
3	-3.56	-3.96	-0.00	0.5000
4	0.49	0.56	0.56	0.0010
5	-0.03	-0.44	0.09	0.3070
6	-0.34	-0.74	-0.00	0.4990
7	0.03	-0.24	0.01	0.7210
8	0.37	0.52	0.52	0.0010
9	-0.15	-0.48	-0.00	0.5000
10	-0.34	-0.74	-0.00	0.4990
11	0.45	0.30	0.35	0.0710
12	-3.47	-3.78	-0.00	0.5050
13	-3.86	-4.21	-0.00	0.5010
14	-0.52	-1.66	-0.00	0.4980
15	-1.32	-2.34	0.00	0.5180
16	-4.20	-4.95	0.16	0.8590
Total:	-20.62	-27.74		

BAV may have incomplete penetrance in a number of families [13]; therefore we chose to calculate LOD scores at 70% and 90% penetrance to allow for the presence of potential carrier individuals in our pedigrees (Table 3.1). We arbitrarily chose to set the locus exclusion cut-off ($Z = -2.0$) at 90% penetrance.

We calculated LOD scores with the MLINK program at various θ values (data shown for $\theta = 0.0$ only, Table 3.1). The LODSCORE program calculates the peak of the LOD score (Z_{max}) and also returns the θ value at which Z_{max} was attained (θ_{max}). Z_{max} will occur at $\theta_{max} = 0.0$ when there is no recombination between the disease locus and the marker locus (families 1, 4, 8), and at another θ value (except 0.5) when some recombinations are detected (families 5, 7, 11, 16). When $\theta_{max} = 0.5$, Z_{max} always equals zero because it represents a random number of recombinants. This is what would be expected by chance for two unlinked loci and therefore is consistent with the negative LOD scores obtained (families 2, 3, 6, 9, 10, 12, 13, 14, 15).

Results in Table 3.1 show that the highest Z values at $\theta = 0$ (denoted by $Z(0)$) obtained in our families for this locus were 0.49 and 0.56 for family 4 at 70% and 90% penetrance respectively. The next highest were families 1, 8 and 11 with LOD scores of 0.52, 0.52 and 0.30 at 90% penetrance. All the other families yielded LOD scores below zero. Families 2, 3, 12, 13, 15 and 16 had $Z(0)$ values lower than our threshold of –2.0 at 90% penetrance, hence linkage for these six families was excluded at this locus under an autosomal dominant model of inheritance.

3.3.2 Evaluation of the *NOS3* gene by DNA sequencing in ten families

Ten families could not be formally excluded at this locus because they had LOD scores greater than –2.0 at 90% penetrance (families 1, 4, 5, 6, 7, 8, 9, 10, 11, 14). In these families, the *NOS3* gene was evaluated by DNA sequencing of the 26 exons, flanking splice sites, 3'- and 5'-UTRs (untranslated regions) in the proband (Figure 3.1, arrows). Several polymorphisms were detected in the sequence, all of which were present in the NCBI single nucleotide polymorphism (SNP) database (Table 3.2). Intronic polymorphisms did not create or alter splice site sequences. Four exonic polymorphisms were found, two of which are silent and do not create new splice sites. The other two polymorphisms, in exons 7 and 19 of *NOS3*, were non-synonymous and were not present in the unaffected control's DNA sequence. However, we have determined below that these polymorphisms are not implicated in the BAV disorder in our patients.

According to the NCBI SNP database, the mutant T allele of SNP #1799983 in exon 7 has an average frequency of 0.308, which is far more common than the BAV prevalence of 1-2% (and even less for congenital BAV) in the general population. SNP #3918232 in exon 19 was only present in one individual (#8088, from family 1) out of the ten patients that were sequenced, and the mutant A allele has a very low reported frequency of 0.013, similar to that of BAV. To determine whether or not this polymorphism segregated with the affected status in family 1, we screened all members of this family by restriction digest with the NcoI enzyme, which discriminates between the two alleles (Figure 3.2). The results demonstrated that the other affected individual in this family (#8134) did not carry the polymorphism as shown by the uncut DNA band.

Table 3.2. Single nucleotide polymorphisms identified in the *NOS3* gene. DNA sequencing of the coding, flanking splice sites and untranslated regions of *NOS3* was performed in ten BAV patients plus one unaffected control. **Abbreviations:** SNP: single nucleotide polymorphism. a.a.: amino acid. No s.s.: no new splice site was created.

NOS3 exon or intron #	Polymorphism	dbSNP #	Position	Codon change	a.a. or splice site change	Genotypes found in patients	Genotype of unaffected control
Exon 6	T/C	1549758	Asp258	GAT-GAC	Silent	C/C, T/T, C/T	C/C
Exon 7	G/T	1799983	Glu298	GAG-GAT	Glu-Asp	G/G, T/T, T/G	G/G
Intron 11	G/A	1800780	-30 of exon 12	---	No s.s.	G/A, A/A, G/G	G/A
Intron 12	T/G	1800782	-38 of exon 13	---	No s.s.	G/T, G/G	G/T
Exon 16	C/G	2566514	Ala666	GCC-GCG	Silent	C/C, G/G, C/G	C/G
Intron 16	A/C	3730305	+36 of exon 16	---	No s.s.	C/C, A/C	C/C
Intron 18	A/C	753482	+28 of exon 18	---	No s.s.	A/A, A/C	A/A
Exon 19	G/A	3918232	Val827	GTG-ATG	Val-Met	G/G, G/A	G/G
Intron 22	G/A	891512	+15 of exon 22	---	No s.s.	G/G, G/A	G/G
Intron 23	T/G	1065299	+11 of exon 23	---	No s.s.	G/G, T/G	T/T

Figure 3.2. NcoI digest of *NOS3* exon 19 in BAV family 1. NcoI cuts the CCATGG sequence, but not the wild-type CCGTGG sequence. The PCR product comprising *NOS3* exons 17-18-19 is 838 bp long. NcoI cuts in exon 19 between bases #709 and #710 of the PCR product. Fragments to be expected are 709 bp long (bases 1 to 709) and 129 bp long (bases 710 to 838). Patient #8088 (G/A) and the unaffected control (G/G) serve as the cut and uncut controls respectively, since their genotypes have been confirmed by DNA sequencing.

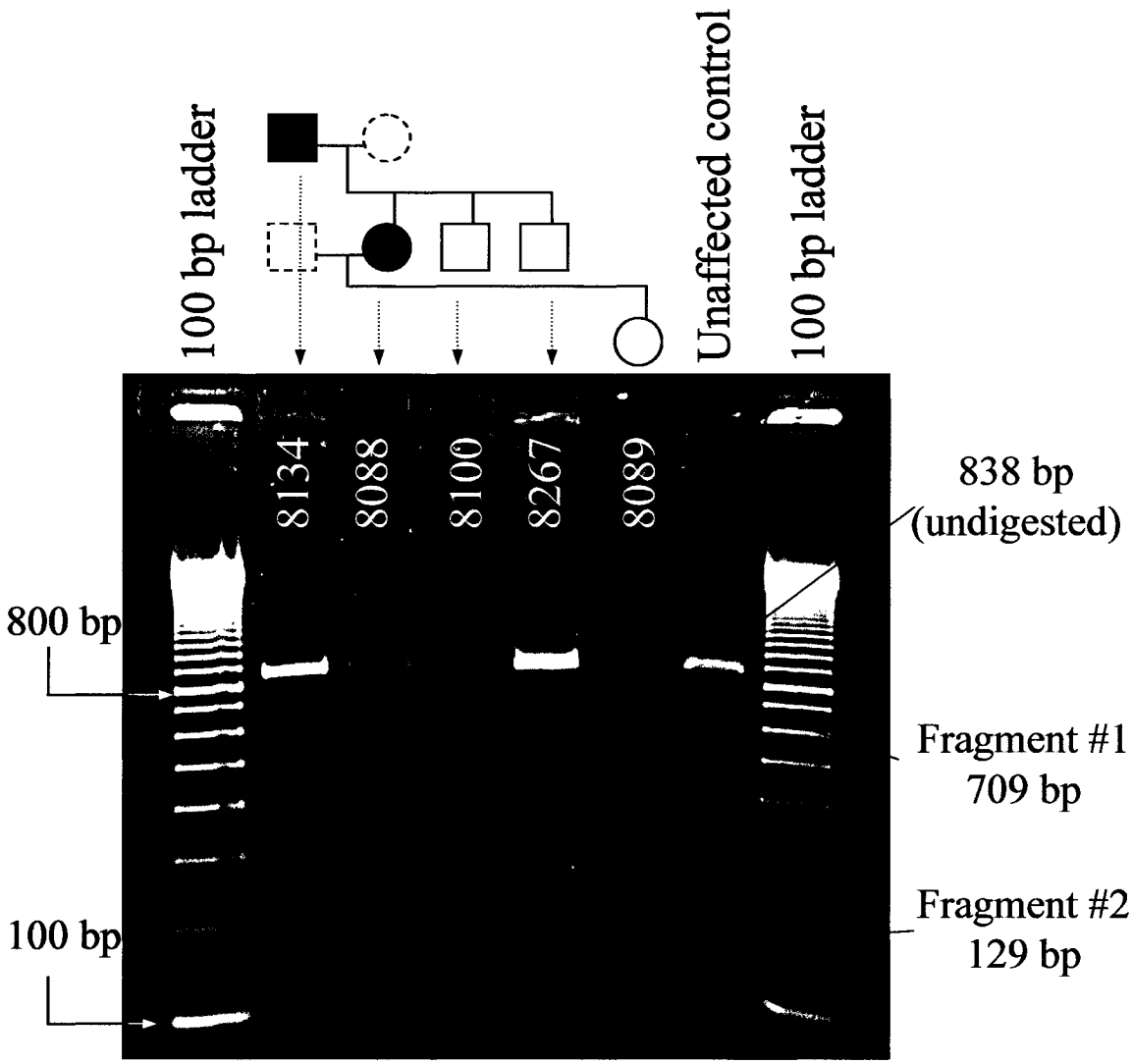
100 bp ladder
Unaffected control
100 bp ladder
8134
8088
8100
8267
8089
838 bp
(undigested)
800 bp
Fragment #1
709 bp
Fragment #2
129 bp
100 bp

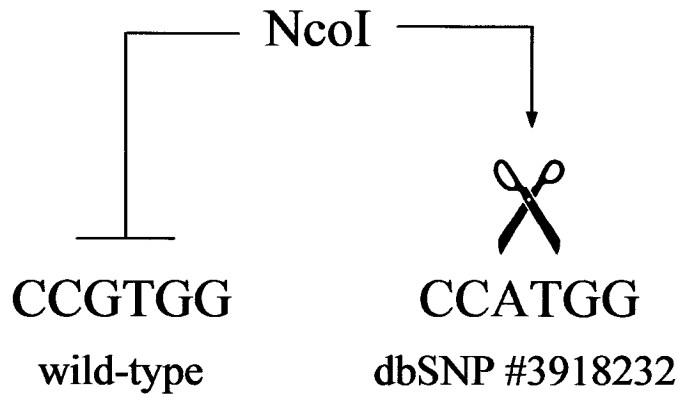
NcoI
CCGTGG
wild-type
CCATGG
dbSNP #3918232

In summary, six families were excluded for linkage at the *NOS3* locus under an autosomal dominant model by linkage analysis with the D7S636 polymorphic marker. In the remaining ten families, we have excluded the presence of mutations in the entire transcribed region and flanking splice sites of *NOS3* as a cause for cBAV.

3.4 Discussion

3.4.1 Interpretation of the linkage results

None of the families reached LOD scores that were significantly high enough to consider the D7S636 locus to be linked to BAV under an autosomal dominant model. Six families were excluded, but the absence of significant LOD scores in the remaining ten families does not preclude the presence of disease-causing mutations in our gene of interest. Several of our pedigrees include individuals from two generations only, which means that the genotypes are phase unknown and therefore less informative. Nevertheless, genetic linkage analysis is not restricted to large families as LOD scores are additive across pedigrees. The combined LOD score of a group of pedigrees represents the likelihood that all those families are linked to the locus [159]. Adding up the LOD scores of several small pedigrees can thus allow linkage detection at a locus that would otherwise be overlooked based on individual LOD scores.

In our sixteen families, the combined LOD score at D7S636 (see "Total" in Table 3.1) was much too low to consider this locus responsible for cBAV. However, if cBAV were a genetically heterogeneous disorder, we would expect only certain families to be linked to a particular locus. In such a case, the combined LOD score might be driven

down by the unlinked families, but until we can show the presence of heterogeneity, we are obligated to keep all the families together when performing linkage analysis.

3.4.2 Interpretation of the sequencing results

Although we did not find any disease-causing mutations in the coding, UTR and splice site sequence of *NOS3* in ten families, it is possible that other mutations in the promoter region or deeper inside introns are present and affect the gene's expression or mRNA splicing. Splice site sequences may also vary from the consensus sequence considered here (section 3.2). However, approximately 89% of mutations underlying disease phenotypes are found in the coding region of genes, compared with approximately 10% and 1% for splice site and regulatory mutations, respectively [160]. Therefore, sequencing the entire transcribed region (coding and UTRs) and flanking splice sites of *NOS3* constitutes a good starting point when searching for disease-causing mutations. To study the presence of regulatory and splicing mutations, it would be interesting to assess *NOS3* mRNA expression and stability in BAV patients as compared with controls, but these experiments would require tissue biopsies from patients and are beyond the scope of this thesis.

3.4.3 Regulation of *NOS3* gene and protein expression

Across species, the amino acid sequence of eNOS is well conserved (~94% identity with mouse, rat, cow and pig) [122], which allows one to think that the protein serves similar functions in humans and mice. The apparent exclusion of *NOS3* reported here in ten families suggests that congenital bicuspid aortic valve in these families results

from mutations in gene(s) other than *NOS3*, or possibly that the regulation of *NOS3* expression is disrupted. In this regard, a number of factors influence *NOS3* gene and protein expression. Endothelial NOS is a constitutive enzyme, but several factors upregulate its expression at the gene and/or protein level, namely shear stress from flowing blood, cell proliferation, growth factors (TGF-β, FGF, VEGF, PDGF) and certain hormones. On the other hand, TNF-α downregulates eNOS expression, and NO itself also acts on eNOS through a negative feedback mechanism in the systemic circulation [122,145]. A disruption in the expression or function of any of these compounds could possibly affect valve development indirectly.

3.4.4 eNOS polymorphisms and their role in susceptibility to ischemic heart disease

Many studies have associated certain eNOS polymorphisms to different forms of ischemic heart or blood vessel disease such as coronary spasm, ruptured intracranial aneurysms, coronary atherosclerosis and giant cell arteritis [161-163]. A recent meta-analysis of 26 studies revealed the importance of two eNOS polymorphisms: the Glu298Asp polymorphism in exon 7 and the "a/b" VNTR (variable number of tandem repeats) in intron 4. Homozygosity for the Asp298 allele or the intron 4 "a" allele is strongly associated with an increased risk of ischemic heart disease [164]. A direct effect of the polymorphisms on the pathology of ischemic heart disease remains to be demonstrated.

The region of *NOS3* containing the intron 4 polymorphism was not sequenced in our patients, but we have identified the Glu298Asp polymorphism in six out of ten BAV

patients (Table 3.2). Two of the six patients are homozygous for aspartic acid (families 4 and 6) and four are heterozygous. The unaffected control is homozygous for glutamic acid. We have excluded this polymorphism as a cause for BAV based on its high frequency in the general population (section 3.3.2), but it is nonetheless interesting to note that it can be associated with ischemic heart disease, especially since ischemic/hypoxic episodes during embryonic development can lead to cardiac malformations such as septation defects, semilunar valve anomalies and artery malformations in animal models [116,165].

Chapter 4: Genetic Screening of the Chromosome 3p Region in 16 BAV Families

4.1 Introduction

The positional cloning approach has been successful in identifying numerous genes responsible for hereditary diseases in the past when functional candidates could not be directly identified [166,167]. The efficiency of this method has increased tremendously today with the availability of highly accurate transcript maps in public databases, which allowed replacing the time-consuming cloning and mapping procedures with rapid *in silico* searches for candidate genes having a role related to the pathophysiology of the disease [167]. This version of the method has been dubbed the "positional candidate" approach [166].

The first step of this approach is to perform genome-wide linkage analysis on affected families with a set of polymorphic DNA markers distributed throughout the genome. These microsatellite DNA sequences are of known chromosomal location and are multiallelic, short tandem repeat polymorphisms (STRPs) [168,169]. The alleles vary in length and their segregation can be compared to that of the disease status in each family, yielding information about the location of a potential disease gene. Each individual is genotyped, and then a LOD score can be calculated for each marker in each family using linkage software [149,150]. Following the identification of linked markers, one should define a critical region that is flanked by recombinant (non-linked) markers. Candidate genes located in this critical interval can next be selected and screened for mutations.

4.1.1 Genome-wide screen in 11 BAV families

A genome-wide genetic screen with autosomal markers was performed on families 1 to 11 by this laboratory prior to the beginning of the present Master's project (Bulman *et al*, unpublished data). Families 12 to 16 were recruited after the completion of the genome screen. A total of 196 markers spaced ~20 centimorgans (cM) apart were genotyped. When the mode of inheritance is not known, "model-free" linkage analysis should be performed to prevent false-positive and false-negative results due to model misspecification [170]. For a genome scan of a complex disorder, LOD scores between 2.2 and 3.5 are considered to be suggestive of linkage and further screening of the region is recommended [171,172]. We have used the MFLINK model-free linkage software, which tests a number of Mendelian disease transmission models varying from recessive to dominant [170,172,173]. The program returns the combined LOD score for a group of pedigrees at the best transmission model and also assumes heterogeneity by maximizing the LOD score over "α", the proportion of families linked (maximized admixture LOD score, MALOD) [173].

MALOD scores of 1.0 or higher were obtained for six markers on different chromosomes (Table 4.1). The highest score was obtained at the D3S1259 marker locus on chromosome 3p25 with a score of ~2.54. This score was obtained under a purely dominant model with the proportion of families linked $\alpha = 0.8$.

Marker	MALOD
D3S1259	2.5442*
D6S1021	1.1805
D8S1106	1.2348
D9S910	1.7280
D14S606	1.1412
D22S420	1.1814

Table 4.1. Partial results of a 20 cM genome screen in BAV families 1 to 11. The combined model-free scores assuming heterogeneity (MALOD) were obtained with the MFLINK program at 70% penetrance.
* p = 0.00145.

We decided to look further into the region surrounding chromosome 3p25 in our 16 BAV families in order to confirm or dispute these results.

4.2 Material and Methods

Genotyping

Genotyping procedures were as described in Chapter 3 (section 3.2). Primer sequences for amplifying DNA markers were found at the NCBI UniSTS web site (Appendix I). An M13 tail sequence was added to the forward primer sequences. Primers were synthesized and diluted as described in Chapter 3 (section 3.2). Refer to Appendix V for primer sequences and PCR conditions.

Linkage analysis

Linkage analysis with MLINK for chromosome 3 was performed as described in Chapter 3 (section 3.2), except that the penetrance values were set to 70%, 90% and 99%. Model-free linkage assuming admixture (MALOD) was performed on our 16 families with the MFLINK software (MFMAP, version 5.1) [170,172,173] using a penetrance of 70% and relative marker allele frequencies. The disease allele frequency was set to 0.01.

P values

MALOD can be viewed as a one-tailed statistical test having two degrees of freedom. The MALOD score can be multiplied by 2ln(10) = 4.6 to obtain an equivalent chi-squared statistic (MFMAP documentation and [170,172]). P values were calculated with the GraphPad QuickCalcs online calculator (Appendix I), which calculates the two-tailed

p value. This value is divided by 2 to obtain the one-tailed p value. Only the p value for marker D3S1259 is shown, but the MALOD scores in Table 4.1 were all statistically significant. $P < 0.05$ was considered to be statistically significant.

4.3 Results

4.3.1 Two-point linkage analysis in the 3p25 region

The highest LOD score from the genome screen performed on BAV families 1 to 11 was obtained with marker D3S1259 on chromosome 3p25. The 3p region surrounding D3S1259 was saturated with 18 additional polymorphic markers that were genotyped in all 16 families (Figure 4.1). The markers are di- or tetranucleotide repeats, and have a heterozygosity range of 0.63 to 0.85 (average: 0.77). They are spaced 3-5 cM apart, with less spacing around D3S1259 (Table 4.2). The genotypes (data not shown) were used to calculate two-point LOD scores for each marker in each family under an autosomal dominant model with the MLINK program. This mode of inheritance was chosen based on the structure of our pedigrees, on reports from the literature and on the MALOD results from the genome screen (section 4.1.1).

We calculated LOD scores with equal and relative marker allele frequencies to assess the effects of this parameter in our families. The LOD scores were essentially identical under both settings (data not shown). The results presented below were obtained with equal marker allele frequencies.

Figure 4.1. Schematic representation of nineteen STRP markers located on chromosome 3p. Genotypes were obtained in our sixteen families for each of those markers. The heterozygosity index of the markers ranges from 0.63 to 0.85. Shown in pink is the D3S1259 marker, which gave the highest admixture LOD score in our genome screen of 11 families. These markers are spaced on average 5 cM away from each other, with a few markers spaced at 1-2 cM around D3S1259. The region of chromosome 3 comprised between the first and last marker shown spans about 56 cM (Marshfield map), which corresponds to approximately 36 megabases of genomic DNA. The region shown represents approximately 40% of the short arm of chromosome 3.

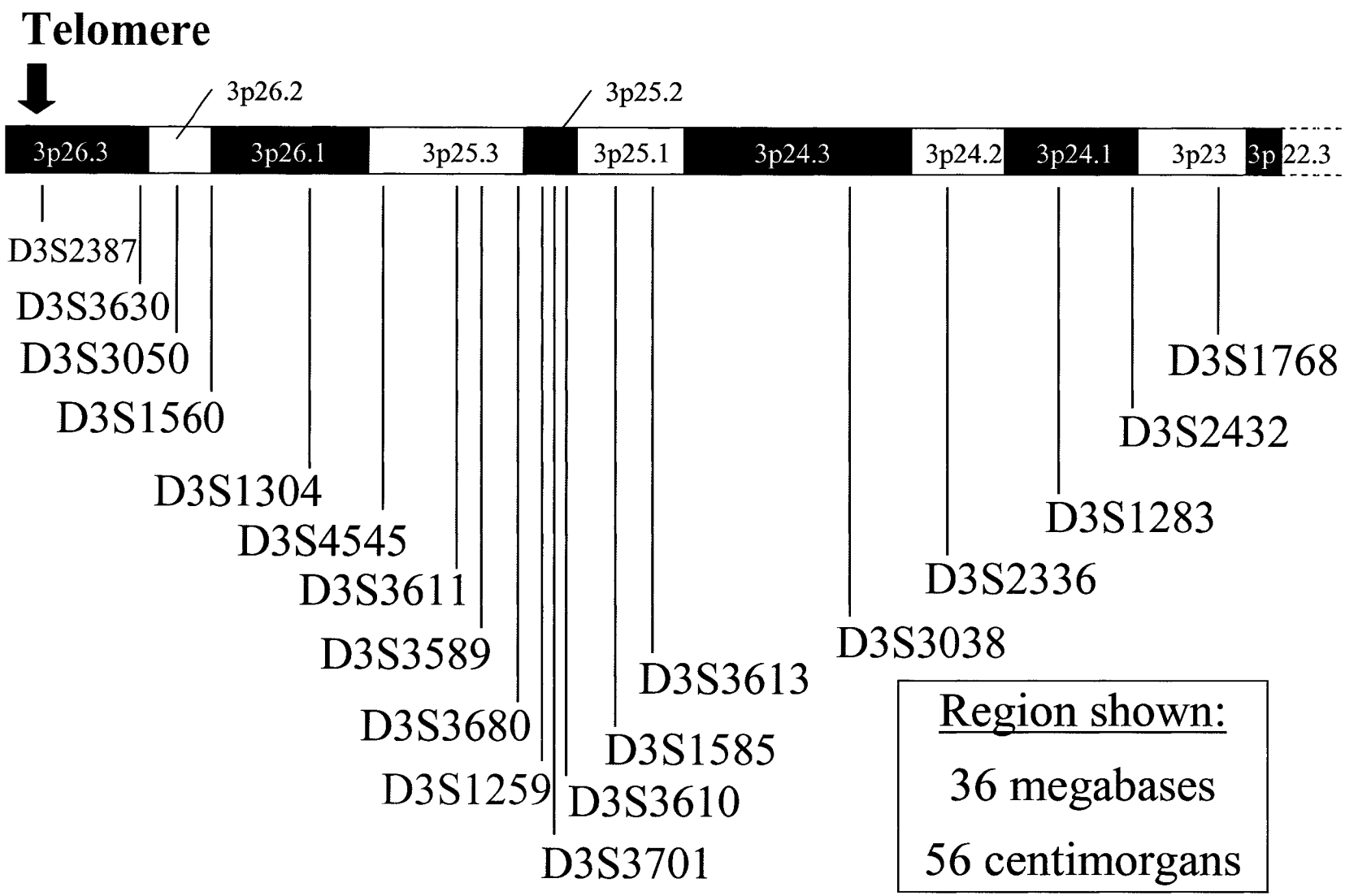
Telomere
3p26.2
3p25.2
3p26.3
3p26.1
3p25.3
3p25.1
3p24.3
3p24.2
3p24.1
3p23
3p 22.3
D3S2387
D3S3630
D3S3050
D3S1560
D3S1304
D3S4545
D3S3611
D3S3589
D3S3680
D3S1259
D3S3701
D3S3610
D3S1585
D3S3613
D3S3038
D3S2336
D3S1283
D3S2432
D3S1768
Region shown:
36 megabases
56 centimorgans

Table 4.2. Location and features of 19 polymorphic microsatellite markers in the 3p region. The heterozygosity index and position in cM are according to the Marshfield sex-averaged map (NCBI Map Viewer). The chromosomal bands and genomic distance in kilobases are according to the UCSC Genome Browser (Human May 2004 Assembly). All data is accurate in date of August 2004. **Abbreviations**: di: dinucleotide repeat. Tetra: tetranucleotide repeat. cM: centimorgan.

Marker	Chromosomal band	Position (cM)	Repeat type	Heterozygosity index	Distance from previous (kilobases)	Distance from previous (cM)
D3S2387	3p26.3	5.54	tetra	0.85	---	---
D3S3630	3p26.3	10.70	di	0.81	1,664	5.16
D3S3050	3p26.2	14.46	tetra	0.76	596	3.76
D3S1560	3p26.1	18.97	di	0.81	3,697	4.51
D3S1304	3p26.1	22.33	di	0.80	2,870	3.36
D3S4545	3p25.3	26.25	tetra	0.82	1,665	3.92
D3S3611	3p25.3	31.13	di	0.82	1,969	4.88
D3S3589	3p25.3	32.36	di	0.72	295	1.23
D3S3680	3p25.3	36.10	di	0.76	876	3.74
D3S1259	3p25.2	36.65	di	0.83	372	0.55
D3S3701	3p25.2	36.65	di	0.68	519	0.00
D3S3610	3p25.2	37.20	di	0.70	388	0.55
D3S1585	3p25.1	38.83	di	0.63	936	1.63
D3S3613	3p25.1	41.56	di	0.85	1,420	2.73
D3S3038	3p24.3	44.81	tetra	0.77	6,587	3.25
D3S2336	3p24.2	49.18	di	0.79	2,975	4.37
D3S1283	3p24.1	52.60	di	0.71	3,802	3.42
D3S2432	3p24.1	57.92	tetra	0.84	3,438	5.32
D3S1768	3p23	61.52	tetra	0.77	2,459	3.60
				Total:	36,528	55.98

We arbitrarily chose to calculate LOD scores at 70%, 90% and 99% penetrance to allow for the presence of potential carrier individuals (data not shown for 90%). Two-point LOD scores at $\theta = 0.0$ are presented in Tables 4.3 and 4.4, and the same results were also plotted against the genomic position of each marker (Figures 4.2, 4.3). For the purpose of clarity, the graphs were split into three panels for each figure. In general, changing the penetrance from 70% to 99% made the positive LOD scores increase and the negative LOD scores decrease even further. This was true for every family except for families 15 and 16, which saw their positive LOD scores decrease when the penetrance was increased. Among all the markers screened, the highest LOD score obtained was 1.78 for family 2 at 99% penetrance, and 1.24 for family 15 at 70% penetrance (Tables 4.3 and 4.4). Only two other families yielded LOD scores above 1.0; they were families 11 and 15 at 99% penetrance with scores of 1.19 and 1.05 respectively.

The LOD score curves were quite different for each family, but most of them could be roughly grouped into categories based on the major pattern of each curve (Figures 4.2 and 4.3). At 70% penetrance, four families (families 2, 4, 13, 15) had positive LOD scores over at least two consecutive markers, as seen by a plateau in the LOD score curve (Figure 4.2). The plateau seemed to disappear for family 15 when the penetrance was changed to 99%, but not for the other three families (Figure 4.3). This plateau covers a distance ranging from at least 2 megabases (family 4) to possibly over 15 megabases (family 2). Notably, the plateau did not always overlap the same marker loci in these four families. At all penetrance values tested, families 3, 5, 7, 12 and 14 appeared unlinked to chromosome 3p with LOD scores below –2.0 at several marker loci, while families 6 and 10 were mostly uninformative with LOD scores of zero or very

Table 4.3. LOD scores at 19 chromosome 3 marker loci, 70% penetrance. Two-point LOD scores ($Z(\theta)$) were calculated under an autosomal dominant mode of inheritance with the MLINK program. Also shown in the "Simul" row are the maximum theoretical LOD scores for each family. **Colour legend:** Blank: $Z \leq 0.00$. **Light blue:** $0.01 \leq Z \leq 0.49$. **Medium blue:** $0.50 \leq Z \leq 0.99$. **Dark blue:** $1.00 \leq Z \leq 1.49$.

Marker	$Z(0)$ (70% penetrance)																
	BAV family #																Total
	1	2	3	4	5	6	7	8	9	10	11	12	13	14	15	16	
D3S2387	0,31	-4,07	-0,17	-0,03	-3,77	0,19	0,05	-0,15	-0,67	0,19		-0,36		0,19	-3,10	-0,52	-10,55
D3S3630	0,13	-3,80	-0,18	-0,03	-0,58	0,00	0,07	0,00	-0,67	0,00	0,03	-0,50	-0,15	0,19	-3,57	-0,03	-9,09
D3S3050	-0,05	-0,64	-0,20	-3,74	0,19	0,00	0,19	-0,15	-0,34	0,00		0,05	0,53	0,19	-4,11	0,04	-7,49
D3S1560	0,12	0,14	0,31	0,00	-3,79	0,00	-0,17	-0,15	-0,67	0,00	0,03	-0,22	-0,10	-0,34	-0,64	0,00	-5,48
D3S1304	0,04	1,12	-3,23	-3,74	-3,96	0,00	0,03	-0,15	-0,67	-0,34	0,39	0,16		-4,55	-3,62	-0,03	-17,98
D3S4545	0,04		-0,14	-3,67	0,19	0,00	-3,79	-0,15	-0,67	-0,34	0,05	-3,09		0,19	0,26	0,00	-9,80
D3S3611	0,19		-3,56	-3,67	-4,06	0,00	-3,60	-0,15	-0,11	0,00	-0,65	-3,10		-4,65	-0,36	0,04	-22,20
D3S3589	0,19		-3,42	-3,67	0,01	0,00	-3,60	-0,09	0,00	0,00	-0,10	0,11	-0,09	-4,49		0,00	-13,46
D3S3680	0,19		-0,23	-3,67	0,19	0,00	-3,59	0,00	-0,67	0,00	-0,76	-0,40	-0,13	-4,39		0,04	-11,83
D3S1259	0,19		-0,17	0,49	-3,70	0,00	-3,58	-0,15	0,19	0,00	-0,30	-0,24	-0,16	-4,13	1,24	0,00	-9,53
D3S3701	0,19	-0,08	-3,56	0,00	0,19	0,00	-3,55	0,00	-0,15	0,00	-0,78	-0,14	-0,14	-4,24	-0,64	0,00	-12,90
D3S3610	0,19		-3,56	0,49	-0,42	0,00	-3,60	-0,15	-0,15	0,00	-0,72	-3,31	-0,14	-0,15	1,06	0,00	-9,69
D3S1585	-0,22	-0,09	-0,13	0,49	-0,12	0,00	-3,56	-0,15	-0,15	0,00	0,19	0,16	-0,15	-4,05	0,23	0,34	-7,21
D3S3613	-0,26		-3,56	0,49	-3,70	0,00	-3,60	-0,15	0,00	0,00	-0,30	-3,28	-0,18	-4,24	1,05	0,00	-16,79
D3S3038	0,04	1,12	-0,16	0,00	0,19	-0,34	-0,23	-0,15	0,00	-0,34	-1,14	-0,03	-0,48	-4,13	1,24	-0,03	-4,44
D3S2336	0,19	1,12	-3,56	-3,74	-0,15	0,00	-0,93	0,00	-0,34	0,00	-0,30	0,16	-4,07	0,04		0,53	-10,52
D3S1283	0,13		-0,20	-3,83	-4,34	0,00	-3,56	0,19	-0,15	0,00	-0,47	-0,43	-4,07	0,37	0,45	0,00	-15,16
D3S2432	0,04	1,12	-0,14	-3,67	-0,15	0,00	-3,59	0,00	0,00	-0,34	-1,15	-0,23	-0,15	0,04	-0,11		-7,77
D3S1768	0,37	1,12	0,12	-3,67	0,33	0,19	0,03	-0,15	-0,15	-0,34	-0,11	0,05	-3,79	-4,31	-0,43	-0,34	-11,08
Simul	0,56	1,12	0,49	0,49	0,68	0,19	0,49	0,37	0,37	0,19	0,94	0,68	0,61	1,24	1,76	1,05	---

Table 4.4. LOD scores at 19 chromosome 3 marker loci, 99% penetrance. Two-point LOD scores ($Z(\theta)$) were calculated under an autosomal dominant mode of inheritance with the MLINK program. Also shown in the "Simul" row are the maximum theoretical LOD scores for each family. **Colour legend:** Blank: $Z \leq 0.00$. **Light blue:** $0.01 \leq Z \leq 0.49$. **Medium blue:** $0.50 \leq Z \leq 0.99$. **Dark blue:** $1.00 \leq Z \leq 1.49$. **Violet:** $Z \geq 1.5$.

Marker	Z(0) (99% penetrance)																
	BAV family #																Total
	1	2	3	4	5	6	7	8	9	10	11	12	13	14	15	16	
D3S2387		-6,80	-0,62	-1,40	-5,11	0,30	-0,37	-1,41	-3,41	0,30	1,19	-1,16		-2,22	-4,21	-4,51	-28,04
D3S3630	0,29	-6,22	-0,57	-1,40	-2,37	0,00	-0,29	0,00	-3,41	0,00	-0,51	-1,29	-0,48	-2,22	-6,21	-1,40	-26,08
D3S3050	-0,33	-2,00	-0,55	-5,22	0,30	0,00	0,30	-1,41	-1,70	0,00		-0,19		-2,22	-9,44	-1,11	-21,99
D3S1560	0,29	0,43	0,42	0,00	-5,39	0,00	-0,39	-1,41	-3,41	0,00	0,00	-0,61	-0,27	-1,70	-3,45	-2,51	-18,00
D3S1304	-1,11	1,78	-3,39	-5,22	-5,95	0,00	0,05	-1,41	-3,41	-1,70		-0,06		-9,91	-6,21	-1,40	-36,37
D3S4545	-1,11	1,19	-0,59	-5,10	0,30	0,00	-4,95	-1,41	-3,41	-1,70	-0,99	-3,05		0,30	-0,81	-2,51	-22,98
D3S3611	0,30	1,48	-4,93	-5,10	-6,38	0,00	-4,19	-1,41	-0,60	0,00	-2,10	-3,05		-10,21	-3,06	-1,11	-39,44
D3S3589	0,30	1,48	-3,68	-5,10	0,02	0,00	-4,19	-0,44	0,00	0,00	-0,20	0,11	-0,24	-9,91	-0,21	-2,51	-24,57
D3S3680	0,30	1,48	-0,49	-5,10	0,30	0,00	-4,13	0,00	-3,41	0,00	-2,21	-0,65	-0,42	-7,69		-1,11	-22,57
D3S1259	0,30	1,19	-0,60		-5,10	0,00	-4,10	-1,41	0,30	0,00	-0,38	-0,28	-0,49	-8,21	0,38	-2,51	-20,31
D3S3701	0,30	-0,21	-4,93	0,00	0,30	0,00	-3,97	0,00	-1,41	0,00	-2,24	-0,07	-0,44	-8,50	-2,28	-2,51	-25,96
D3S3610	0,30	1,19	-4,93		-1,92	0,00	-4,19	-1,41	-1,41	0,00	-2,24	-3,80	-0,44	-1,41	1,05	-2,51	-21,12
D3S1585	-0,58	-0,24	-0,32		-0,27	0,00	-4,02	-1,41	-1,41	0,00	-0,22	0,29	-0,46	-6,81	-2,21	-0,81	-17,87
D3S3613	-0,77	1,48	-4,93		-5,10	0,00	-4,22	-1,41	0,00	0,00	-2,81	-3,94	-2,81	-8,50	0,09	-2,51	-34,83
D3S3038	-1,11	1,78	-0,54	0,00	0,30	-1,70	-0,59	-1,41	0,00	-1,70	-4,00	-0,38	-3,11	-8,21	0,38	-1,40	-21,69
D3S2336	0,30	1,78	-4,93	-5,22	-1,41	0,00	-1,29	0,00	-1,70	0,00	-2,81	0,13	-6,80	-1,11	-1,91	-0,51	-25,48
D3S1283	0,29	1,19	-0,55	-5,39	-7,66	0,00	-4,02	0,30	-1,41	0,00	-2,99	-0,87	-6,80		-0,56	0,00	-27,88
D3S2432	-1,11	1,78	-0,59	-5,10	-1,41	0,00	-4,13	0,00	0,00	-1,70	-4,05	-0,59	-1,41	-1,11	-3,92		-22,45
D3S1768		1,78	-0,19	-5,10		0,30	0,06	-1,41	-1,41	-1,70	-0,21	-0,18	-5,11	-8,41	-1,71	-1,70	-23,86
Simul	0,89	1,78	0,60	0,60	0,89	0,30	0,60	0,59	0,59	0,30	1,48	0,89	0,92	1,78	2,38	1,49	---

Figure 4.2. Two-point LOD scores at 19 microsatellite marker loci on chromosome 3p in 16 BAV families at 70% penetrance. For the purpose of clarity, the graph was split into three panels (each panel uses the same scale). Families with positive LOD scores are shown in the top panel, families with mostly negative LOD scores are shown in the middle panel and families with mostly uninformative LOD scores are shown in the bottom panel. The genetic markers are spaced 1-5 cM apart and are plotted on the X axis according to their genomic position in base pairs (UCSC Genome Browser). Each LOD score is represented on the graph by a datapoint label (see figure legend) and the datapoints are linked together by a line. Two-point LOD scores ($Z(\theta)$) were calculated with the MLINK program under an autosomal dominant model. Mb: Megabases.

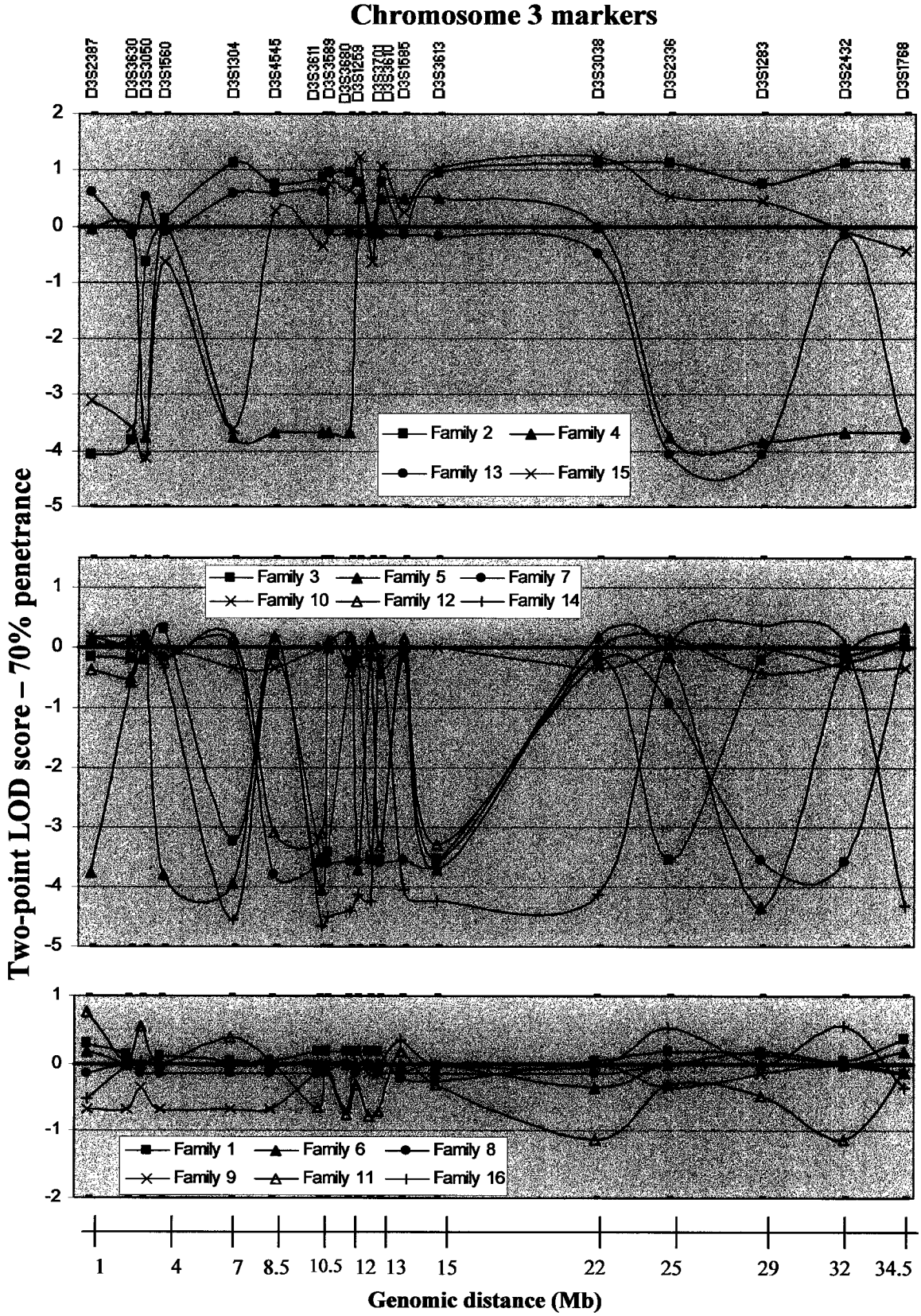
Chromosome 3 markers
D3S2387
D3S3630
D3S3050
D3S1560
D3S1304
D3S4545
D3S3611
D3S3589
D3S3680
D3S1259
D3S3701
D3S3610
D3S1685
D3S3613
D3S3038
D3S2336
D3S1283
D3S2432
D3S1768
Two-point LOD score – 70% penetrance
Family 2
Family 4
Family 13
Family 15
Family 3
Family 5
Family 7
Family 10
Family 12
Family 14
Family 1
Family 6
Family 8
Family 9
Family 11
Family 16
1
4
7
8.5
10.5
12
13
15
22
25
29
32
34.5
Genomic distance (Mb)

Figure 4.3. Two-point LOD scores at 19 microsatellite marker loci on chromosome 3p in 16 BAV families at 99% penetrance. For the purpose of clarity, the graph was split into three panels (each panel uses the same scale). Families with positive LOD scores are shown in the top panel, families with mostly negative LOD scores are shown in the middle panel and families with mostly uninformative LOD scores are shown in the bottom panel. The genetic markers are spaced 1-5 cM apart and are plotted on the X axis according to their genomic position in base pairs (UCSC Genome Browser). Each LOD score is represented on the graph by a datapoint label (see figure legend) and the datapoints are linked together by a line. Two-point LOD scores ($Z(\theta)$) were calculated with the MLINK program under an autosomal dominant model. Mb: Megabases.

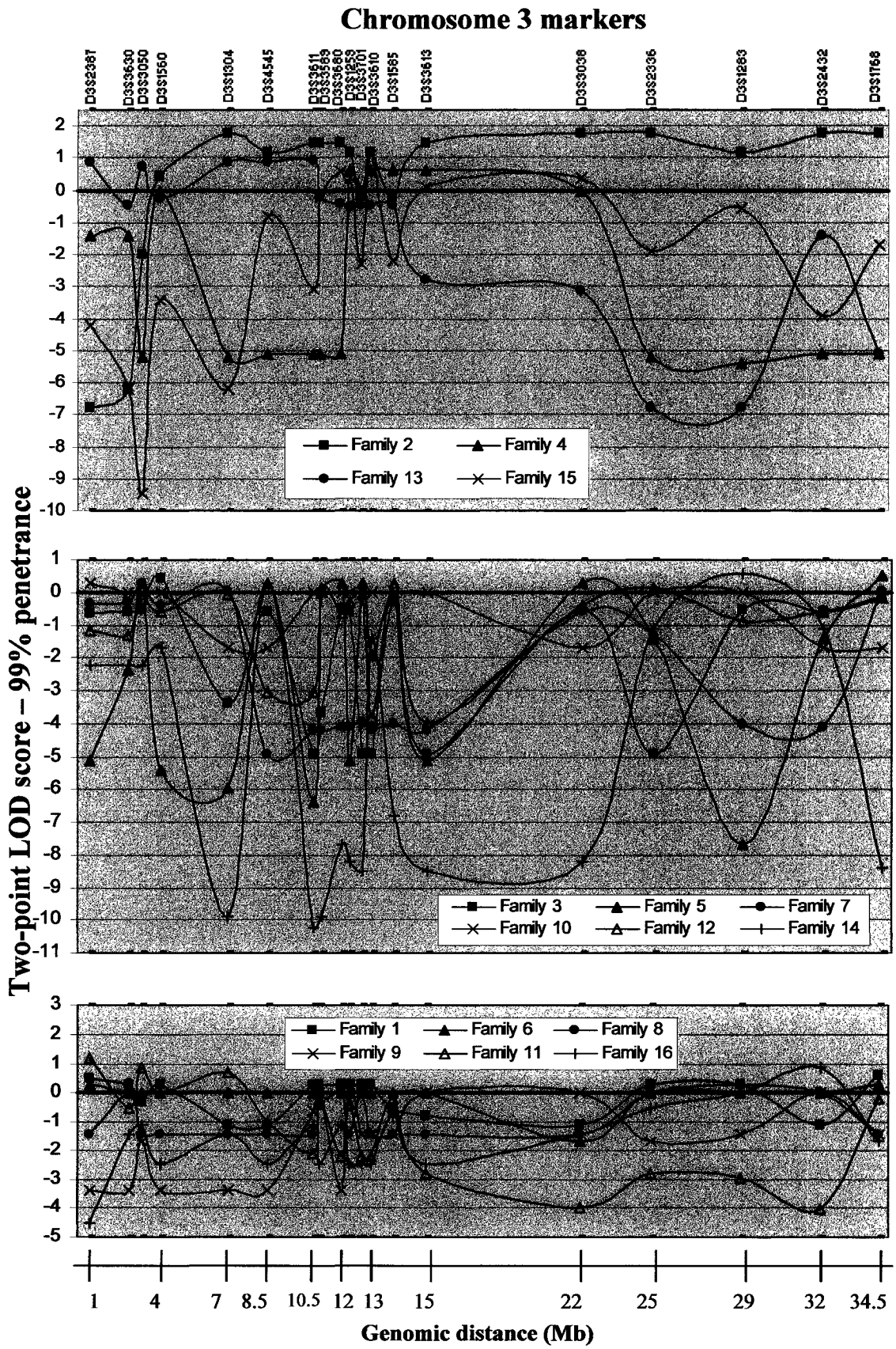
Chromosome 3 markers
D3S2387
D3S3630
D3S3050
D3S1560
D3S1304
D3S4545
D3S3611
D3S3589
D3S3660
D3S1253
D3S1701
D3S3610
D3S1565
D3S3613
D3S3038
D3S2336
D3S1283
D3S2432
D3S1768
Family 2
Family 4
Family 13
Family 15
Family 3
Family 5
Family 7
Family 10
Family 12
Family 14
Family 1
Family 6
Family 8
Family 9
Family 11
Family 16
Two-point LOD score – 99% penetrance
1
4
7
8.5
10.5
12
13
15
22
25
29
32
34.5
Genomic distance (Mb)

close to zero across the entire region. Families 8 and 9 appear unlinked to chromosome 3p although the LOD scores did not always descend below the –2.0 threshold. Families 1, 11 and 16 show a less simple pattern with a mix of positive, negative and uninformative LOD scores at different marker loci. No single family is considered to be formally linked to any marker locus since LOD scores of 3.0 were not attained. In addition, the combined LOD score for all 16 families was below –2.0 at every marker locus (Tables 4.3 and 4.4, "Total").

4.3.2 Calculation of the maximum theoretical LOD scores under an autosomal dominant model

Since our pedigrees are small and some are phase unknown, we suspected that high LOD scores would be hard to obtain in our individual families. To get a general idea of the LOD scores that would be obtained if a marker locus was truly linked to the affected status, we simulated linkage under an autosomal dominant model by manually distributing the genotypes in such a way that only one allele segregates perfectly with the affected status in each family. These maximum theoretical LOD scores are presented in the "Simul" row of Tables 4.3 and 4.4. These scores are quite low in most families with only four families yielding maximum theoretical LOD scores above 1.0 at 99% penetrance (families 2, 11, 14, 16) and one family reaching a LOD score above 2.0 (family 15; Z_{simul} = 2.38). When comparing the Z_{simul} scores with $Z(0)$ obtained at the chromosome 3 marker loci, we notice that some markers gave scores equal to the simulated LOD scores. Indeed, 5 families reached their maximum potential LOD scores

for at least one marker in the region (families 2, 4, 6, 10, 13), and for several consecutive markers in families 2 and 4 (Tables 4.3 and 4.4).

4.3.3 Model-free linkage analysis at the D3S1259 marker locus

Since BAV families 12 to 16 were not originally included in the genome screen, we wanted to determine the effect of adding those families to the genome screen data at the D3S1259 marker locus. We performed model-free linkage analysis with MFLINK to obtain the combined maximized admixture LOD score (MALOD) for families 1 to 16 at the D3S1259 locus. A MALOD score of ~1.94 was obtained under a mainly dominant transmission model (Table 4.5).

Marker	MALOD
D3S1259	1.9453*

Table 4.5. Model-free linkage analysis at the D3S1259 locus in BAV families 1 to 16. The combined model-free score assuming heterogeneity (MALOD) was obtained with the MFLINK program at 70% penetrance.
* p = 0.0057.

This MALOD score is lower than the previous score obtained with families 1 to 11 only (Table 4.1, MALOD = ~2.54). The proportion of families linked (α) also decreased from 0.8 to 0.6. It seems therefore that BAV families 12 to 16 do not support the preliminary evidence of suggestive linkage at this locus.

4.4 Discussion

4.4.1 Interpretation of the two-point linkage results for chromosome 3 markers

The second objective for this project was to look further into the genome screen results for chromosome 3 in order to determine whether the "hit" at marker D3S1259 had been obtained by chance or not. The region was saturated with additional markers and two-point model-based LOD scores were calculated at three different penetrance values. Changing the penetrance did not considerably affect the positive LOD scores in most families except for families 15 and 16, which suggests that unaffected carriers might be present in these two families.

We also calculated the maximum theoretical LOD scores as a guide demonstrating the ability of our families to attain a certain LOD score in the presence of linkage. An important observation that was made is that a LOD score of 3.0 would not be attained in any of our families even in the presence of linkage with fully informative marker genotypes. Hence we saw the importance of relying on combined LOD scores from multiple pedigrees in order to detect linkage in our families. Unfortunately, the combined LOD scores suggested exclusion across the entire 3p region (Tables 4.3 and 4.4, "Total"). With the possibility of genetic heterogeneity for cBAV in mind, we looked at individual linkage data from each family to see the different linkage patterns in the region (Figures 4.2 and 4.3).

Of the 11 families that were part of the original genome screen, only families 2 and 4 yielded positive LOD scores over a small region of consecutive markers in the vicinity of D3S1259 (Figures 4.2 and 4.3). This suggests that, in the other nine families,

the genome screen hit was spurious, i.e. did not represent real linkage for the region. Moreover, families 2 and 4 alone were probably making the largest contribution to the ~2.54 score from the genome screen according to our results in Tables 4.3 and 4.4.

Families 12 to 16 were recruited after the completion of the genome screen. Our analysis with chromosome 3 markers revealed LOD scores close to- or above 1.0 in the 3p region in two families (13 and 15) that were not included in the original genome screen. Families 12, 14 and 16 do not appear linked to chromosome 3p under an autosomal dominant model at 99% penetrance although it is less clear for family 16 at 70% penetrance.

In short, families 3, 5, 7, 12 and 14 can most likely be excluded from the region surrounding 3p25 under an autosomal dominant model. To clarify the involvement of this region in the remaining families, expansion of the families or recruitment of additional families would be required.

4.4.2 Interpretation of the model-free linkage analysis in 16 families

The fact that the MALOD score at D3S1259 decreased when adding the newest BAV families (families 12 to 16) to the data set indicates that these new families augmented the level of heterogeneity at that locus, and this was confirmed by the decrease of the α value of from 0.8 to 0.6. The addition of these new families reduced the confidence of finding linkage in this region of chromosome 3p. Nonetheless, it appears that the hit at D3S1259 was not a false-positive, since we have in fact found two families from the original genome screen (families 2 and 4) that show a potentially linked region over a minimum distance of 2 megabases. Since our results favour admixture in our BAV

families, an important future challenge will be to clearly separate the families based on locus or etiologic heterogeneity when performing linkage analysis. This will only become possible once a defective gene is identified as the cause of cBAV in certain families and not in others, or once it can be shown that subgroups of phenotypic variants have a different etiology.

In conclusion, our results do not clearly confirm or infirm linkage in the 3p25 area in our BAV families, but rather suggest that if linkage is truly present, it is restricted to a small number of families, most likely including families 2 and 4.

Chapter 5: Identification and Mutation Screening of Functional Candidates on Chromosome 3p25

5.1 Introduction

The genome screen results at marker D3S1259 prompted us to search the NCBI database for candidate genes in the 3p25 region. Since this work was done concomitantly to the chromosome 3 marker genotyping, we arbitrarily chose a large search region corresponding to the entire 3p25 chromosomal band, which encompasses marker D3S1259 (3p25.2). The region spans ~16 cM, corresponding to 8.2 megabase pairs of physical map, and extends a little beyond the D3S4545 and D3S3613 markers (Figure 4.1) (UCSC genome browser, NCBI Map Viewer). 109 known genes (confirmed and predicted genes) are located in the 3p25 band (NCBI Map Viewer), 48 of which are known to be expressed in heart tissue (UniGene at NCBI). Our search prioritized genes encoding proteins with high expression in embryonic cardiac tissue that were known or thought to contribute to the development or remodelling of the truncal endocardial cushions. Two genes fulfilled these criteria: *FBLN2* (3p25.1) and *TIMP4* (3p25.2). *FBLN2* is flanked by the D3S3610 and D3S1585 markers, and *TIMP4* is flanked by the D3S1259 and D3S3701 markers (Figure 5.1) (UCSC Genome Browser). These genes were deemed excellent functional candidates because of their strong expression in heart tissue and their role in the extracellular matrix, which is important during valve development (Chapter 1, section 1.8.1). We have screened those genes for mutations by DNA sequencing in our 16 families.

Figure 5.1. Genomic organization of two candidate genes for cBAV located on chromosome 3p. The *TIMP4* and *FBLN2* genes are located inside the 3p25.2 and 3p25.1 chromosomal bands respectively. Both genes encode extracellular matrix proteins and are expressed in embryonic heart tissue. The enlarged view depicts the intron/exon structure of the genes. Elevated boxes or small vertical lines represent exons (including untranslated regions), and horizontal lines in between exons represent introns. Drawing not to scale.

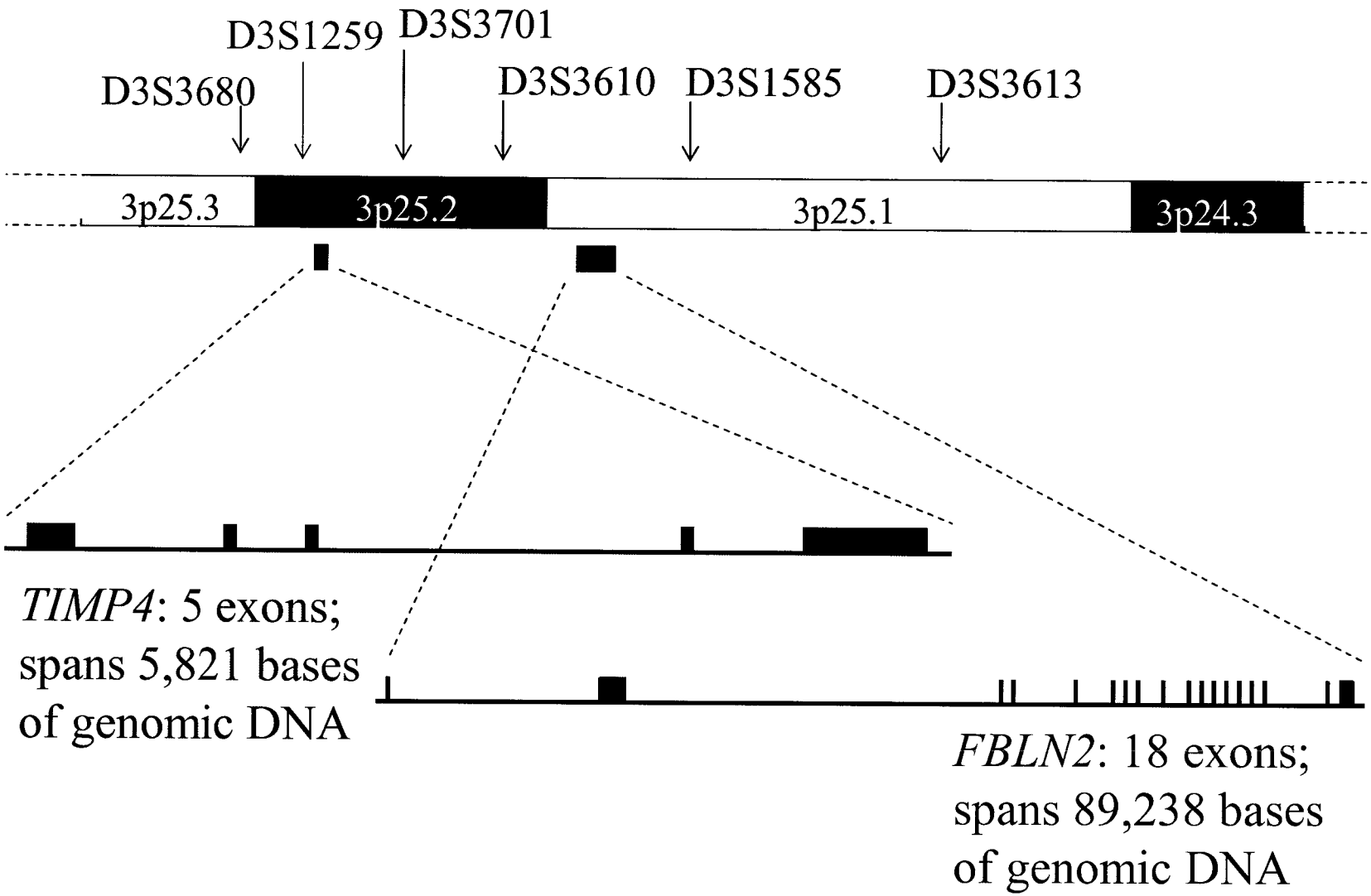
D3S1259
D3S3701
D3S3680
D3S3610
D3S1585
D3S3613
3p25.3
3p25.2
3p25.1
3p24.3
TIMP4: 5 exons;
spans 5,821 bases
of genomic DNA
FBLN2: 18 exons;
spans 89,238 bases
of genomic DNA

5.1.1 The *FBLN2* candidate gene

The *FBLN2* gene encodes fibulin-2, a multi-domain extracellular matrix (ECM) protein expressed abundantly in human heart, placenta and ovary, with lower expression in a variety of other tissues [174]. The mouse ortholog is highly conserved and is expressed in the endocardial cushions during heart development, and more specifically in the truncal cushions, the aorticopulmonary septum, and the aortic wall and valve [174,175]. Fibulin-2 is considered to be a very specific marker of the developing cardiac cushions [175]. Notably, fibulin-2 remains expressed in the adult valve tissue [175].

Human *FBLN2* encodes an 1184 amino acid (a.a.) precursor protein with a 27 a.a. signal peptide [174]. The amino acid sequence of fibulin-2 is cysteine-rich and contains N-linked oligosaccharide acceptor sites. The protein also has anaphylatoxin-related motifs and several epidermal growth factor (EGF)-like repeats, most of which possess a consensus sequence for calcium binding [174,176]. Of particular interest, exon 9 of the human gene is alternatively spliced in certain tissues; the longer isoform (comprising exon 9) is abundantly expressed in heart, with lower expression in skeletal muscle and pancreas (mRNA: AY130459) [177]. The corresponding domain in the mouse protein, which represents one of the calcium-binding EGF-like motifs, also shows alternative splicing [176]. The restricted expression of this fibulin-2 isoform suggests a tissue-specific function for the longer protein.

Fibulin-1 (*FBLN1*, chr. 22) is another protein of the fibulin family that is also expressed in the developing heart. The fibulin-1 and -2 proteins have a similar domain organization, although fibulin-1 is much shorter and has fewer domains [176]. Both fibulins are expressed in the cardiac jelly in areas of epithelial-to-mesenchymal

transformation, except that fibulin-1 is also expressed in the myocardium at certain stages of heart development [175,178]. Moreover, fibulin-1 and -2 are found in adult valve tissue, although fibulin-2 has a stronger expression and is also found in the walls of the coronary arteries [175,179].

The fibulins are thought to have a structural role in the maintenance of the tensile strength in the valves and septum, which have to resist mechanical forces from the beating heart and blood flow [175]. They interact and bind with a number of ECM proteins, which contributes to creating a highly ordered matrix that will facilitate cell migration and cushion remodelling during valve development [89]. In the ECM, fibulins bind to versican, which in turn is associated with hyaluronic acid [89]. Fibulin-2 also binds with fibrillin-1 and elastin [179]. Notably, *in vitro* studies revealed little to no interaction between fibulin-1 and -2. On the other hand, mouse and human fibulin-2 bind strongly with fibronectin in a calcium-dependent manner [180]. Weaker interactions were also detected with perlecan and collagen IV.

Another study also found fibulin-2 to be expressed in the aortic arch vessel walls and coronary arteries, both during development and adult life [179]. Fibulin-2 in these regions is synthesized from smooth muscle precursor cells, neural crest- and epicardium-derived cells, and not from endocardially-derived cells of the cardiac cushions. Fibulin-2 is thought to have an anchoring role to support aortic wall assembly during development [179].

In summary, *FBLN2* is a good candidate gene for cBAV because it is expressed in the truncal cushions and aortic wall during and after the development of the aortic valve, and is directly implicated in maintenance of the cardiac jelly and development of the

aorta. These functions may potentially be accomplished by the heart-specific isoform of fibulin-2.

5.1.2 The *TIMP4* candidate gene

TIMP4 encodes the TIMP-4 enzyme, the tissue inhibitor of metalloproteinase 4 [181-183]. TIMP-4 is expressed abundantly in human heart, and is a member of the TIMP family. The TIMP proteins are natural, endogenous inhibitors of the matrix metalloproteinases (MMPs). MMPs are a family of proteases that degrade ECM proteins. There are at least 23 known human MMPs with different substrate specificity (NCBI LocusLink) [102]. MMPs mediate ECM remodelling as well as disruption of cell-cell and cell-ECM interactions, all of which are important in numerous physiological processes such as organ development, pregnancy, wound healing, angiogenesis and apoptosis [102,103]. Matrix metalloproteinases are also activated in pathological processes such as arthritis, cancer, cardiovascular disease and ulcers [103,184,185]. The proteolytic activity of MMPs also serves functions other than ECM turnover; for example, the cleavage of a specific domain in a substrate protein can expose binding sites for ligands or release an active peptide [102,103]. Of particular interest is the role of MMPs in cardiac cushion remodelling and blood vessel wall integrity. ECM degradation by MMPs in the cardiac cushions facilitates cell migration and tissue remodelling [88], while deficient MMP activity is associated with aortic dilatation [186]. To achieve their inhibitory activity, TIMP proteins physically bind to MMPs and block their active site [103]. In short, MMPs and TIMPs together maintain ECM homeostasis in various tissues, including the developing heart and aorta.

Currently, four *TIMP* genes are known (*TIMP1* to *4*), and they are each located on a different chromosome. *TIMP4* encodes a 224 a.a. precursor protein, and like fibulin-2, has a 29 a.a. signal peptide sequence and conserved cysteine residues. Notably, the VIRAK amino acid sequence near the N-terminal end is a hallmark of the TIMP family of proteins [181]. TIMP-4 is distinguished from the other TIMPs by its very limited tissue distribution. TIMP-1 to -3 are widely expressed, whereas TIMP-4 mRNA is found in cardiac muscle cells of the embryonic and adult mouse, as well as in ovary and brain [183]. In contrast, human TIMP-4 mRNA was not found in brain, but was strongly expressed in heart tissue, and to a much lesser extent in kidney, pancreas, colon and testes [181]. The expression of TIMP-4 in the myocardium and not in the cardiac jelly does not make it a less significant candidate for BAV, as the integrity of the myocardium is essential for correct epithelial-to-mesenchymal transformation and cushion remodelling.

The proposed function for TIMP-4 is tissue remodelling in the heart [181,183]. Interestingly, it appears that tissue remodelling in the murine heart is not restricted to the embryonic period, as TIMP-4 expression is strongest soon after birth [187]. In addition, *TIMP4* has a TATA-less promoter with potential GATA and Ets binding elements. The activity of these transcription factors is associated with tissue-specific expression of genes, and they are upregulated in heart tissue at the correct time to influence *TIMP4* expression [187]. The biological function of the TIMPs is not restricted to inhibition of the MMPs; they also have effects on cell growth [103]. Notably, *in vitro* experiments on transformed cardiac fibroblasts revealed that TIMP-4 could inhibit cell invasion and migration and induce apoptosis [185].

TIMP-4 is also found to be active in the context of cardiovascular disease. Namely, TIMP-4 is overexpressed in the endothelium after induced injury to large vessels in rats, and controls smooth muscle cell migration and collagen accumulation in the injured arterial wall [188]. In contrast, downregulation of the expression of TIMP-4 and other TIMP proteins is found in the heart of patients with ischemic heart disease [185,189]. Also, certain MMPs and TIMPs are active in the context of degenerative valvular disease [190]. A disruption of the MMP/TIMP activity in general is also widely recognized in aortic aneurysm disease. Aneurysmal tissue is found to express a multitude of proteases as compared with normal aortic tissue [186]. Currently, aortic expansion in aneurysm disease is thought to be caused by excessive extracellular matrix breakdown by MMPs derived from inflammatory cells [186,191]. A genetic disorder involving MMP or TIMP genes could potentially mimic this pathological process in familial cases of aortic aneurysms and dissections.

Interestingly, an altered extracellular matrix is emerging as being part of the pathology of BAV. It appears that the structural weakness of the aortic wall could be explained by a disruption of the ECM in BAV patients [42,49,55,56,59,63]. Particularly, in BAV patients with thoracic aortic aneurysm, vascular smooth muscle cells had a reduced extracellular distribution of the ECM proteins fibrillin, fibronectin, and tenascin [63]. A disruption in the expression or function of TIMP-4 would result in increased MMP activity in the ECM, and thus could quite conceivably be responsible for the loss of matrix components in the aortic wall. Similarly, a disturbance in the balance of the TIMP/MMP activity in the ECM during development could result in abnormal remodelling of the cardiac cushions and cause cBAV.

In summary, *TIMP4* is a good candidate gene for cBAV because of its strong expression in heart tissue and its role in the regulation of extracellular matrix remodelling and cell death, two processes known to be essential for the correct development of the aortic arch and valve.

5.2 Material and methods

DNA sequencing of *FBLN2* and *TIMP4*

The sequencing procedures were as described in Chapter 3 (section 3.2). The *FBLN2* and *TIMP4* genes contain 18 and 5 exons, respectively. One individual from each of the 16 families (Figure 3.1, arrows) plus one unaffected, unrelated control were sequenced. The 3'UTR of both *FBLN2* and *TIMP4* was amplified by PCR and sent to the Ontario Genomics Innovation Centre (Ottawa, ON) for sequencing. PCR and sequencing primers were designed and diluted as described in Chapter 3 (section 3.2). Refer to Appendix VI for primers and conditions.

5.3 Results

5.3.1 DNA sequencing of *FBLN2*

We have screened the *FBLN2* gene for mutations by DNA sequencing of the proband in our 16 BAV families (Figure 3.1, arrows). Patients from families apparently unlinked to 3p (Chapter 4) serve as controls. All 18 exons of *FBLN2* (corresponding to the longest isoform), flanking splice sites and untranslated regions (UTRs) were sequenced. Several polymorphisms were detected in the sequence, some of which were unreported in the NCBI SNP database (Table 5.1). All the intronic polymorphisms did

Table 5.1. Single nucleotide polymorphisms identified in the *FBLN2* gene. DNA sequencing of the coding, flanking splice sites and untranslated regions of *FBLN2* was performed in sixteen BAV patients plus one unaffected control. Exons/introns and amino acids are numbered according to the longest isoform of fibulin-2, which has 1184 amino acids and 18 exons in the mRNA (GenBank: AY130459). In the "Position" column, "+" indicates "upstream of exon…" and "—" indicates "downstream of exon…" by the number of bases indicated. *This polymorphism is in fact a mistake in the genomic contig sequence. See text for details. **Abbreviations:** No s.s.: no new splice site sequence was created. NR: not reported in NCBI dbSNP as of May 31st 2004. SNP: single nucleotide polymorphism. a.a.: amino acid. STRP: short tandem repeat polymorphism. Polym: polymorphism.

FBLN2 exon or intron #	Polym.	dbSNP #	Position	Codon change	AA or splice site change	Genotypes found in patients	Genotype of unaffected control
Exon 2 (5'UTR)	T/C	37326	-6 of start codon	---	No s.s.	T/C, T/T	T/T
Exon 2	(mistake)* A/G	11365766 3732666	Ala313 Ser361	CC-C AGC-GGC	(mistake)* Ser-Gly	C A/A, G/G, G/A	C G/A
Intron 4	A/C	2276746	-63 of exon 5	---	No s.s.	C/C, A/C	C/C
Intron 5	C/T	3773270	+18 of exon 5	---	No s.s.	C/C, C/T	C/T
Exon 6	G/A	NR	Pro601	CCG-CCA	Silent	G/G, G/A	G/G
Intron 8	A/C	NR	-42 of exon 9	---	No s.s.	C/C	A/C
Exon 12	G/A G/A G/A	2242023 NR 9843344	Thr882 Ala891 Thr901	ACA-ACG GCG-GCA ACC-GCC	Silent Silent Thr-Ala	G/A, G/G, A/A G/A, G/G G/A, G/G, A,A	A/A G/A A/A
Exon 13	T/C	4684968	Phe942	TTT-TTC	Silent	T/C, C/C, T/T	T/T
Intron 13	T/G T/C	4684969 NR	+45 of exon 13 -47 of exon 14	--- ---	No s.s. No s.s.	T/G, G/G, T/T C/C, T/C	T/T C/C
Exon 18	G/A C/T	1061375 1061376	Thr1160 Asp1204	ACG-ACA GAC-GAT	Silent Silent	G/G, G/A C/C, T/C	G/G C/C
Exon 18 (3'UTR)	T/A C/A C/A T/C A/T STRP	1061390 1061398 12968 7820 7596 NR	+268 after stop +275 after stop +288 after stop +409 after stop +435 after stop +442,443 after stop	--- --- --- --- --- ---	No s.s. No s.s. No s.s. No s.s. No s.s. No s.s.	T/T, T/A C/C, C/A C/C, C/A T/C, T/T, C/C A/A, A/T, T/T AA/AA, AA/--, --/--, AA/A-	T/T C/C C/C T/C A/T AA/--

not create or alter splice site sequences. We found a mistake in the reported sequence of exon 2 at the alanine 313 position. According to the NT_022517 genomic contig sequence, two cytosines should be present at this position whereas we only found one C in all of the individuals that were sequenced (Table 5.1). This variation was given the dbSNP #11365766. If this C were really present, it would be spliced out during mRNA maturation based on its absence from every reported mRNA sequence (NCBI mRNA accession numbers: BC051690, NM_001998, AY130456, AH011811, AY130459). In fact, we believe that this extra nucleotide represents a mistake in the sequence; it appears rather unusual, if not impossible, for the splicing machinery to splice out only one base from the sequence. We have therefore confirmed a mistake in the genomic contig sequence (NT_022517) that was also previously pointed out by others (see for example BC051690); the correct sequence has only one cytosine at this position.

We found eight exonic polymorphisms in the coding sequence, six of which are silent (Table 5.1). The silent G/A SNP at threonine 1160 in exon 18 is not carried by the unaffected control and creates a new splice acceptor site by changing the CCTTCACGGG sequence into the consensus CCTTCACAGG acceptor sequence [157]. However, the population frequency of the A allele is approximately 0.15 (NCBI dbSNP), which is ~10 times more frequent than the BAV prevalence and thus makes it unlikely to be a disease-causing mutation.

Two other exonic polymorphisms were non-synonymous. The G/A transition in exon 2 (dbSNP #3732666) was found in nine patients and creates a serine-to-glycine change, but this SNP was also found in one allele of the unaffected control's DNA sequence, and the reported frequencies for the G/A alleles are approximately 0.6/0.4 in

the population (NCBI dbSNP). Another A/G transition in exon 12 (dbSNP #9843344) was identified in BAV patients, but not in the unaffected control's DNA sequence. This SNP changes threonine 901 for an alanine, and the allele frequencies are not available. However, the G/G genotype was found in nine patients, G/A in six patients, and A/A in one patient plus in the control's DNA sequence. The presence of many homozygote G individuals indicates that the G allele is very frequent, which makes it unlikely to be a disease-causing mutation.

We found what appears to be a 1-2 bp STRP (short tandem repeat polymorphism) at the end of the 3'UTR of *FBLN2* (Table 5.1). This sequence variation is not reported in dbSNP. Some individuals had two adenosines (AA) positioned 442 and 443 bases downstream of the stop codon, whereas others had only one A (indicated by A-), or none (--). The unaffected control was heterozygous AA/--, and this sequence variation does not create a new splice site. The genomic contig sequence indicates AA at this position, but according to our results, the AA and -- alleles are approximately equally frequent. Therefore it appears that this variation in the number of adenosines at this position should probably be regarded as a STRP instead of an insertion/deletion polymorphism, especially because of the occurrence of the A- allele.

5.3.2 DNA sequencing of *TIMP4*

We have screened the *TIMP4* gene for mutations by DNA sequencing of the 5 exons, flanking splice sites and UTRs in the proband of our sixteen families (Figure 3.1, arrows). Only one polymorphism was detected in all the sequence obtained from our reactions, and it is located in the 3'UTR of exon 5 (Table 5.2). This G/A transition is not

Table 5.2. Single nucleotide polymorphism identified in the *TIMP4* gene. DNA sequencing of the coding, flanking splice sites and untranslated regions of *TIMP4* was performed in sixteen BAV patients plus one unaffected control. In the "Position" column, "+386 after stop" indicates that the SNP is located 386 bases downstream of the stop codon. **Abbreviations:** SNP: single nucleotide polymorphism. Polym: polymorphism. NR: not reported in NCBI dbSNP as of May 31st 2004.

TIMP4 exon #	Polym.	dbSNP #	Position	Codon change	New splice site created?	Genotypes found in patients	Genotype of unaffected control
Exon 5 (3'UTR)	G/A	NR	+386 after stop	---	No.	G/G, G/A	G/A

reported in NCBI's dbSNP, but it does not create a new splice site and the unaffected control is heterozygous for this SNP.

In summary, no potential disease-causing mutations were found in the *FBLN2* and *TIMP4* DNA sequence in our sixteen BAV patients.

5.4 Discussion

We have excluded the presence of mutations in the entire transcribed sequence and flanking splice sites of *FBLN2* and *TIMP4* as a cause for cBAV in sixteen families. As discussed earlier for *NOS3* (section 3.4.2), the possibility of intronic and regulatory mutations remains, but this possibility was not studied here. To date, no mutations in the *FBLN2* and *TIMP4* genes are known to cause any disease, however their expression is altered in a number of pathological processes (sections 5.1.1 and 5.1.2).

Other genes in the 3p region could also be considered acceptable candidate genes for BAV. The *CRELD1* gene (Cysteine-Rich with EGF-Like Domains 1, 3p25.3) is ubiquitously expressed with stronger expression in certain developing tissues including the heart [192]. This gene encodes a putative cell adhesion protein and is deleted in patients with the 3p- syndrome (section 1.7.3) [192]. *CRELD1* is thought to be an atrioventricular septal defect (AVSD)-susceptibility gene since missense mutations have been associated with a low proportion of sporadic AVSD patients [193]. However, the development of the aortic valve is not affected in 3p- or in AVSD patients despite the deletion or mutation of *CRELD1*, which raises doubts about the involvement of this gene in the pathogenesis of BAV.

The *RARB* gene (retinoic acid receptor-beta, 3p24) is a reasonable candidate expressed in heart (unclear for fetal heart), although it is also expressed in a wide variety of other tissues (AceView). Proteins from the RAR family are known to be involved in embryonic morphogenesis (NCBI LocusLink). Particularly, retinoid X receptor α (RXR-α)-null mice have endocardial cushion defects (*RXRA*: human chr. 9) [88]. Mapping slightly outside of the area that we have studied, the *TGFBR2* gene (transforming growth factor receptor-2, 3p22) is known to have a direct role in valve development (section 1.8.1). However, it contributes to the development of all four heart valves (not just the semilunar valves) [88], and mutations in this gene are known to cause colon cancer (OMIM). Further downstream of the 3p arm reside the *HYAL1*, *-2*, and *-3* genes (3p21.3), which are hyaluronoglucosaminidases, hyaluronic acid-degrading enzymes. Hyaluronic acid is the major component of the cardiac jelly (section 1.8.1), although it is not clear whether these genes are expressed in the developing fetal heart (AceView).

Although we could not clearly confirm linkage to the 3p25 region with our genetic marker analysis (Chapter 4), it is still possible that a defective gene causing cBAV is located in this area. We have excluded the involvement of the transcribed sequence and flanking splice sites in the best two candidate genes, although regulatory mutations could still be present. On the other hand, other genes in this region may have yet unidentified functions in semilunar valve development. This is quite conceivable considering the vast amount of knowledge left to be discovered in the field of cardiac development. Additionally, one of the predicted genes in the region may in the future be confirmed as a bona fide gene with a role in valve development.

In conclusion, the sequencing of *FBLN2* and *TIMP4* in our BAV families did not allow confirming linkage to the 3p25 region, which would have required the identification of a disease-causing mutation. Therefore, the issue of linkage in the 3p region remains an open-ended story, at least for four BAV families with potential linkage in this region (families 2, 4, 13, 15).

Chapter 6: General Discussion and Conclusions

6.1 Summary of our findings

Our initial hypothesis stated that congenital BAV was inherited as an autosomal dominant disorder, with possible genetic heterogeneity. Our results did not allow confirming the mode of inheritance of cBAV nor the presence of heterogeneity. This will await the identification of disease-causing mutations.

The first objective of this project was to study the *NOS3* candidate gene based on the reported phenotype of a mouse model. We have excluded linkage at this locus in six families and subsequently excluded the presence of mutations in the transcribed region and flanking splice sites of the gene in ten other families. A mouse model with a greater penetrance of the BAV phenotype and an absence of other anomalies is yet to be generated. Notably, the effects of gene knockouts in mouse models may represent severe phenotypes as compared with point mutations, which account for most disease-causing mutations in humans [160]. Mouse mutants resulting in truncal cushion malformations (Table 1.1) may show a less severe phenotype upon mutation of a single amino acid or domain.

The second objective was to screen the chromosome 3p region with genetic markers to clarify the involvement of this region in our 16 BAV families. Our two-point linkage results did not allow finding significant linkage in this region, although we have excluded a minimum of five families under an autosomal dominant transmission model. In addition, our results suggested that the LOD score of ~2.54 obtained from the genome screen had been most likely obtained by chance in most families. Further analysis will be necessary to clarify the involvement of this region in the remaining families.

We concomitantly studied two genes located on chromosome 3p, *FBLN2* and *TIMP4*, in our 16 families based on their known function in cardiac development. We have ruled out the presence of mutations in the transcribed region and flanking splice sites of these genes.

6.1.1 The question of genetic heterogeneity

The high incidence of BAV and its occurrence at low penetrance in certain syndromes strongly favours heterogeneity for this disorder [129]. Locus heterogeneity could occur when a different member of the same signalling cascade is defective in different individuals during cardiac morphogenesis, for example.

Until it can be demonstrated that multiple loci can independently cause cBAV in different families, we will not be able to confirm locus heterogeneity in our families. However, we believe that the results from the model-free analysis in our 16 families support this possibility.

6.1.2 Study limitations

The two major limitations of our study were the small size of our pedigrees and their insufficient number, and the unknown mode of transmission for cBAV. A recent report indicated that a larger study sample was associated with increased success in a genome screen [194]. Because of the small number of affected individuals in most of our pedigrees, a greater number of families would have facilitated the detection of linkage. Additionally, since the mode of transmission for cBAV remains uncertain, we are unable to draw clear conclusions from our linkage analyses. Model-free analysis has the

advantage of being powerful enough to detect linkage when the mode of inheritance is not known, however we obtain the combined results of a potentially heterogeneous group of pedigrees. On the other hand, with model-based analysis we are forced to assume the transmission model, which can result in failure to detect linkage. For example, we might have excluded different families at the *NOS3* locus had we performed the analysis under a different model. We however continue to believe that cBAV is most likely inherited as an autosomal dominant trait in several families based on the presence of affected individuals in three generations.

6.3 Congenital bicuspid aortic valve: a complex disorder?

In this study, our hypothesis assumed that cBAV was a monogenic disorder, although other scenarios are possible. The presence of what appears to be unaffected carriers in some families hints at the existence of modifier genes and/or the contribution of environmental factors and susceptibility genes (for example see families 14 and 15, Figure 3.1). Nora and Nora proposed that as many as 90% of congenital heart defects may have an important genetic-environmental interaction [195].

Complex disorders result from the interaction of several genes with each other and/or with environmental factors. They are mainly characterized by variability in the severity of symptoms and age of onset, multiple etiological mechanisms, and the involvement of several genes each with a small overall contribution to the phenotype [196]. In the case of cBAV, the "environmental" component could be embryonic blood flow (section 1.9.1.1), which could cause BAV only in the presence of a genetic predisposition. Although altered cardiac hemodynamics are sufficient to cause BAV in

animal models (section 1.9.1.1, [115,116]), it is hard to explain how this factor alone could be responsible for congenital BAV in multigenerational human families, unless this perturbation was of a congenital nature itself.

Another interesting possibility to consider is that cBAV may be an oligogenic disorder. Oligogenic disorders remain primarily genetic in etiology, but require the synergistic action of mutant alleles at a small number of loci [197]. Indications of oligogenicity include strain/background-dependent expression of the phenotype in animal models, confirmation of linkage at multiple loci and the difficulty to successfully apply Mendelian models in genetic analyses [197]. The BAV phenotype was indeed background dependent in Syrian hamsters and mice (section 1.9.2). Substantial inter- and intra-familial phenotypic variability is also strongly suggestive of the presence of modifier genes [197]. Future research will hopefully clarify whether the different subtypes of congenitally bicuspid aortic valves, and possibly the severity of the complications, are genetically determined.

Complex disorders unquestionably represent a future challenge for linkage studies. Genes with a low contribution to the phenotype will be hard to detect by linkage [194]. However, modified linkage approaches that do not rely exclusively on attaining significant LOD scores are emerging as efficient methods to detect such loci [198].

6.4 Importance of this work

This work is important because it represents the first effort to investigate the molecular genetic component of familial congenital BAV in humans. Although our results remain preliminary, our study constitutes a framework to lead future research.

Moreover, we have presented six previously unpublished BAV families, raising the count of reported families to 52.

Our work also has clinical importance. Almost every patient affected with BAV will eventually develop symptoms that will require examination, prophylactic medication, follow-up and potentially surgery, and thus become a regular user of the health care system [6,12,23,42]. An early diagnosis allows for a better management of the complications [24]. Research on cBAV aims to uncover its causes, and eventually to allow diagnosing the condition before the appearance of symptoms. Furthermore, the association of BAV with aortic medial weakness has implications for aortic valve surgery and for research in the field of cardiac embryogenesis. The demonstration of a genetic cause to this association would positively impact both domains.

6.5 Future directions

In order to increase the likelihood of success of future genetic analyses, it will be essential to recruit many additional congenital BAV families, especially with the possibility of genetic heterogeneity. The efforts of our laboratory and collaborators from the Heart Institute are currently aimed in this direction.

The next important step will be to conduct a finer genome screen in all of our BAV families by genotyping additional STRP markers located in between the markers from the first set to achieve 10 cM spacing. Chromosome X will also be included. This "grid-tightening" process will be repeated until the detection of potentially linked loci, which will be further examined. Until the true mode of inheritance of BAV is identified,

it will be prudent to keep to model-free or to non-parametric linkage analysis to avoid the consequences of model misspecification.

Future challenges in the field of cardiac development will include defining the pathology of cBAV on a molecular level, which will be of great assistance to genetic analyses by providing additional information for the selection of candidate genes.

References

1. Online Mendelian Inheritance in Man, OMIM (TM). McKusick-Nathans Institute for Genetic Medicine, Johns Hopkins University (Baltimore, MD) and National Center for Biotechnology Information, National Library of Medicine (Bethesda, MD), **2000**. World Wide Web URL: http://www.ncbi.nlm.nih.gov/omim/.

2. Roberts, W.C. The congenitally bicuspid aortic valve. A study of 85 autopsy cases. *Am J Cardiol.* **1970**; 26(1): 72-83.

3. Larson, E.W. and W.D. Edwards. Risk factors for aortic dissection: a necropsy study of 161 cases. *Am J Cardiol.* **1984**; 53(6): 849-55.

4. Hoffman, J.I. and S. Kaplan. The incidence of congenital heart disease. *J Am Coll Cardiol.* **2002**; 39(12): 1890-900.

5. Walley, V.M., et al. Congenitally bicuspid aortic valves: study of a variant with fenestrated raphe. *Can.J.Cardiol.* **1994**; 10(5): 535-542.

6. Sabet, H.Y., et al. Congenitally bicuspid aortic valves: a surgical pathology study of 542 cases (1991 through 1996) and a literature review of 2,715 additional cases. *Mayo Clin Proc.* **1999**; 74(1): 14-26.

7. Dare, A.J., et al. New observations on the etiology of aortic valve disease: a surgical pathologic study of 236 cases from 1990. *Hum Pathol.* **1993**; 24(12): 1330-8.

8. Antecol, D.H. and K.L. Chan, Congenital bicuspid aortic valve: diagnosis, complications, and progression, in *Primary Cardiology*, L. Goldman and E. Braunwald, Editors. **1994**, W.B. Saunders Company: Philadelphia. p. 15-18.

9. Yotsumoto, G., et al. Congenital bicuspid aortic valve: analysis of 63 surgical cases. *J Heart Valve Dis.* **1998**; 7(5): 500-3.

10. Angelini, A., et al. The morphology of the normal aortic valve as compared with the aortic valve having two leaflets. *J Thorac Cardiovasc Surg.* **1989**; 98(3): 362-7.

11. Waller, B.F., et al. Bicuspid aortic valve. Comparison of congenital and acquired types. *Circulation.* **1973**; 48(5): 1140-50.

12. Ward, C. Clinical significance of the bicuspid aortic valve. *Heart.* **2000**; 83(1): 81-5.

13. Huntington, K., A.G. Hunter, and K.L. Chan. A prospective study to assess the frequency of familial clustering of congenital bicuspid aortic valve. *J.Am.Coll.Cardiol.* **1997**; 30(7): 1809-1812.

14. Lindsay, J., Jr. Coarctation of the aorta, bicuspid aortic valve and abnormal ascending aortic wall. *Am J Cardiol.* **1988**; 61(1): 182-4.

15. Kappetein, A.P., et al. The neural crest as a possible pathogenetic factor in coarctation of the aorta and bicuspid aortic valve. *J Thorac Cardiovasc Surg.* **1991**; 102(6): 830-6.

16. Sadee, A.S., et al. Aortic valve regurgitation and the congenitally bicuspid aortic valve: a clinico-pathological correlation. *Br Heart J.* **1992**; 67(6): 439-41.

17. Lerer, P.K. and W.D. Edwards. Coronary arterial anatomy in bicuspid aortic valve. Necropsy study of 100 hearts. *Br Heart J.* **1981**; 45(2): 142-7.

18. Brandenburg, R.O., Jr, et al. Accuracy of 2-dimensional echocardiographic diagnosis of congenitally bicuspid aortic valve: echocardiographic-anatomic correlation in 115 patients. *Am.J.Cardiol.* **1983**; 51(9): 1469-1473.

19. Nakamura, K., et al. Rare cases of congenital bicuspid aortic valve with an abnormal fibrous band. *Ann Thorac Cardiovasc Surg.* **1999**; 5(5): 343-6.

20. Yamagishi, M., N. Anzai, and M. Yamada. An exceptional form of congenitally bicuspid aortic valve resulting in pure aortic regurgitation. *Jpn Heart J.* **1986**; 27(2): 267-71.

21. Duran, A.C., et al. Bicuspid aortic valves in hearts with other congenital heart disease. *J.Heart Valve.Dis.* **1995**; 4(6): 581-590.

22. Chan, K.L., W.A. Stinson, and J.P. Veinot. Reliability of transthoracic echocardiography in the assessment of aortic valve morphology: pathological correlation in 178 patients. *Can.J.Cardiol.* **1999**; 15(1): 48-52.

23. Pachulski, R.T. and K.L. Chan. Progression of aortic valve dysfunction in 51 adult patients with congenital bicuspid aortic valve: assessment and follow up by Doppler echocardiography. *Br.Heart J.* **1993**; 69(3): 237-240.

24. Glancy, D.L. Congenitally bicuspid aortic valves in adults. *J La State Med Soc.* **2002**; 154(6): 296-301; quiz 301-2.

25. Yener, N., et al. Bicuspid aortic valve. *Ann Thorac Cardiovasc Surg.* **2002**; 8(5): 264-7.

26. Campbell, M. Calcific aortic stenosis and congenital bicuspid aortic valves. *Br Heart J.* **1968**; 30(5): 606-16.

27. Fowles, R.E., et al. Two-dimensional echocardiographic features of bicuspid aortic valve. *Chest.* **1979**; 75(4): 434-40.

28. Edwards, J.E. The congenital bicuspid aortic valve. *Circulation.* **1961**; 23: 485-8.

29. Subramanian, R., L.J. Olson, and W.D. Edwards. Surgical pathology of pure aortic stenosis: a study of 374 cases. *Mayo Clin Proc.* **1984**; 59(10): 683-90.

30. Alegret, J.M., et al. Prevalence of and predictors of bicuspid aortic valves in patients with dilated aortic roots. *Am J Cardiol.* **2003**; 91(5): 619-22.

31. Fenoglio, J.J., Jr., et al. Congenital bicuspid aortic valve after age 20. *Am J Cardiol.* **1977**; 39(2): 164-9.

32. Novaro, G.M., et al. Features and predictors of ascending aortic dilatation in association with a congenital bicuspid aortic valve. *Am J Cardiol.* **2003**; 92(1): 99-101.

33. Espinola-Zavaleta, N., et al. Anatomic three-dimensional echocardiographic correlation of bicuspid aortic valve. *J Am Soc Echocardiogr.* **2003**; 16(1): 46-53.

34. Ando, M., et al. Thoracic aortic aneurysm associated with congenital bicuspid aortic valve. *Cardiovasc Surg.* **1998**; 6(6): 629-34.

35. Pauperio, H.M., A.C. Azevedo, and C.S. Ferreira. The aortic valve with two leaflets--a study in 2,000 autopsies. *Cardiol Young.* **1999**; 9(5): 488-98.

36. Clementi, M., et al. Familial congenital bicuspid aortic valve: a disorder of uncertain inheritance. *Am.J.Med.Genet.* **1996**; 62(4): 336-338.

37. Emanuel, R., et al. Congenitally bicuspid aortic valves. Clinicogenetic study of 41 families. *Br Heart J.* **1978**; 40(12): 1402-7.

38. Nabulsi, M.M., et al. Parental consanguinity and congenital heart malformations in a developing country. *Am J Med Genet.* **2003**; 116A(4): 342-7.

39. Glick, B.N. and W.C. Roberts. Congenitally bicuspid aortic valve in multiple family members. *Am J Cardiol.* **1994**; 73(5): 400-4.

40. Cripe, L., et al. Bicuspid aortic valve is heritable. *J Am Coll Cardiol.* **2004**; 44(1): 138-43.

41. Brown, C., D.C. Sane, and D.W. Kitzman. Bicuspid aortic valves in monozygotic twins. *Echocardiography.* **2003**; 20(2): 183-4.

42. Fedak, P.W., et al. Clinical and pathophysiological implications of a bicuspid aortic valve. *Circulation.* **2002**; 106(8): 900-4.

43. Presbitero, P., et al. Long term results (15-30 years) of surgical repair of aortic coarctation. *Br Heart J.* **1987**; 57(5): 462-7.

44. Stewart, A.B., et al. Coarctation of the aorta life and health 20-44 years after surgical repair. *Br Heart J.* **1993**; 69(1): 65-70.

45. Roos-Hesselink, J.W., et al. Aortic valve and aortic arch pathology after coarctation repair. *Heart.* **2003**; 89(9): 1074-7.

46. Moore, G.W., et al. Congenital malformations of the semilunar valves. *Hum Pathol.* **1980**; 11(4): 367-72.

47. Basso, C., et al. Congenital heart disease and sudden death in the young. *Hum Pathol.* **1995**; 26(10): 1065-72.

48. Dore, A., et al. Progressive dilation of the diameter of the aortic root in adults with a bicuspid aortic valve. *Cardiol Young.* **2003**; 13(6): 526-31.

49. Braverman, A.C. Bicuspid aortic valve and associated aortic wall abnormalities [editorial]. *Curr Opin Cardiol.* **1996**; 11(5): 501-3.

50. Pachulski, R.T., A.L. Weinberg, and K.L. Chan. Aortic aneurysm in patients with functionally normal or minimally stenotic bicuspid aortic valve. *Am J Cardiol.* **1991**; 67(8): 781-2.

51. Hahn, R.T., et al. Association of aortic dilation with regurgitant, stenotic and functionally normal bicuspid aortic valves. *J Am Coll Cardiol.* **1992**; 19(2): 283-8.

52. Keane, M.G., et al. Bicuspid aortic valves are associated with aortic dilatation out of proportion to coexistent valvular lesions. *Circulation.* **2000**; 102(19 Suppl 3): III35-9.

53. Edwards, W.D., D.S. Leaf, and J.E. Edwards. Dissecting aortic aneurysm associated with congenital bicuspid aortic valve. *Circulation.* **1978**; 57(5): 1022-1025.

54. Roberts, C.S. and W.C. Roberts. Dissection of the aorta associated with congenital malformation of the aortic valve. *J Am Coll Cardiol.* **1991**; 17(3): 712-6.

55. Parai, J.L., et al. Aortic medial changes associated with bicuspid aortic valve: myth or reality? *Can J Cardiol.* **1999**; 15(11): 1233-8.

56. de Sa, M., et al. Histologic abnormalities of the ascending aorta and pulmonary trunk in patients with bicuspid aortic valve disease: clinical relevance to the ross procedure. *J Thorac Cardiovasc Surg.* **1999**; 118(4): 588-94.

57. Gale, A.N., et al. Familial congenital bicuspid aortic valve: secondary calcific aortic stenosis and aortic aneurysm. *Chest.* **1977**; 72(5): 668-70.

58. McKusick, V.A. Association of congenital bicuspid aortic valve and erdheim's cystic medial necrosis [letter]. *Lancet.* **1972**; 1(7758): 1026-7.

59. Niwa, K., et al. Structural abnormalities of great arterial walls in congenital heart disease: light and electron microscopic analyses. *Circulation.* **2001**; 103(3): 393-400.

60. Nistri, S., et al. Bicuspid aortic valve: abnormal aortic elastic properties. *J Heart Valve Dis.* **2002**; 11(3): 369-73; discussion 373-4.

61. Schmid, F.X., et al. Ascending aortic aneurysm associated with bicuspid and tricuspid aortic valve: involvement and clinical relevance of smooth muscle cell apoptosis and expression of cell death-initiating proteins. *Eur J Cardiothorac Surg.* **2003**; 23(4): 537-43.

62. Bonderman, D., et al. Mechanisms underlying aortic dilatation in congenital aortic valve malformation. *Circulation.* **1999**; 99(16): 2138-43.

63. Nataatmadja, M., et al. Abnormal extracellular matrix protein transport associated with increased apoptosis of vascular smooth muscle cells in marfan syndrome and bicuspid aortic valve thoracic aortic aneurysm. *Circulation.* **2003**; 108 Suppl 1: II329-34.

64. Robicsek, F. Bicuspid versus tricuspid aortic valves. *J Heart Valve Dis.* **2003**; 12(1): 52-3.

65. Stehbens, W.E. Structural and architectural changes during arterial development and the role of hemodynamics. *Acta Anat (Basel).* **1996**; 157(4): 261-74.

66. Agozzino, L., et al. Non-inflammatory aortic root disease and floppy aortic valve as cause of isolated regurgitation: a clinico-morphologic study. *Int J Cardiol.* **1994**; 45(2): 129-34.

67. Ferencik, M. and L.A. Pape. Changes in size of ascending aorta and aortic valve function with time in patients with congenitally bicuspid aortic valves. *Am J Cardiol.* **2003**; 92(1): 43-6.

68. Nkomo, V.T., et al. Bicuspid aortic valve associated with aortic dilatation: a community-based study. *Arterioscler Thromb Vasc Biol.* **2003**; 23(2): 351-6.

69. Warnes, C.A. Bicuspid aortic valve and coarctation: two villains part of a diffuse problem. *Heart.* **2003**; 89(9): 965-6.

70. Carlson, B.M., *Human embryology and developmental biology.* 3rd ed. **2004**, St Louis: Mosby - Year Book, Inc. 527 pages.

71. Kirby, M.L. and K.L. Waldo. Neural crest and cardiovascular patterning. *Circ Res.* **1995**; 77(2): 211-5.

72. Yasuda, H., et al. Failure to prevent progressive dilation of ascending aorta by aortic valve replacement in patients with bicuspid aortic valve: comparison with tricuspid aortic valve. *Circulation.* **2003**; 108 Suppl 1: II291-4.

73. Schwarze, U., et al. Haploinsufficiency for one COL3A1 allele of type III procollagen results in a phenotype similar to the vascular form of Ehlers-Danlos syndrome, Ehlers-Danlos syndrome type IV. *Am J Hum Genet.* **2001**; 69(5): 989-1001.

74. Loeys, B., et al. Genotype and phenotype analysis of 171 patients referred for molecular study of the fibrillin-1 gene FBN1 because of suspected Marfan syndrome. *Arch Intern Med.* **2001**; 161(20): 2447-54.

75. Vaughan, C.J., et al. Identification of a chromosome 11q23.2-q24 locus for familial aortic aneurysm disease, a genetically heterogeneous disorder. *Circulation.* **2001**; 103(20): 2469-2475.

76. Guo, D., et al. Familial thoracic aortic aneurysms and dissections: genetic heterogeneity with a major locus mapping to 5q13-14. *Circulation.* **2001**; 103(20): 2461-2468.

77. Hasham, S.N., et al. Mapping a locus for familial thoracic aortic aneurysms and dissections (TAAD2) to 3p24-25. *Circulation.* **2003**; 107(25): 3184-90.

78. Disse, S., et al. Mapping of a first locus for autosomal dominant myxomatous mitral-valve prolapse to chromosome 16p11.2-p12.1. *Am J Hum Genet.* **1999**; 65(5): 1242-51.

79. Freed, L.A., et al. A locus for autosomal dominant mitral valve prolapse on chromosome 11p15.4. *Am J Hum Genet.* **2003**; 72(6): 1551-9.

80. Surerus, E., I.C. Huggon, and L.D. Allan. Turner's syndrome in fetal life. *Ultrasound Obstet Gynecol.* **2003**; 22(3): 264-7.

81. Van Praagh, S., et al. Cardiac malformations in trisomy-18: a study of 41 postmortem cases. *J Am Coll Cardiol.* **1989**; 13(7): 1586-97.

82. Drumheller, T., et al. Precise localisation of 3p25 breakpoints in four patients with the 3p-syndrome. *J Med Genet.* **1996**; 33(10): 842-7.

83. Mowrey, P.N., et al. Clinical and molecular analyses of deletion 3p25-pter syndrome. *Am J Med Genet.* **1993**; 46(6): 623-9.

84. Phipps, M.E., et al. Molecular genetic analysis of the 3p- syndrome. *Hum Mol Genet.* **1994**; 3(6): 903-8.

85. Green, E.K., et al. Detailed mapping of a congenital heart disease gene in chromosome 3p25. *J.Med.Genet.* **2000**; 37(8): 581-587.

86. Eisenberg, L.M. and R.R. Markwald. Molecular regulation of atrioventricular valvuloseptal morphogenesis. *Circ Res.* **1995**; 77(1): 1-6.

87. Fishman, M.C. and K.R. Chien. Fashioning the vertebrate heart: earliest embryonic decisions. *Development.* **1997**; 124(11): 2099-117.

88. Barnett, J.V. and J.S. Desgrosellier. Early events in valvulogenesis: a signaling perspective. *Birth Defects Res Part C Embryo Today.* **2003**; 69(1): 58-72.

89. Schroeder, J.A., et al. Form and function of developing heart valves: coordination by extracellular matrix and growth factor signaling. *J Mol Med.* **2003**; 81(7): 392-403.

90. Larsen, W.J., *Human embryology.* 2nd ed. **1997**, New York: Churchill Livingstone Inc. pp. 170-180.

91. Rothenberg, F., S.A. Fisher, and M. Watanabe. Sculpting the cardiac outflow tract. *Birth Defects Res Part C Embryo Today.* **2003**; 69(1): 38-45.

92. Hurle, J.M. and J.L. Ojeda. Cell death during the development of the truncus and conus of the chick embryo heart. *J Anat.* **1979**; 129(2): 427-39.

93. Hurle, J.M., E. Colvee, and A.M. Blanco. Development of mouse semilunar valves. *Anat Embryol (Berl).* **1980**; 160(1): 83-91.

94. Hurle, J.M. and E. Colvee. Changes in the endothelial morphology of the developing semilunar heart valves. A TEM and SEM study in the chick. *Anat Embryol (Berl).* **1983**; 167(1): 67-83.

95. Hurle, J.M. Scanning and light microscope studies of the development of the chick embryo semilunar heart valves. *Anat Embryol (Berl).* **1979**; 157(1): 69-80.

96. Olson, E.N. and D. Srivastava. Molecular pathways controlling heart development. *Science.* **1996**; 272(5262): 671-6.

97. Bartram, U., et al. Double-outlet right ventricle and overriding tricuspid valve reflect disturbances of looping, myocardialization, endocardial cushion differentiation, and apoptosis in TGF-beta(2)-knockout mice. *Circulation.* **2001**; 103(22): 2745-52.

98. Brown, C.B., et al. Requirement of type III TGF-beta receptor for endocardial cell transformation in the heart. *Science.* **1999**; 283(5410): 2080-2.

99. Delot, E.C., et al. BMP signaling is required for septation of the outflow tract of the mammalian heart. *Development.* **2003**; 130(1): 209-20.

100. Dor, Y., et al. A novel role for VEGF in endocardial cushion formation and its potential contribution to congenital heart defects. *Development.* **2001**; 128(9): 1531-8.

101. Galvin, K.M., et al. A role for smad6 in development and homeostasis of the cardiovascular system. *Nat Genet.* **2000**; 24(2): 171-4.

102. Werb, Z. ECM and cell surface proteolysis: regulating cellular ecology. *Cell.* **1997**; 91(4): 439-42.

103. Nagase, H. and J.F. Woessner, Jr. Matrix metalloproteinases. *J Biol Chem.* **1999**; 274(31): 21491-4.

104. Costell, M., et al. Hyperplastic conotruncal endocardial cushions and transposition of great arteries in perlecan-null mice. *Circ Res.* **2002**; 91(2): 158-64.

105. van den Hoff, M.J., et al. Myocardialization of the cardiac outflow tract. *Dev Biol.* **1999**; 212(2): 477-90.

106. Takamura, K., et al. Association of cephalic neural crest cells with cardiovascular development, particularly that of the semilunar valves. *Anat Embryol (Berl).* **1990**; 182(3): 263-72.

107. Waldo, K., et al. Cardiac neural crest cells provide new insight into septation of the cardiac outflow tract: aortic sac to ventricular septal closure. *Dev Biol.* **1998**; 196(2): 129-44.

108. Kirby, M.L. and K.L. Waldo. Role of neural crest in congenital heart disease. *Circulation.* **1990**; 82(2): 332-40.

109. Poelmann, R.E., T. Mikawa, and A.C. Gittenberger-de Groot. Neural crest cells in outflow tract septation of the embryonic chicken heart: differentiation and apoptosis. *Dev Dyn.* **1998**; 212(3): 373-84.

110. Watanabe, M., et al. Developmental remodeling and shortening of the cardiac outflow tract involves myocyte programmed cell death. *Development.* **1998**; 125(19): 3809-20.

111. Abdelwahid, E., L.J. Pelliniemi, and E. Jokinen. Cell death and differentiation in the development of the endocardial cushion of the embryonic heart. *Microsc Res Tech.* **2002**; 58(5): 395-403.

112. Ya, J., et al. Sox4-deficiency syndrome in mice is an animal model for common trunk. *Circ Res.* **1998**; 83(10): 986-94.

113. Hirooka, K., et al. Combined abnormalities of semilunar valves: quadricuspid pulmonary and bicuspid aortic valves. *Circulation.* **2001**; 103(1): E7.

114. Rosenberg, H.S. Coarctation as a deformation. *Pediatr Pathol.* **1990**; 10(1-2): 103-15.

115. Hogers, B., et al. Unilateral vitelline vein ligation alters intracardiac blood flow patterns and morphogenesis in the chick embryo. *Circ Res.* **1997**; 80(4): 473-81.

116. Hogers, B., et al. Extraembryonic venous obstructions lead to cardiovascular malformations and can be embryolethal. *Cardiovasc Res.* **1999**; 41(1): 87-99.

117. Colvee, E. and J.M. Hurle. Malformations of the semilunar valves produced in chick embryos by mechanical interference with cardiogenesis. An experimental approach to the role of hemodynamics in valvular development. *Anat Embryol (Berl).* **1983**; 168(1): 59-71.

118. Garcia-Martinez, V. and J.M. Hurle. Cell shape and cytoskeletal organization of the endothelial cells of the semilunar heart valves in the developing chick. *Anat Embryol (Berl).* **1986**; 174(1): 83-9.

119. Malek, A.M. and S. Izumo. Mechanism of endothelial cell shape change and cytoskeletal remodeling in response to fluid shear stress. *J Cell Sci.* **1996**; 109 (Pt 4): 713-26.

120. Fisher, A.B., et al. Endothelial cellular response to altered shear stress. *Am J Physiol Lung Cell Mol Physiol.* **2001**; 281(3): L529-33.

121. Ohno, M., et al. Fluid shear stress induces endothelial transforming growth factor beta-1 transcription and production. Modulation by potassium channel blockade. *J Clin Invest.* **1995**; 95(3): 1363-9.

122. Li, H., T. Wallerath, and U. Forstermann. Physiological mechanisms regulating the expression of endothelial-type NO synthase. *Nitric Oxide.* **2002**; 7(2): 132-47.

123. Sans-Coma, V., et al. Bicuspid aortic and pulmonary valves in the Syrian hamster. *Int J Cardiol.* **1992**; 34(3): 249-54.

124. Sans-Coma, V., et al. Evidence for a quantitative genetic influence on the formation of aortic valves with two leaflets in the Syrian hamster. *Cardiol Young.* **1993**; 3: 132-140.

125. Sans-Coma, V., et al. Fusion of valve cushions as a key factor in the formation of congenital bicuspid aortic valves in Syrian hamsters. *Anat Rec.* **1996**; 244(4): 490-8.

126. Novaro, G.M., M. Mishra, and B.P. Griffin. Incidence and echocardiographic features of congenital unicuspid aortic valve in an adult population. *J Heart Valve Dis.* **2003**; 12(6): 674-8.

127. Hwang, D.M., C.M. Feindel, and J.W. Butany. Quadricuspid semilunar valves: report of two cases. *Can J Cardiol.* **2003**; 19(8): 938-42.

128. Lee, T.C., et al. Abnormal aortic valve development in mice lacking endothelial nitric oxide synthase. *Circulation.* **2000**; 101(20): 2345-8.

129. Biben, C., et al. Cardiac septal and valvular dysmorphogenesis in mice heterozygous for mutations in the homeobox gene Nkx2-5. *Circ Res.* **2000**; 87(10): 888-95.

130. Macatee, T.L., et al. Ablation of specific expression domains reveals discrete functions of ectoderm- and endoderm-derived FGF8 during cardiovascular and pharyngeal development. *Development.* **2003**; 130(25): 6361-74.

131. Chen, B., et al. Mice mutant for Egfr and Shp2 have defective cardiac semilunar valvulogenesis. *Nat Genet.* **2000**; 24(3): 296-9.

132. Sibilia, M., et al. Mice humanised for the EGF receptor display hypomorphic phenotypes in skin, bone and heart. *Development.* **2003**; 130(19): 4515-25.

133. Crispino, J.D., et al. Proper coronary vascular development and heart morphogenesis depend on interaction of GATA-4 with FOG cofactors. *Genes Dev.* **2001**; 15(7): 839-44.

134. Ranger, A.M., et al. The transcription factor NF-ATc is essential for cardiac valve formation. *Nature.* **1998**; 392(6672): 186-90.

135. de la Pompa, J., et al. Role of the NF-ATc transcription factor in morphogenesis of cardiac valves and septum. *Nature.* **1998**; 392(6672): 182-186.

136. Kim, R.Y., E.J. Robertson, and M.J. Solloway. Bmp6 and Bmp7 are required for cushion formation and septation in the developing mouse heart. *Dev Biol.* **2001**; 235(2): 449-66.

137. Zhou, H.M., et al. Essential role for ADAM19 in cardiovascular morphogenesis. *Mol Cell Biol.* **2004**; 24(1): 96-104.

138. Svensson, E.C., et al. A syndrome of tricuspid atresia in mice with a targeted mutation of the gene encoding Fog-2. *Nat Genet.* **2000**; 25(3): 353-6.

139. Lee, P.C., et al. Impaired wound healing and angiogenesis in eNOS-deficient mice. *Am J Physiol.* **1999**; 277(4 Pt 2): H1600-8.

140. Gregg, A.R., et al. Limb reduction defects in endothelial nitric oxide synthase-deficient mice. *Am J Physiol.* **1998**; 275(6 Pt 2): H2319-24.

141. Murohara, T., et al. Nitric oxide synthase modulates angiogenesis in response to tissue ischemia. *J Clin Invest.* **1998**; 101(11): 2567-78.

142. Lake-Bruse, K.D., et al. Gene transfer of endothelial nitric oxide synthase (eNOS) in eNOS-deficient mice. *Am J Physiol.* **1999**; 277(2 Pt 2): H770-6.

143. Rudic, R.D., et al. Direct evidence for the importance of endothelium-derived nitric oxide in vascular remodeling. *J Clin Invest.* **1998**; 101(4): 731-6.

144. Huang, P.L., et al. Hypertension in mice lacking the gene for endothelial nitric oxide synthase. *Nature.* **1995**; 377(6546): 239-42.

145. Forstermann, U., et al. Nitric oxide synthase isozymes. Characterization, purification, molecular cloning, and functions. *Hypertension.* **1994**; 23(6 Pt 2): 1121-31.

146. Moncada, S. and A. Higgs. The L-arginine-nitric oxide pathway. *N Engl J Med.* **1993**; 329(27): 2002-12.

147. Prior, B.M., et al. Arteriogenesis: role of nitric oxide. *Endothelium.* **2003**; 10(4-5): 207-16.

148. Feng, Q., et al. Development of heart failure and congenital septal defects in mice lacking endothelial nitric oxide synthase. *Circulation.* **2002**; 106(7): 873-9.

149. Terwilliger, J.D. and J. Ott, *Handbook of human genetic linkage.* **1994**, Baltimore: The Johns Hopkins University Press. 307 pages.

150. Ott, J., *Analysis of human genetic linkage.* Third ed. **1999**, Baltimore and London: The Johns Hopkins University Press. 382 pages.

151. Schiller, N.B., et al. Recommendations for quantitation of the left ventricle by two-dimensional echocardiography. American Society of Echocardiography Committee on Standards, Subcommittee on Quantitation of Two-Dimensional Echocardiograms. *J Am Soc Echocardiogr.* **1989**; 2(5): 358-67.

152. Sambrook, J., E.F. Fritsch, and T. Maniatis, *Molecular Cloning; A Laboratory Manual.* 2nd ed. Vol. 3. **1989**, USA: Cold Spring Harbor Laboratory Press.

153. Lathrop, G.M. and J.M. Lalouel. Easy calculations of lod scores and genetic risks on small computers. *Am J Hum Genet.* **1984**; 36(2): 460-5.

154. Lathrop, G.M., et al. Strategies for multilocus linkage analysis in humans. *Proc Natl Acad Sci U S A.* **1984**; 81(11): 3443-6.

155. Lathrop, G.M., et al. Multilocus linkage analysis in humans: detection of linkage and estimation of recombination. *Am J Hum Genet.* **1985**; 37(3): 482-98.

156. Schaffer, A.A., et al. Avoiding recomputation in linkage analysis. *Hum.Hered.* **1994**; 44(4): 225-237.

157. Voet, D., Voet, J G., *Biochimie.* 2ième ed. **1998**, Paris, Bruxelles: De Boeck Université. p. 947.

158. Rozen, S., Skaletsky, Helen J., Primer3 on the WWW for general users and for biologist programmers., in *Bioinformatics Methods and Protocols: Methods in Molecular Biology*, S. Krawetz and S. Misener, Editors. **2000**, Humana Press: Totowa, NJ. p. 365-386.

159. Curtis, D., Data Analysis for Genetic Studies, in *SNP and Microsatellite Genotyping: Markers for Genetic Analysis*, A. Hajeer, J. Worthington, and S. John, Editors. **2000**, Eaton Publishing: Natick, MA. p. 81-116.

160. Botstein, D. and N. Risch. Discovering genotypes underlying human phenotypes: past successes for mendelian disease, future approaches for complex disease. *Nat Genet.* **2003**; 33 Suppl: 228-37.

161. Yoshimura, M., et al. Genetic risk factors for coronary artery spasm: significance of endothelial nitric oxide synthase gene T-786-->C and missense Glu298Asp variants. *J Investig Med.* **2000**; 48(5): 367-74.

162. Khurana, V.G., et al. Endothelial nitric oxide synthase T-786C single nucleotide polymorphism: a putative genetic marker differentiating small versus large ruptured intracranial aneurysms. *Stroke.* **2003**; 34(11): 2555-9.

163. Salvarani, C., et al. Endothelial nitric oxide synthase gene polymorphisms in giant cell arteritis. *Arthritis Rheum.* **2003**; 48(11): 3219-23.

164. Casas, J.P., et al. Endothelial nitric oxide synthase genotype and ischemic heart disease: meta-analysis of 26 studies involving 23028 subjects. *Circulation.* **2004**; 109(11): 1359-65.

165. Dor, Y., et al. VEGF modulates early heart valve formation. *Anat Rec.* **2003**; 271A(1): 202-8.

166. Collins, F.S. Positional cloning moves from perditional to traditional. *Nat Genet.* **1995**; 9(4): 347-50.

167. Lander, E.S., et al. Initial sequencing and analysis of the human genome. *Nature.* **2001**; 409(6822): 860-921.

168. Weber, J.L. and P.E. May. Abundant class of human DNA polymorphisms which can be typed using the polymerase chain reaction. *Am J Hum Genet.* **1989**; 44(3): 388-96.

169. Ghebranious, N., et al. STRP screening sets for the human genome at 5 cM density. *BMC Genomics.* **2003**; 4(1): 6.

170. Curtis, D. and P.C. Sham. Model-free linkage analysis using likelihoods. *Am J Hum Genet.* **1995**; 57(3): 703-16.

171. Lander, E. and L. Kruglyak. Genetic dissection of complex traits: guidelines for interpreting and reporting linkage results. *Nat Genet.* **1995**; 11(3): 241-7.

172. Curtis, D., J.H. Zhao, and P.C. Sham. Comparison of GENEHUNTER and MFLINK for analysis of COGA linkage data. *Genet Epidemiol.* **1999**; 17 Suppl 1: S115-20.

173. Sham, P.C., et al. Power comparison of parametric and nonparametric linkage tests in small pedigrees. *Am J Hum Genet.* **2000**; 66(5): 1661-8.

174. Zhang, R.Z., et al. Fibulin-2 (FBLN2): human cDNA sequence, mRNA expression, and mapping of the gene on human and mouse chromosomes. *Genomics.* **1994**; 22(2): 425-30.

175. Zhang, H.Y., et al. Extracellular matrix protein fibulin-2 is expressed in the embryonic endocardial cushion tissue and is a prominent component of valves in adult heart. *Dev Biol.* **1995**; 167(1): 18-26.

176. Pan, T.C., et al. Structure and expression of fibulin-2, a novel extracellular matrix protein with multiple EGF-like repeats and consensus motifs for calcium binding. *J Cell Biol.* **1993**; 123(5): 1269-77.

177. Li, D., Marian, A.J., Roberts, R. Identification of a novel alternatively spliced isoform of human fibulin-2 gene abundantly expressed in heart and genetic evaluation in patients with ARVD (abstract). *Abstracts of the 52nd annual meeting of the American Society of Human Genetics.* **2002**; 71 (Suppl).(4): 323, A881.

178. Spence, S.G., et al. Fibulin is localized at sites of epithelial-mesenchymal transitions in the early avian embryo. *Dev Biol.* **1992**; 151(2): 473-84.

179. Tsuda, T., et al. Fibulin-2 expression marks transformed mesenchymal cells in developing cardiac valves, aortic arch vessels, and coronary vessels. *Dev Dyn.* **2001**; 222(1): 89-100.

180. Sasaki, T., et al. Binding of mouse and human fibulin-2 to extracellular matrix ligands. *J Mol Biol.* **1995**; 254(5): 892-9.

181. Greene, J., et al. Molecular cloning and characterization of human tissue inhibitor of metalloproteinase 4. *J Biol Chem.* **1996**; 271(48): 30375-80.

182. Olson, T.M., et al. Cloning of the human tissue inhibitor of metalloproteinase-4 gene (TIMP4) and localization of the TIMP4 and Timp4 genes to human chromosome 3p25 and mouse chromosome 6, respectively. *Genomics.* **1998**; 51(1): 148-51.

183. Rahkonen, O.P., et al. Characterization of the murine Timp4 gene, localization within intron 5 of the synapsin 2 gene and tissue distribution of the mRNA. *Biochim Biophys Acta.* **2002**; 1577(1): 45-52.

184. Yamada, H., et al. Processing of beta-dystroglycan by matrix metalloproteinase disrupts the link between the extracellular matrix and cell membrane via the dystroglycan complex. *Hum Mol Genet.* **2001**; 10(15): 1563-9.

185. Tummalapalli, C.M., B.J. Heath, and S.C. Tyagi. Tissue inhibitor of metalloproteinase-4 instigates apoptosis in transformed cardiac fibroblasts. *J Cell Biochem.* **2001**; 80(4): 512-21.

186. Shah, P.K. Inflammation, metalloproteinases, and increased proteolysis: an emerging pathophysiological paradigm in aortic aneurysm. *Circulation.* **1997**; 96(7): 2115-7.

187. Young, D.A., et al. Identification of an initiator-like element essential for the expression of the tissue inhibitor of metalloproteinases-4 (Timp-4) gene. *Biochem J.* **2002**; 364(Pt 1): 89-99.

188. Dollery, C.M., et al. TIMP-4 is regulated by vascular injury in rats. *Circ Res.* **1999**; 84(5): 498-504.

189. Li, Y.Y., et al. Differential expression of tissue inhibitors of metalloproteinases in the failing human heart. *Circulation.* **1998**; 98(17): 1728-34.

190. Soini, Y., et al. Expression of MMP2, MMP9, MT1-MMP, TIMP1, and TIMP2 mRNA in valvular lesions of the heart. *J Pathol.* **2001**; 194(2): 225-31.

191. McMillan, W.D., et al. Size matters: the relationship between MMP-9 expression and aortic diameter. *Circulation.* **1997**; 96(7): 2228-32.

192. Rupp, P.A., et al. Identification, genomic organization and mRNA expression of CRELD1, the founding member of a unique family of matricellular proteins. *Gene.* **2002**; 293(1-2): 47-57.

193. Robinson, S.W., et al. Missense mutations in CRELD1 are associated with cardiac atrioventricular septal defects. *Am J Hum Genet.* **2003**; 72(4): 1047-52.

194. Altmuller, J., et al. Genomewide scans of complex human diseases: true linkage is hard to find. *Am J Hum Genet.* **2001**; 69(5): 936-50.

195. Nora, J.J. and A.H. Nora. The evolution of specific genetic and environmental counseling in congenital heart diseases. *Circulation.* **1978**; 57(2): 205-13.

196. Tabor, H.K., N.J. Risch, and R.M. Myers. Opinion: Candidate-gene approaches for studying complex genetic traits: practical considerations. *Nat Rev Genet.* **2002**; 3(5): 391-7.

197. Badano, J.L. and N. Katsanis. Beyond Mendel: an evolving view of human genetic disease transmission. *Nat Rev Genet.* **2002**; 3(10): 779-89.

198. Wiltshire, S., L.R. Cardon, and M.I. McCarthy. Evaluating the results of genomewide linkage scans of complex traits by locus counting. *Am J Hum Genet.* **2002**; 71(5): 1175-82.

Appendix I
Electronic Database Information and Accession Numbers

AceView:
http://www.ncbi.nlm.nih.gov/IEB/Research/Acembly/

GraphPad QuickCalcs (p value calculator):
http://www.graphpad.com/quickcalcs/PValue1.cfm

National Centre for Biotechnology Information (NCBI):
http://www.ncbi.nlm.nih.gov/

Nos3 genomic sequence: NT_039299 Nos3 mRNA: NM_008713
NOS3 genomic sequence: NT_007914.13 *NOS3* mRNA: NM_000603
FBLN2 and *TIMP4* genomic sequence: NT_022517.16
FBLN2 mRNA (longest isoform): AY130459 *TIMP4* mRNA: BC010553

NCBI LocusLink:
http://www.ncbi.nlm.nih.gov/LocusLink/

LocusID: *NOS3*: 4846 Nos3: 18127 *FBLN2*: 2199 *TIMP4*: 7079

NCBI Map Viewer:
http://www.ncbi.nlm.nih.gov/mapview/map_search.cgi?taxid=9606

NCBI Single Nucleotide Polymorphism (SNP) database:
http://www.ncbi.nlm.nih.gov/entrez/query.fcgi?db=Snp

NCBI UniGene
http://www.ncbi.nlm.nih.gov/entrez/query.fcgi?db=unigene

NCBI UniSTS
http://www.ncbi.nlm.nih.gov/entrez/query.fcgi?db=unists

Online Mendelian Inheritance in Man (OMIM):
http://www.ncbi.nlm.nih.gov/entrez/query.fcgi?db=OMIM

BAV: 109730

Primer3 online primer design software:
http://frodo.wi.mit.edu/cgi-bin/primer3/primer3_www.cgi

Swiss-Prot:
http://ca.expasy.org/sprot/

eNOS: P29474 Fibulin-2: P98095 TIMP-4: Q99727

University of California Santa-Cruz (UCSC) Genome Browser:
http://genome.cse.ucsc.edu/cgi-bin/hgGateway

Appendix II
PCR conditions for genotyping at the D7S636 marker locus

PCR conditions in each sample (10 µl reactions):

- 20-100 ng of genomic DNA;
- 10 mM TRIS-HCl (pH 8.3);
- 50 mM KCl;
- 0.1 µg/ml bovine serum albumin;
- 1.5 mM of $MgCl_2$;
- 0.2 mM dNTPs;
- 0.0625 pmol of M13 Forward (-29) IRD™ Dye-Labelled primer (Li-Cor, Lincoln, NE);
- 1 pmol of each primer (forward and reverse);
- 1 unit of Taq polymerase.

PCR program for genotyping:

1. 94 °C for 5:00 min;
2. 10 cycles:
   a. 94 °C for 30 s;
   b. 69 °C (minus 1°C per cycle) for 30 s;
   c. 72 °C for 30 s;
3. 21 cycles:
   a. 94 °C for 30 s;
   b. 60 °C for 30 s;
   c. 72 °C for 30 s;
4. 72 °C for 5:00 min;
5. End.

PCR primers:

Primer	Primer sequence (5'-3')
Forward	CACGACGTTGTAAAACGACTGAGGAGAGACTCAGAATTGGA
Reverse	GCTTGTGTGGGGTTTCAGGCT

Table A1. Oligonucleotide sequence of the PCR primers used to amplify the D7S636 marker (underlined: the M13 label sequence).

This primer pair yields PCR products in the range of 155-200 base pairs (including the M13 tail).

Appendix III
PCR conditions for sequencing of the *NOS3* gene

The PCR program and conditions described below are for the initial amplification of the PCR products to be sequenced. The actual sequencing reaction (unidirectional PCR) was performed under the conditions described in the kit manual (see Methods, section 3.2).

PCR conditions in each sample (25 µl reactions):

- 20-100 ng of genomic DNA;
- 10 mM TRIS-HCl (pH 8.3);
- 50 mM KCl;
- 0.1 µg/ml bovine serum albumin;
- 1.0 to 2.0 mM of $MgCl_2$;
- 0.26 mM dNTPs;
- 8.5 pmol of each primer (forward and reverse);
- 1 unit of Taq polymerase.

PCR program (for both the amplification and the sequencing reactions):

1. 94 °C for 5:00 min;
2. 35 cycles:
    a. 94 °C for 30 s;
    b. 1 °C/s to X °C, then X °C for 30 s; *(see note below)
    c. 1 °C/s to 72 °C, then 72 °C for 30 s;
3. 72 °C for 5:00 min;
4. End.

*In step 2b of this program, X represents the annealing temperature in °C, as indicated in the third column of Table A2 below.

PCR and sequencing primers:

See Tables A2 and A3 below.

Table A2 (next page). Primers and conditions for amplification and sequencing of the *NOS3* gene.

NOS3 exon #	PCR primers	PCR annealing temperature (°C)	PCR product size (bp)	Sequencing primers
1 (coding + 5'UTR)	eNOSx1F eNOSx1R	65.0	340	eNOSx1F
2	eNOSx2F eNOSx2R	65.5	226	eNOSx2F
3	eNOSx3F eNOSx3R	66.0	287	eNOSx3F eNOSx3R
4	eNOSx4F eNOSx4R	66.0	295	eNOSx4F eNOSx4R
5	eNOSx5-6F eNOSx5-6R	62.5	463	eNOSx5-6F
6	eNOSx5-6F eNOSx5-6R	62.5	463	eNOSx5-6R
7	eNOSx7-8F eNOSx7-8R	65.2	573	eNOSx7intR
8	eNOSx7-8F eNOSx7-8R	65.2	573	eNOSx8intF
9	eNOSx9F eNOSx9R	65.5	318	eNOSx9F
10	eNOSx10-11F eNOSx10-11R	65.0	559	eNOSx10intR
11	eNOSx10-11F eNOSx10-11R	65.0	559	eNOSx11intF
12	eNOSx1213F eNOSx1213R	62.0	782	eNOSx1213F
13	eNOSx1213F eNOSx1213R	62.0	782	eNOSx13intF
14	eNOSx14F eNOSx14R	62.0	334	eNOSx14F eNOSx14R
15	eNOSx15F eNOSx15R	66.0	293	eNOSx15F
16	eNOSx15F eNOSx16R	66.0	535	eNOSx16intF
17	eNOSx17F eNOSx17R	67.0	293	eNOSx17F
18	eNOSx17F eNOSx19R	63.0	836	eNOSx18F
19	eNOSx17F eNOSx19R	63.0	836	eNOSx19R
20	eNOSx20F eNOSx20R	64.0	298	eNOSx20F eNOSx20R
21	eNOSx21F eNOSx22R	64.0	592	eNOSx21R
22	eNOSx21F eNOSx22R	64.0	592	eNOSx22R
23	eNOSx23aF eNOSx23aR	66.0	299	eNOSx23aF eNOSx23aR
24	eNOSx24F eNOSx24R	64.0	386	eNOSx24F
25	eNOSx25F eNOSx25R	64.0	520	eNOSx25R
26 (coding)	eNOSx26aF eNOSx26aR	65.2	504	eNOSx26aF eNOSx26aR
26 (3'UTR)	eNOSx26aF eNOSx26utrR	65.0	1030	eNOSx26intF

Primer name	Primer sequence (5'-3')
eNOSx1F	GTGTATGGGATAGGGGCGG
eNOSx1R	CACCACCCTTGTTGCCCAC
eNOSx2F	CATCTGGGAAGGCTGAAAGG
eNOSx2R	CCTTACCCACCCTTTCCCTG
eNOSx3F	CAACTCCCATCCCACCCCT
eNOSx3R	GGGTCATGGGAAGGTCGTC
eNOSx4F	CACTTGCACAAAGCCTGGAG
eNOSx4R	CCGCTCCCCTTTTGGTAG
eNOSx5-6F	CTCTGGAGCTGATACTCAAGACC
eNOSx5-6R	GCCTTCTCCCACTGGTTTC
eNOSx7-8F	CAGGAGACAGTGGATGGAGG
eNOSx7-8R	TTGGGGATGGAGTGAGAGC
eNOSx7intR	CAGGATGTTGTAGCGGTGAGG
eNOSx8intF	CCCAGGAAACGGTCGCTT
eNOSx9F	CTCACCTCACTCCTTCCAGC
eNOSx9R	CTGTCCAAATCCTGCCCTA
eNOSx10-11F	GGAGTGGTGGAGGAAGAATG
eNOSx10-11R	TAGGCCCAGAACACTGCTG
eNOSx10intR	GAAAGGTTAGAGGTCCCCAGG
eNOSx11intF	CCTGGGGACCTCTAACCTTTC
eNOSx1213F	GCATCACCAGGAAGAAGACCT
eNOSx1213R	TCACTCCAATTCTGAGTCTCTCC
eNOSx13intF	TGTTCAGAGATCAAGTTGGGG
eNOSx14F	GGGGTGGTCTTTGTCTTATC
eNOSx14R	CCCTTTCTGTTTGTGTCTCC
eNOSx15F	ACCCTGAAGCCGTCCCTG
eNOSx15R	CAGGGGTCGTCAGTGGAGC
eNOSx16R	TGAGGCAGGAGGAGGCATC
eNOSx16intF	TTGGCGGCGGAAGAGGAAG
eNOSx17F	AGCAAGACGCAGTGAAGCC
eNOSx17R	CCCAGAGTGCTTTAGTCCCG
eNOSx18F	GGACTAAAGCACTCTGGGGC
eNOSx19R	CTGGGTCGGGTCCTGAGC
eNOSx20F	AACACAAACATCAGCCCAGG
eNOSx20R	CCAGCTCATCCCGTCTCTC
eNOSx21F	GGGGTCAAGAAGGGAGGTTAC
eNOSx21R	TCTGGGGGTGGGAAGGAG
eNOSx22R	CTAATGACACCACACCCTTGAC
eNOSx23aF	TCCTTGCTCCACCCACCCTGC
eNOSx23aR	TGCCCTCTCTTTCCTATTTCCTGCC
eNOSx24F	AAGTAATGGTGGTTTCAGCCC
eNOSx24R	TGAGTGGTCGTGGGAGGC
eNOSx25F	CGACCACTCAGCCACCCC
eNOSx25R	TCGGAAAAGAGCACAGTGGATC
eNOSx26aF	TGAGCGTGCGGGGTTCC
eNOSx26aR	CTAAGAAACAGGAAGCGGGTGG
eNOSx26intF	CCAGGAAGGAGCAAAACGC
eNOSx26utrR	CCACCACATACCCACAACTGC

Table A3. DNA sequence of the *NOS3* PCR and sequencing primers described in Table A2.

Appendix IV
PCR conditions for amplification of *NOS3* exons 17-18-19 (for NcoI restriction digest)

PCR conditions* (in 25 µl volumes):
- 20-100 ng of genomic DNA;
- 50 mM TRIS-HCl (pH 9.2)
- 16 mM ammonium sulphate ($(NH_4)_2SO_4$)
- 1.75 mM of $MgCl_2$;
- 200 mM dNTPs;
- 8.5 pmol of each primer (forward and reverse);
- 1 unit of Taq polymerase.

*These conditions were used because amplification was not obtained with the conventional conditions described in Appendix III.

PCR primers:

The eNOSx17F and eNOSx19R primers were used (see Appendix III).

PCR program:

As described in Appendix III. An annealing temperature of 63.0 °C was used.

Appendix V
PCR conditions for genotyping BAV families

PCR conditions for genotyping (in 10 µl volumes):

As described in Appendix II.

PCR programs:

TD50:

1. 94 °C for 5:00 min;
2. 16 cycles:
    a. 94 °C for 30 s;
    b. 66 °C for 30 s, minus 1 °C per cycle;
    c. 72 °C for 30 s;
3. 23 cycles:
    a. 94 °C for 45 s;
    b. 50 °C for 30 s;
    c. 72 °C for 30 s;
4. 72 °C for 5:00 min;
5. End.

TD55: Same as TD50, except for these modifications:

- Step 2: only 11 cycles;
- Step 2b is done at 65 °C for 30 s, minus 1 °C per cycle;
- Step 3b is done at 55 °C for 30 s.

T49:

1. 94 °C for 5:00 min;
2. 40 cycles:
    a. 94 °C for 30 s;
    b. 49 °C for 30 s;
    c. 72 °C for 30 s;
3. 72 °C for 10:00 min;
4. End.

L50: Same as T49 except for these modifications:

- Step 2: only 30 cycles;
- Step 2b is done at 50 °C.

PCR primers:

See Table A4 below.

Marker name	PCR primers (5'-3') (Top: forward primer; bottom: reverse primer)	PCR program	Amplicon length (bp)
D3S2387	CACGACGTTGTAAAACGACAAAGCTAGAAGGAGCTGGCT GGGTGACAGAGTGAGATGTG	TD50	177-209
D3S3630	CACGACGTTGTAAAACGACAAGGGATAAGCTGCAAATCA ACCAAATACAATTCATGAGACCTGA	L50	172-188
D3S3050	CACGACGTTGTAAAACGACTGGTGGTATGCATTTGTCAG ATTCCCTGACTTCAAGTGCA	TD55	227-242
D3S1560	CACGACGTTGTAAAACGACGCATCTACAGGGGGTGTCT AGGCTGATTTTCAGCACAA	TD50	235-253
D3S1304	CACGACGTTGTAAAACGACCGGGAAGAAAATAGGCCACT TCTGATCAGCTACTTTCCTGCTTA	TD50	253-259
D3S4545	CACGACGTTGTAAAACGACCTGTGATCACACCACTGCAG TGGGGTATCCTGTGTCAGAGC	TD50	192-240
D3S3611	CACGACGTTGTAAAACGACGCTACCTCTGCTGAGCAT TAGCAAGACTGTTGGGG	TD50	107-137
D3S3589	CACGACGTTGTAAAACGACAAGCAATATTTTCTACCACTTTCT TCTGAGCCACCAGCAC	TD55	235-245
D3S3680	CACGACGTTGTAAAACGACAAGGAATTGCAAATGAAAATAGAAA GCCTGGTCCCTAACATAACT	TD55	126-144
D3S1259	CACGACGTTGTAAAACGACGTTCATGTTTCACTAG CCAGGAGGCAGAGGTTTC	TD50	184-245
D3S3701	CACGACGTTGTAAAACGACCCCCAGAACTTAAAGCAAAA TGTTGGAGAATCTGCCAGAC	TD55	171-179
D3S3610	CACGACGTTGTAAAACGACCCAGATTCTCTAAGGCCATGC TGTGGAATATCCGCCCAG	TD55	211-263
D3S1585	CACGACGTTGTAAAACGACTGCACGAGCCAGAAGT TTGGACTGCTGAGGGG	TD55	126-144
D3S3613	CACGACGTTGTAAAACGACCATCTATGTGGCAATCGG CAGCATTTGTTGTAGGGACT	TD50	172-208
D3S3038	CACGACGTTGTAAAACGACCATCTTTCTTTTCCTGTTCCC GATACCATATTCAACATGAAGAGG	TD50	187-219
D3S2336	CACGACGTTGTAAAACGACTCCTTTAGTGGTTTTAACACA TTTACTTGGGCATGTTTG	T49	89-109
D3S1283	CACGACGTTGTAAAACGACGGCAGTACCACCTGTAGAAATG GAGTAACAGAGGCATCGTGTATTC	TD50	150-160
D3S2432	CACGACGTTGTAAAACGACGGCAGGCAGGTAGATAGACA ACACTACACAAGCATAGTCAGGC	TD50	118-170
D3S1768	CACGACGTTGTAAAACGACGGTTGCTGCCAAAGATTAGA CACTGTGATTTGCTGTTGGA	TD50	186-206

Table A4. Oligonucleotide sequences and PCR programs used to amplify polymorphic DNA markers on chromosome 3. Underlined in each forward primer is the M13 tail sequence. The amplicon lengths are from UCSC Genome Browser and do not include the size of the M13 tail.

Appendix VI
PCR conditions for sequencing the *FBLN2* and *TIMP4* genes

PCR conditions and PCR programs:

As described in Appendix III.

PCR primers:

As described in Tables A5, A6, A7 and A8 below.

TIMP4 exon #	PCR primers	Annealing temperature (°C)	PCR product size (bp)	Sequencing primer
1 (5'UTR)	TIMP45utraF TIMP45utraR	62.0	696	TIMP45utraF TIMP45utraR
1 (coding)	TIMP4x1F TIMP4x1R	61.0	464	TIMP4x1R
2	TIMP4x2aF TIMP4x2aR	56.0	234	TIMP4x2aR
3	TIMP4x3F TIMP4x3R	62.0	330	TIMP4x3F
4	TIMP4x4F TIMP4x4R	59.0	383	TIMP4x4F
5 (coding)	TIMP4x5F TIMP4x5R	53.0	534	TIMP4x5R
5 (3'UTR)	TIMP4x5F TIMP43utrR	54.0	934	TIMP43utrR TIMP43utrintF

Table A5. Primers and conditions for amplification and sequencing of the *TIMP4* gene.

Primer name	Primer sequence (5'-3')
TIMP45utraF	CTGTTGCTTTGGAGCCTCAT
TIMP45utraR	CAGCTGCATGCCTCACC
TIMP4x1F	AGCCTCGGGTCCTGCCTC
TIMP4x1R	CACCCATCAGCCTCAGCAAG
TIMP4x2aF	TCCAGACCTCAGGTGTATTGC
TIMP4x2aR	CCTCCCAGAACACAGACTCC
TIMP4x3F	AGTAGGGACATCTGAGGACACA
TIMP4x3R	CCTGGCTCCTTTCTCACTACC
TIMP4x4F	CACCACTGCCACCAAAG
TIMP4x4R	GACTGTATTGCTTTCTCATCC
TIMP4x5F	AGGTCAGTGGTAGAGTAAGG
TIMP4x5R	AAGAGGTCAGGTGGTAATG
TIMP43utrR	TTAGGATGAGTTGAGACAGG
TIMP43utrintF	ACCTGCCTCTCAGGAAGGAG

Table A6. DNA sequence of the *TIMP4* PCR and sequencing primers described in Table A5.

FBLN2 exon #	PCR primers	Annealing temperature (°C)	PCR product size (bp)	Sequencing primers
1 (5'UTR)	Fibu25utrF Fibu25utrR	65.0	231	Fibu25utrF
2 (partially)	Fibu2x1.1F Fibu2x1.2R	65.0	733	Fibu2x1.1R
2 (partially)	Fibu2x1.2F Fibu2x1.2R	65.0	471	Fibu2x1.2F Fibu2x1.2R
2 (partially)	Fibu2x1.3F Fibu2x1.3R	65.0	990	Fibu2x1.3F Fibu2x1.3R Fibu2x1.3intF Fibu2x1.3intR
3	Fibu2x2F Fibu2x2R	63.0	213	Fibu2x2F Fibu2x2R
4	Fibu2x3F Fibu2x3R	62.0	300	Fibu2x3F
5	Fibu2x4F Fibu2x4R	62.0	489	Fibu2x4F Fibu2x4R
6	Fibu2x5F Fibu2x5R	58.5	377	Fibu2x5F
7	Fibu2x6F Fibu2x6R	64.0	267	Fibu2x6F Fibu2x6R
8	Fibu2x7F Fibu2x7R	59.0	321	Fibu2x7F Fibu2x7R
9	Fibu2x8F Fibu2x8R	64.0	294	Fibu2x8F
10	Fibu2x9F Fibu2x9R	58.0	396	Fibu2x9F
11	Fibu2x10F Fibu2x10R	56.0	261	Fibu2x10F Fibu2x10R
12-13	Fibu2x11-12aF Fibu2x11-12R	60.0	676	Fibu2x11-12aF Fibu2x12intF
14	Fibu2x13F Fibu2x13R	61.0	280	Fibu2x13R
15	Fibu2x14F Fibu2x14R	58.5	438	Fibu2x14F
16	Fibu2x15F Fibu2x15R	65.0	248	Fibu2x15F Fibu2x15R
17	Fibu2x16F Fibu2x16R	56.0	289	Fibu2x16F
18 (coding)	Fibu2x17F Fibu2x17R	59.0	565	Fibu2x17F Fibu2x17R
18 (3'UTR)	Fibu23utraF Fibu23utraR	53.0	645	Fibu23utraF Fibu23utrintF Fibu23utrintaF

Table A7. Primers and conditions for amplification and sequencing of the *FBLN2* gene.

Primer name	Primer sequence (5'-3')
Fibu25utrF	GCTGGTCCCGCCTCTCGC
Fibu25utrR	GTCCGAGGGTCCGCCGAG
Fibu2x1.1F	GCGTGTGAGGTGGCTGAGG
Fibu2x1.1R	TCAGTGCTCCCGAAGTCCAC
Fibu2x1.2F	CGCCGCTGGAGAACTGC
Fibu2x1.2R	GGTCTTCGTAGTGTCGCTCGG
Fibu2x1.3F	GCCTGCCACTGCCCTGAC
Fibu2x1.3R	AGCCTCCTGCCCAAACCAAG
Fibu2x1.3intF	AGTCAGCCACTGTCCACCAT
Fibu2x1.3intR	CATCAGGCAGTGATGTGGACA
Fibu2x2F	CTGCTGGACTTGGTGACTTATG
Fibu2x2R	AGAAGGCAAATGGGCAGC
Fibu2x3F	GCCTCACTCACTTTCCACTCT
Fibu2x3R	GGACAGCCTAACTTCTTGGG
Fibu2x4F	GGCAGAGGAGATAAGATAATGG
Fibu2x4R	TGGGTGGTAGTTGGTGGTTA
Fibu2x5F	GTTGTCTCAGCCACCTACTCT
Fibu2x5R	GTAACAGGAAGTGAAGGACC
Fibu2x6F	CCTGGCTGAAGACCTGAGACC
Fibu2x6R	ACATACCCAGCACCAGACAGC
Fibu2x7F	TAGTAGGTTAGAGCCAGGGATG
Fibu2x7R	TCATCATAGCAGCCAAGACTC
Fibu2x8F	CCTTGCTGGGTCTCATTCTCCTG
Fibu2x8R	TGGCGTGGAGCAGAGCGG
Fibu2x9F	GCTCTCTCCCTCCTGGTGGC
Fibu2x9R	CCAGCAGGAAACCCAACTAAGG
Fibu2x10F	GGCTGCTGAGTGTAAAGG
Fibu2x10R	CCACAATGCCTCCAGTAG
Fibu2x11-12aF	TGGCCCTGCAACTCTGAC
Fibu2x11-12R	CCAGCAGGAGGATGAGGC
Fibu2x12intF	AAGTGTGTGGGTAAGGCCAG
Fibu2x13F	CTCTCCCACTTAGCCTCC
Fibu2x13R	TGCCCACTACAGATACCAG
Fibu2x14F	TCCCTTCCCAGTCACCAG
Fibu2x14R	CAAGGTCACACAGCCAGG
Fibu2x15F	GGCTCTGTGGGTGGACG
Fibu2x15R	TTTCTGTGCCTGCTTGGAG
Fibu2x16F	GCTATTCTCACAGGTCCG
Fibu2x16R	ACAGGACCAGGACAGGC
Fibu2x17F	GCTGTGCCATCTGTGTC
Fibu2x17R	ACAGGAGTCAAGTCAGCAA
Fibu23utraF	ACGTGGAGATGAAGCTCTGG
Fibu23utraR	GCCATAGAGCCCTGTGACAT
Fibu23utrintF	TTGCTGACTTGACTCCTGT
Fibu23utrintaF	CTGTGGGTGAGGCTGGGT

Table A8. DNA sequence of the *FBLN2* PCR and sequencing primers described in Table A7.

Contribution of Collaborators

Dr Kwan-Leung Chan (investigator, cardiologist); The University of Ottawa Heart Institute, Ottawa, Canada: patient examination and diagnosis.

Donna Dillon, BScN, RegN (clinical research coordinator); The University of Ottawa Heart Institute, Ottawa, Canada: recruitment of family members and blood collection.

Ruobing Zou and Kelly Westaff (laboratory technicians); Ottawa Health Research Institute (OHRI), Ottawa, Canada: Genotyping of 19 markers on chromosome 3 for families 15 and 16.

Lee Bowman; (coop student); University of Waterloo, Waterloo, Canada: Primer optimization and DNA sequencing of one and nine exons (partial sequence) from the *TIMP4* and *FBLN2* genes respectively.

Lam Pham, Andrew Seto (summer students); OHRI and The University of Ottawa, Ottawa, Canada: DNA sequencing of three and five exons (partial sequence) from the *NOS3* and *FBLN2* genes respectively.

Curriculum Vitae

Jacinthe Le Sage

Education

2001-2004 **Master of Science in Human Molecular Genetics**
University of Ottawa; Ottawa, Ontario
My research project consists of studying the genetics of familial congenital bicuspid aortic valve, a malformation of the aortic heart valve. I identified and evaluated candidate genes for this disorder by linkage analysis and DNA sequencing. Supervisor: Dr Dennis E. Bulman.

1998-2001 **Honours Baccalaureate in Science in Biochemistry**
University of Ottawa; Ottawa, Ontario
I acquired some theoretical and experimental knowledge in biochemistry, molecular biology, metabolism, genetics, as well as in organic, inorganic and analytical chemistry.
My Honour's project consisted of studying the signalling mechanisms of pancreatic cancer cells. Supervisor: Dr Rémy A. Aubin.

1996-1998 **Diplôme d'études collégiales en Sciences de la Nature**
Collège de l'Outaouais; Hull, Québec
I learned the basics of biology, organic chemistry and physics and had some French, English, Spanish and philosophy courses.

Scholarships and Awards

Award name	Awarded by:	Academic year(s)
NSERC scholarship	National Sciences and Engineering Research Council of Canada	2002-2003
Bourse FRSQ	Fonds pour la Recherche en Santé du Québec	Summer 2002
Ontario Graduate Scholarship	Government of Ontario	2001-2002
Excellence scholarship	The University of Ottawa	2001-2003
Admission scholarship	The University of Ottawa	1998-2001
Bourse de promotion des études universitaires auprès de la francophonie	The University of Ottawa	1998-1999

Work Experience

2001-2003 — **Let's Talk Science volunteer**
University of Ottawa; Ottawa, Ontario
The "Let's Talk Science" program aims to increase the awareness and curiosity of grade school and high school students about science in general. As a volunteer, my role was to prepare and carry out hands-on activities with students at their school about various science topics such as DNA and forensics, cloning, and thermochemistry. LTS coordinator: Dr Barbara Vanderhyden.

Fall 2001 — **Teacher's assistant for a molecular biology laboratory course**
University of Ottawa; Ottawa, Ontario
My role was to help the students from the BCH3756 undergraduate course to conduct their experiments and to understand the theoretical aspects of molecular biology. I also evaluated their performance and marked lab books and exams. Supervisor: Dr Ken Dimock.

Summer 2001 — **Creation of a web site for biochemistry laboratory courses**
Biochemistry Department, University of Ottawa; Ottawa, Ontario
My role was to design web sites for three undergraduate biochemistry laboratory courses, as well as their corresponding French versions. The web sites included links to animated tutorials and computerized quizzes. Supervisor: Dr Gabriel Guillet.

Summer 2000 — **Summer student in a research laboratory on pancreatic cancer**
Health Canada, HPB, RSD; Sir F.G. Banting research centre, Tunney's Pasture, Ottawa, Ontario
This summer position was intended to be a preparation to my Honour's project in biochemistry. I performed various molecular biology experiments such as PCR, cloning and Northern blotting. Supervisor: Dr Rémy A. Aubin.

Summer 1999 — **Technician's assistant in animal care**
Health Canada, HPB; ARD, Sir F. G. Banting Research Center Tunney's Pasture, Ottawa, Ontario.
My role consisted of feeding rats, mice and monkeys in the research facility, as well as cleaning their cages and collecting data about them. I assisted the technicians with handling of the animals and preparation of material for routine tests and special projects. Supervisor: Kevin Kittle.